

UNIVERSITÀ DEGLI STUDI DI
CASSINO E DEL LAZIO MERIDIONALE

Corso di Dottorato in
Metodi, modelli e tecnologie per l'ingegneria

Ciclo XXXVII

Numerical assessment of combustion development and emission of spark ignition engines fueled by ammonia and ammonia hydrogen blends

In Partial Fulfillment of the Requirements for the Degree of PHILOSOPHIAE DOCTOR in Civil and mechanical engineering

Coordinatore del Corso
Chiar.mo Prof. Fabrizio Marignetti

Dottorando
Gabriele D'Antuono

Supervisori
Chiar.mo Prof. Enzo Galloni
Chiar.mo Davide Lanni, PhD

Index

Acknowledgment 4

List of figures 5

List of tables 9

List of publications 10

Abstract 11

Introduction 13

Chapter 1: Ammonia as an energy carrier 14

1.1 Ammonia main characteristics 16
1.2 Short overview on ammonia usage for power applications 18
1.3 Ammonia in internal combustion engines 19
1.4 Hydrogen production from ammonia 23
1.5 Ignition delay laminar flame speed and chemical kinetic approach to use ammonia in internal combustion engines 24

Chapter 2: The ammonia and hydrogen-enriched ammonia combustion: a numerical investigation 27

2.1 Cantera environment for ignition delay and laminar flame speed estimation 31

2.2 Spark ignition engine investigated 31

2.3 1D model description 32

2.4 3D CFD model description 36

Chapter 3: Results 40

3.1 Ignition delay estimation 40

3.2 PSA EP6DT engine operative conditions considering different ammonia hydrogen blends 45

3.3 T-jet Engine operative conditions considering different

ammonia hydrogen blends 58

3.3.1 Neat ammonia 60

3.3.2 Ammonia-hydrogen blends 66

3.3.3 Ammonia and ammonia hydrogen comparison 70

3.4 Ammonia cracking system and ammonia-syngas blends analyses 75

Conclusion 80

Bibliografy 83

Acknowledgement

This doctoral thesis marks the end of a long but also satisfying journey and this would not have been possible without the support of many people who I have the duty and pleasure to thank.

First of all I want to thank my family who supported me in this journey and beyond.

I would like to thank my tutor Prof. Enzo Galloni who guided me throughout my doctoral course, always putting me in a position to work at my best to achieve the proposed objectives and helping me in every moment of difficulty.

A sincere thank Prof. Fontana who accompanied me until the end of this journey with his professionalism, competence and infinite patience, always finding a moment for a discussion with me.

A special thanks to my colleagues Davide and Gianni who have become true friends and without whom this journey would have been less fun.

A big thank you also goes to Prof. Perna and Prof. Spazzafumo for their availability during these 3 years.

I would like to thank Prof. Contino from UCLouvain for the opportunity he gave me to attend my period abroad at his university making his professionalism and skills available to me.

I thank my friends, who in one way or another are always a source of carefreeness, having given me the opportunity to lighten the load during these years.

I thank everyone, those who are here and those who have been here; if I have arrived here, it is thanks to all the people I have met in my life so far.

List of figures

Figure 1 - Brown ammonia production scheme 15

Figure 2 - Blue ammonia production scheme 15

Figure 3 - Green ammonia production scheme 16

Figure 4 - Ammonia production and potential usage in power applications 18

Figure 5 - Worldwide greenhouse gases emissions related to human activities7 19

Figure 6 - Ammonia and gasoline laminar flame speed 20

Figure 7 - Peters Borghi diagram 29

Figure 8 - Schematic layout of T-jet engine 36

Figure 9 - T jet engine 38

Figure 10 - The mesh for PSA Engine 38

Figure 11 – Ignition delay estimation 40

Figure 12 - Comparison with experimental data at 1.2 bar. Fuel blend 5% hydrogen content 40

Figure 13 - Comparison with experimental data at 10 bar for 5% hydrogen content (left) and 30% of hydrogen (right) 41

Figure 14 - Calculated Ignition delays. 10 bar, 20% H2 content (left), 50% H2 content (right) 42

Figure 15 - Calculated Ignition delays. 55 bar, 20% H2 content (left), 50% H2 content (right) 42

Figure 16 - Percentage error maps of the proposed correlation as a function of pressure and temperature for the different fuel blends considered 44

Figure 17 - in-cylinder pressure and temperature of the unburned gases during the combustion evolution as a function of crank angle for a spark-ignition engine fueled with an ammonia-hydrogen blend 45

Figure 18 - percentage error maps of the proposed correlation as a function of pressure and temperature for 10 and 20% of hydrogen by volume. Red circles show typical pressure vs temperature trends of unburned gas in a light duty SI engine fuelled with an ammonia-hydrogen blend 45

Figure 19 - Measured in-cylinder pressure curves vs simulated ones 47

Figure 20 - Measured rate of heat release curves vs simulated ones 47

Figure 21 - Calculated temperature field for Case 1 (top), Case 2 (middle) and Case 3 (bottom) 49

Figure 22 - Flame front and end gas region for neat ammonia 49

Figure 23 - Peters Borghi diagram for the investigated mixtures 50

Figure 24 - Ammonia consumption for the three cases investigated 51

Figure 25 - ammonia mass fraction distribution at exhaust valve open 52

Figure 26 - main species concentrations for the three cases investigated: Neat ammonia (left) 5% of hydrogen (middle) and 15% of hydrogen (right) 53

Figure 27 - Main radical and NOx concentrations for the three cases investigated: Neat ammonia (left) 5% of hydrogen (middle) and 15% of hydrogen (right) 53

Figure 28 - Concentrations of some species derived from NH3 the three cases investigated: Neat ammonia (left) 5% of hydrogen (middle) and 15% of hydrogen (right) 53

Figure 29 - Different spark plugs locations 54

Figure 30 - Pressure curves comparisons. Neat ammonia (left), 5% of hydrogen (middle), 15% of hydrogen (right) 55

Figure 31 - Rate of heat release curves comparisons. Neat ammonia (left), 5% of hydrogen (middle), 15% of hydrogen (right) 55

Figure 32 - In cylinder temperature for neat ammonia (left), 5% of hydrogen (middle) and 15% of hydrogen (right) 55

Figure 33 - Ammonia consumption for all the investigated cases. Neat ammonia (left), 5% of hydrogen (middle), 15% of hydrogen (right) 56

Figure 34 - flame propagation for neat ammonia considering one (top) two (middle) and three (bottom) spark plugs 56

Figure 35 - flame propagation for 5% of hydrogen considering two and three spark plugs one (top) two (middle) and three (bottom) spark plugs 56

Figure 36 - flame propagation for 15% of hydrogen considering two and three spark plugs one (top) two (middle) and three (bottom) spark plugs 57

Figure 37 - Hydrogen consumption for all the investigated case. Neat ammonia (left), 5% of hydrogen (middle), 15% of hydrogen (right) 58

Figure 38 - In-cylinder pressure and rate of heat release for both 1D and 3D CFD. Engine running with neat ammonia, stoichiometric mixture, WOT operation, no boost conditions, optimized spark angle at 2000 rom (left) and 3000 rpm (right) 59

Figure 39 - In-cylinder pressure and rate of heat release for both 1D and 3D CFD. Engine running with ammonia-hydrogen blend, stoichiometric mixture, WOT operation, no boost conditions, optimized spark angle at 1500 rpm (left) and 3000 rpm (right) 59

Figure 40 - In-cylinder pressure (left) and brake power (right) for different spark angle considering the equivalence ratio equal to 1, no boost conditions, engine speed equal to 1500 rpm and wide-open throttle conditions 61

Figure 41 - In-cylinder pressure (left) and brake power (right) 62

Figure 42 - combustion duration for different boost levels 63

Figure 43 - Brake efficiency at different boost levels 63

Figure 44 - Brake specific fuel consumption (left) and burned fuel fraction (right) 64

Figure 45 - maximum in-cylinder pressure (left) and exhaust gas temperature (right) 64

Figure 46 - Brake specific fuel consumption (left) and burned fuel fraction (right) for different compression ratio 65

Figure 47 - maximum in-cylinder pressure (left) and exhaust gas temperature(right) for different compression ratio 65

Figure 48 - brake efficiency as a function of the brake torque for 1500 and 3000 rpm. The labels highlight the different throttle opening values 66

Figure 49 -CA 0-90 (left) and burned fuel fraction (right) versus engine torque for 1500 and 3000 rpm 66

Figure 50 - Engine efficiency as a function of engine torque at 3000 rpm for different loads 67

Figure 51 - Burned fuel fraction (left) and CA 0-90 (right) for different loads 68

Figure 52- Engine torque (left) calculated at maximum brake torque at knock limit spark advance and relative combustion duration (right) for different boost levels 68

Figure 53 - Maximum in-cylinder pressure (left), exhaust gas temperature (middle) and burned fuel fraction (right) calculated for the engine running at the maximum torque knock limit spark advance 69

Figure 54 - Boost level, engine efficiency and spark advance as a function of engine speed

and torque 70

Figure 55 - In-cylinder pressure and rate of heat release for ammonia and ammonia hydrogen blend considering an engine speed equal to 3000 rpm and throttle opening equal to 20% 71

Figure 56 - In-cylinder pressure and rate of heat release for ammonia and ammonia hydrogen blend considering an engine speed equal to 3000 rpm and wide-open throttle conditions 71

Figure 57 - In-cylinder pressure and rate of heat release for ammonia and ammonia hydrogen blend considering an engine speed equal to 3000 rpm and boost pressure equal to 1.6 bar 72

Figure 58 - maps for boost pressure for ammonia and ammonia hydrogen blend 73

Figure 59 - maps for engine efficiency for ammonia and ammonia hydrogen blend 74

Figure 60 - Ammonia map vs ammonia hydrogen map for boost pressure 75

Figure 61 - Ammonia map vs ammonia hydrogen map for engine efficiency 75

Figure 62 - pressure curves at different conversion efficiency 76

Figure 63 - temperature curves at different conversion efficiency 76

Figure 64 - Rate of heat release curves considering different conversion efficiency 77

Figure 65 - Pressure (left) and temperature (right) curves for ammonia hydrogen and ammonia syngas blends 79

Figure 66 - Turbulent flame speed assessment for ammonia-hydrogen and ammonia-syngas blends 79

List of tables

Table 1 Ammonia's main properties 17

Table 2 Chemical kinetic mechanism tested 31

Tabel 3 First engine under investigation main characteristics 32

Table 4 Second engine under investigation main characteristics 32

Table 5 Laminar flame speed correlation

Table 6 chemical kinetic mechanism used 34

Table 7 Coefficients for equation 24 37

Table 8 Errors of the proposed correlation 43

Table 9 Reference experimental tests 46

Table 10 Case initialization 47

Table 11 Comparison between mean measured values and calculated data 48

Table 12 Average values calculated in the end gas region at peak pressure 49

Table 13 Calculated mean turbulent flame speed 50

Table 14 Unburned fuel and NOx concentrations in the wet exhaust gas 51

Table 15 Calculated wet concentrations at exhaust valve opening 53

Table 16 $IMEP_H$ comparisons 55

Table 17 Combustion durations 57

Table 18 Unburned fuel and NOx concentrations in the wet exhaust gas 58

Table 19 Burned fuel fraction at exhaust valve open calculated by both 1D and 3D model 60

Table 20 Combustion characteristics and engine performance 61

Table 21 Combustion characteristics and engine performance 62

Table 22 Engine recalibration at 3000 rpm and boost level equal to 1.6 69

Table 23 Combustion durations at different conversion efficiency 77

Table 24 emissions comparison considering different conversion efficiency 77

Table 24 Comparisons 78

List of publications

Galloni, E.; Lanni, D.; Fontana, G.; D'Antuono, G.; Stabile, S. Performance Estimation of a Downsized SI Engine Running with Hydrogen. Energies 2022, 15, 4744. https://doi.org/10.3390/en15134744

Lanni, D.; Galloni, E.; Fontana, G.; D'Antuono, G. Assessment of the Operation of an SI Engine Fueled with Ammonia. Energies 2022, 15, 8583. https://doi.org/10.3390/en15228583

D'Antuono, G.; Lanni, D.; Galloni, E.; Fontana, G. Numerical Modeling and Simulation of a Spark-Ignition Engine Fueled with Ammonia-Hydrogen Blends. Energies 2023, 16, 2543. https://doi.org/ 10.3390/en16062543

Fraioli, V., Di Maio, D., Napolitano, P., Lanni, D., D'Antuono, G., Galloni, E., ... & Maestro, D. (2023). A Joint Work to Develop a Predictive 1D Modelling Approach for Heavy Duty Gaseous Fueled Engines through Experiments and 3D CFD Simulations (No. 2023-24-0007). SAE Technical Paper.

D'Antuono, G., Lanni, D., Galloni, E., & Fontana, G. (2023). Comparison of the Performance and Operation Limits of an SI Engine Fueled with Neat Ammonia and Hydrogen-Ammonia Blends (No. 2023-24-0042). SAE Technical Paper.

Raimondi, G., Greco, G., Ongis, M., D'Antuono, G., Lanni, D., & Spazzafumo, G. (2024). Techno-Economical Assessment for Combined Production of Hydrogen, Heat, and Power from Residual Lignocellulosic Agricultural Biomass in Huesca Province (Spain). Energies, 17(4), 813.

D'Antuono, G., Galloni, E., Lanni, D., & Fontana, G. (2024). A Relationship for Estimating the Ignition Delay of Hydrogen-Enriched Ammonia-Air Mixtures. Engineered Science, 28, 1074.

D'Antuono, G., Galloni, E., Lanni, D., Contino, F., Brequigny, P., & Mounaïm-Rousselle, C. (2024). Assessment of combustion development and pollutant emissions of a spark ignition engine fueled by ammonia and ammonia-hydrogen blends. International Journal of Hydrogen Energy, 85, 191-199.

Abstract

Nowadays, the interest in carbon free fuels for internal combustion engines has increased due to the high levels of CO_2 in the atmosphere. In particular, ammonia is a promising carbon-free fuel for internal combustion engines, but its combustion properties are very poor if compared with conventional fuels. Thus, hydrogen enrichment can be the proper solution to overtake the issues related to neat ammonia fuelling. Adding hydrogen to ammonia is important to improve the combustion characteristics of this fuel, like the laminar flame speed. Furthermore, ammonia, and its blends usage in internal combustion engines needs to be further investigated and the 1D and 3D CFD code can be very useful for these analyses.

The present research activity is aimed at the definition of the allowable operational range of light duty spark ignition engine considering both ammonia and ammonia hydrogen blend. The 3D CFD model has been used to reproduce some experimental data and then to do an in-depth analysis of the combustion process and the emissions. Then multiple spark strategy has been tested on the same engine to improve the combustion behaviour of this engine fuelled by ammonia and ammonia-hydrogen blends.

Considering double spark plug the pressure peak increases of about 43% considering the engine running with neat ammonia, 28% with 5% of hydrogen by volume and 18% with hydrogen-enrichment equal to 15% by volume. Then the effect of multiple spark plugs seems to be very sensitive to the amount of hydrogen considered in the fuel mixture, therefore it might be useful to adopt this strategy with lower ammonia-hydrogen-enriched blends. The $IMEP_H$, moving from single to twin spark strategy increases respectively of 9%, 11% and 6.5% for neat ammonia, 5% and 15% of hydrogen by volume in the fuel mixture. These results confirm that multiple spark strategy better fit with lower amounts of hydrogen-enrichment considered. The improvement in emission is smaller: in fact, for each mixture considered the reduction is respectively of about 13%, 8% and 3%. This is also confirmed for NOx emissions, and, in this case, the effect is less than unburned ammonia.

In the second part of the thesis the same calibration has been moved to the t-jet engine the same calibration has been used to the second engine under investigation and this choice can be justified by the fact that the two engines are very similar from a geometrical point of view, the application range for both is the same and also the turbulent motions inside the combustion chamber are very close to each other.

After that the 1D predictive model has been recalibrated by a hierarchic approach 3D-1D and it has been used to obtain the engine map considering ammonia and ammonia hydrogen blends.

Finally, a cracking system has been modelled in order to obtain the hydrogen necessary for the combustion directly from the ammonia dissociation, and then the syngas which flows from the outlet of the system has been tested in blends with ammonia.

The aim of this thesis is to assess the potential of ammonia as a fuel for internal combustion engine to overcome the problems related to the use of conventional fuel which produce CO_2 due to the presence of carbon in their molecules.

Introduction

Nowadays ammonia has gained considerable interest as a fuel and as an energy carrier, but the lack in the knowledge for these kinds of applications is big, therefore it is fundamental to improve the understanding of the combustion properties of this substance, as a neat fuel and in blends. In this thesis the potential of ammonia for light duty spark ignition engine has been assessed by means of both 1D and 3D CFD approaches. The 1D model has been coupled with correlations available in the literature for the laminar flame speed (presented in the following equation), while for the ignition delay Cantera model has been used to create a database able to cover the whole investigated operative points. For the CFD analysis the AVL tool has been used to better catch the combustion properties of the blend investigated. All these methods will be widely explained in the following chapter. The obtained results can be useful for the validation of the chemical kinetic mechanisms used and to fill the gap existing in the current literature. In particular, in this thesis only neat ammonia and ammonia hydrogen blends have been considered, with a maximum hydrogen enrichment equal to 15% by volume to keep ammonia as the main fuel, also emissions have been considering covering all the problems related to ammonia combustion. Finally, a specific relationship for the ignition delay estimation has been obtained and a catalytic cracking system aimed to the production of the hydrogen required for combustion directly from ammonia has been proposed.

The objective of this thesis is to investigate the feasibility of utilizing ammonia as a fuel for internal combustion engines, with the intention of mitigating the issues linked to conventional fuels that generate CO_2 due to their carbon-based molecular structure.

In chapter 1 there is an overview of the ammonia in the energy system focusing the attention especially on its usage in spark ignition internal combustion engine.

In chapter 2 are described the investigated engine and all the models used to perform the simulations, while chapter 3 presents all the obtained results.

Chapter 1: Ammonia as an energy carrier

The global energy scenario is undergoing a significant transformation, driven by the urgent need to reduce greenhouse gas (GHG) emissions and mitigate the effects of climate change. The transportation sector, responsible for nearly a quarter of global CO2 emissions, is at the forefront of this transition, and internal combustion engines (ICEs), which have dominated transportation for over a century, are a major contributor to these emissions. As a result, there is a growing interest in alternative fuels, that can reduce the carbon footprint of ICEs while maintaining their widespread use and infrastructure.

The Electrofuels, like alcohols, are of particular interest to solve this problem because they allow to compensate the carbon dioxide emission. Alcohols are relatively dense and liquid at normal condition, furthermore they can be produced via various pathways based on both renewable sources and fossil fuels [1,2]. Some of these e-fuels have been widely studied for engine's applications, like methanol, dimethyl ether and ethanol, but for their commercialization there is a problem related to the cost, especially if these kinds of fuels are obtained by renewable sources.

Ammonia [3] can play a significant role in this energy transition, also because it can be used as a hydrogen carrier. Comparing ammonia and hydrogen some advantages of ammonia over hydrogen are its lower cost per unit of stored energy, i.e. over 182 days ammonia storage would cost 0.54 $/kg-H 2 compared to 14.95 $/kg-H 2 of pure hydrogen storage [4], higher volumetric energy density (7.1–2.9 MJ/L), easier and more widespread production, handling and distribution capacity, and better commercial viability. Generally, ammonia market is estimated at 91-225 bn per year with the capital costs that varies from 1350 to 1590 $/kW. The distribution of anhydrous ammonia around the world is done via pipelines, railroads, barges, ships, road trailers and storage deport. Furthermore, the main properties of ammonia can be summarized as:

- It is a carbon-free, has no direct greenhouse gas effect, and can be synthesized with an entirely carbon-free process from renewable power sources.
- It has an energy density of 22.5 MJ/kg, comparable to that of fossil fuels (low-ranked coals have around 20 MJ/kg; natural gas has around 55 MJ/kg, LNG 54 MJ/kg, and hydrogen 142 MJ/kg).
- It is liquid at 0.8 MPa at atmospheric temperature.

Basing on that nowadays the interest in ammonia as an energy carrier, as a fuel and for power system strongly increased. For example, Japan has clearly recognised the potential of ammonia to serve as the hydrogen carrying energy vector, and a 22-member consortium led by Tokyo Gas has been created to cu- rate "Green Ammonia" promoted by the Cross-Ministerial Strategic Innovation Program (SIP) of Japan. Within European nations, the Netherlands are leading the promotion of ammonia, because it possesses a substantial quantity of renewable resources because of the high investment from government and industry.

An ammonia energy system is globally based on carbon free synthesis of ammonia, power generation, respect of safety regulations and public acceptance of the facilities and economic viability.

The aims of using ammonia for energy system are related to emissions reduction, but it important improving security of supply and reduces the cost of energy. Considering ammonia production there are different methods currently used, in fact ammonia can be produced through fossil fuel (brown ammonia), using still fossil fuel, but with a carbon capture (blue ammonia) and using sustainable energy sources (green ammonia). An overview of these systems is presented in figures from 1 to 3 [5], while in equation 1 is presented the global ammonia production reaction, starting from nitrogen and hydrogen.

$$N_2 + 3H_2 \rightarrow 2NH_3 \Delta H = -92 \frac{kJ}{mol} (1)$$

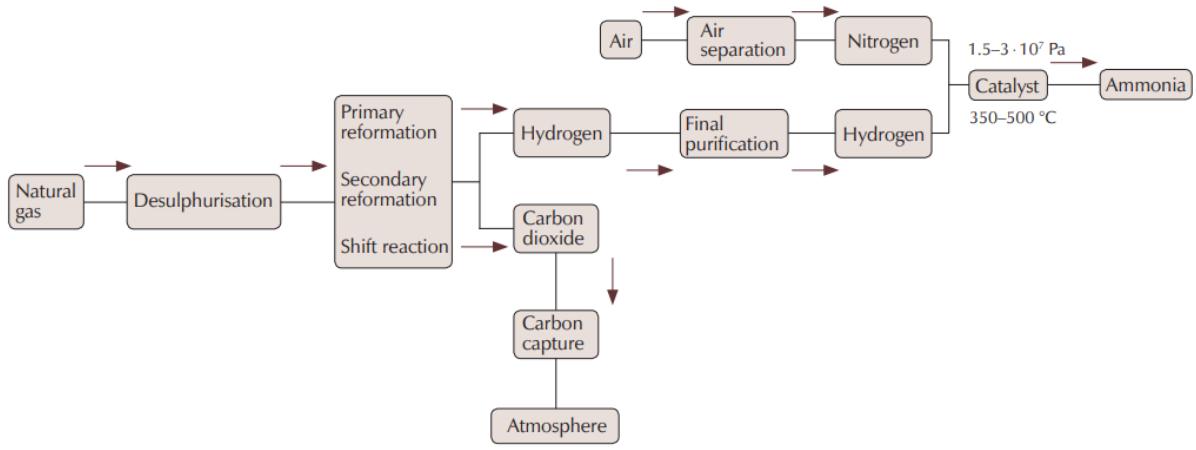


Figure 1: Brown ammonia production scheme

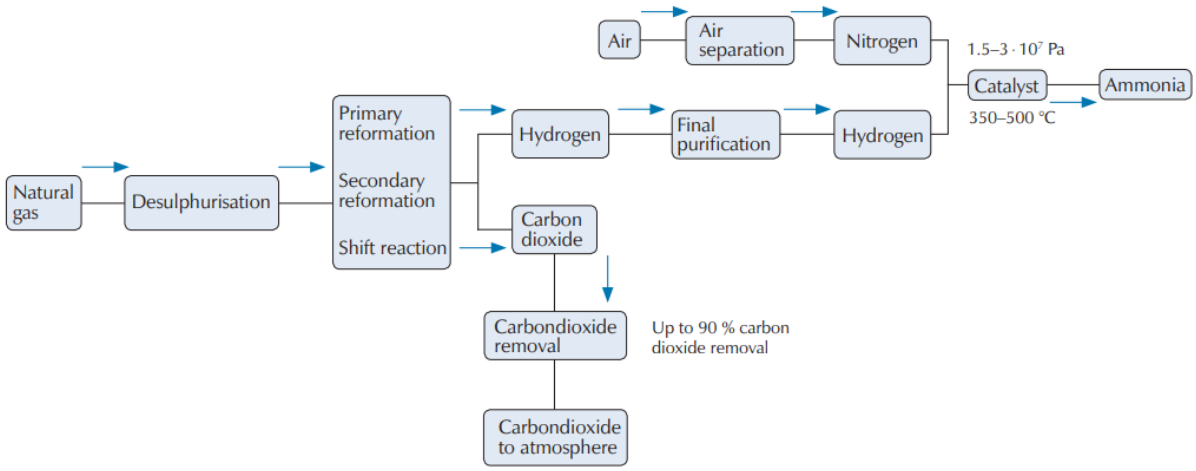


Figure 2: Blue ammonia production scheme

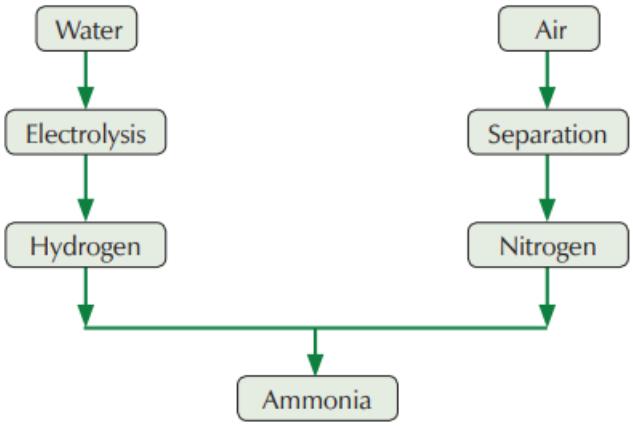


Figure 3: Green ammonia production scheme

Brown ammonia production is based on the use of a fossil fuel as a raw material for hydrogen production, with an emission of approximately 2.86 t of carbon dioxide per 1t of ammonia during production, and the main process used to product ammonia following this street is the well-known Haber-Bosch process (which was historically used to product ammonia as a fertilizer). During this phase, the ammonia production occurs as a catalytic reaction of hydrogen produced as a starting product and nitrogen, which is separated from the air by a separation unit process. Generally, the brown ammonia process requires enormous energy consumption, such as 8 MWh t^{-1}. The Haber-Bosch process can be used also for blue ammonia production, but in this case the advantage is related to ensure extremely low carbon emissions during the production process, which are at least 90 % lower compared to the emissions during the brown ammonia production process. This low concentration is made possible by the application of a carbon capture process after the hydrogen production process. Finally, the main techniques available for green ammonia production are water electrolysis, which on average allows the production of up to 10 ton of ammonia with respect to conventional method, and by air separation unit. Furthermore, renewable ammonia production facilities could also store local variable renewable energy resources and satisfy local ammonia consumption, possibly in small-scale decentralized concepts.

1.1 Ammonia main characteristics

Ammonia is a colourless substance with a sharp, penetrating odour characterized by the properties summarized in table 1. Furthermore, ammonia can be easily stored as a liquid in thermally insulated containers. The ammonia molecules have a trigonal pyramidal shape with the three hydrogen atoms and an unshared pair of electrons attached to the nitrogen atom. It is a polar molecule and is highly associated because of strong intermolecular hydrogen bonding, and the relative dielectric constant is equal to 22 at 239.2K, less than other substances like water.

Table 1: Ammonia's main properties

Ammonia main characteristics	
Boiling point [K]	239.8
Freezing point [K]	195.5
Density [kg/m^3]	0.73
Auto Ignition temperature [K]	930
Octane number	130
Heat of vaoporization [KJ/kg]	1371
Explosion limit [% volume ratio]	16:28
Laminar burning velocity [m/s] at ambient conditions	0.015
Heat released by a volume unit of stoichiometric air-fuel mixture [MJ/m^3]	2.81
Lower Heating Value [MJ/kg]	18.8

The ammonia combustion is challenging due to the lower laminar flame speed compared to conventional fuel, and the lower reactivity of ammonia. Ammonia cannot sustain lean or reach combustion, it is necessary to keep the air to fuel ratio next to the stoichiometric one (6.05). In equation 2 it is presented the global combustion reaction of ammonia-air mixture.

$$4NH_3 + 3O_2 + (3.76 * nO_2)N_2 \rightarrow 6H_2O + 2N_2 + (3.76 * nO_2)N_2 + heat \quad (2)$$

Even if ammonia is very useful for many applications, it is also important to pay attention on its health and safety risks, in fact, ammonia is classified as a toxic and corrosive substance. Human exposure limit of ammonia is not globally regulated, but mainly depends on legislation of the different country around the world. The mean limits can be identified as 25 and 500 ppm, dangerous consequences appear for exposure to concentrations above 300 ppm, with an exposure time of about 8 hours. To better define the limit that leads to a toxic effect on human health, the Acute Exposure Guideline Levels (AEGL), which is divided into three levels, can be used [6]:

- Level 1 defines the airborne concentration above which it is predicted that the general population, including susceptible individuals, could experience notable discomfort, irritation, or certain asymptomatic, non-sensory effects, but these effects are transient and reversible upon cessation of exposure.
- Level 2 defines the concentration at which there are irreversible and serious consequences on human health.
- Level 3 defines the concentration at which lethal effect on human health could appear.

It is also important to focus the attention on the potential secondary contamination which are irritation of eyes and nose with a sore throat, cough, chest tightness, headache, confusion and burns to the mouth and throat (if ingested). Fortunately, ammonia is lighter than air and this allows the leakages to tome quickly through the rising plums of air reducing the exposure. Furthermore, it is important to take attention also on the environmental impact of ammonia, in fact, ammonia is a natural part of the nitrogen-cycle since it is produced by some living organisms via

the nitrogenase enzyme and excessive ammonia release in the environment, either from agriculture or directly in the atmosphere, can be a serious cause of pollution, finally ammonia spillage, or infiltration due to leaching of intensive agricultural activities is highly toxic to aquatic life and this might have also disastrous effects on human life. Considering ammonia emission in the atmosphere, in Europe, ammonia emissions were first regulated in the Euro VI norm for heavy-duty vehicles, which includes on-road tests and real driving emissions assessments with a concentration limit of 10 ppm

Considering the usage of ammonia as a fuel it is important to pay attention on the corrosive behaviour of ammonia, especially if it is used in internal combustion engine.

1.2 Short overview on ammonia usage for power applications

The first use of ammonia for powertrain applications was related to locomotives, then during the second world war it was used as a fuel due to the unavailability of diesel and petrol. Moving forward in time ammonia became also a working fluid for power cycle, and it can be used instead of a Rankine cycle in a combined cycle. Recently ammonia has also been studied for gas turbines fuel cells applications, keeping the attention mainly on stationary usage. In figure 4 the whole cycle of ammonia from production to usage in power applications is summarized [7].

In this work, the attention is focused only on the possibility of using ammonia in internal combustion engines and that is deep explored in the following section.

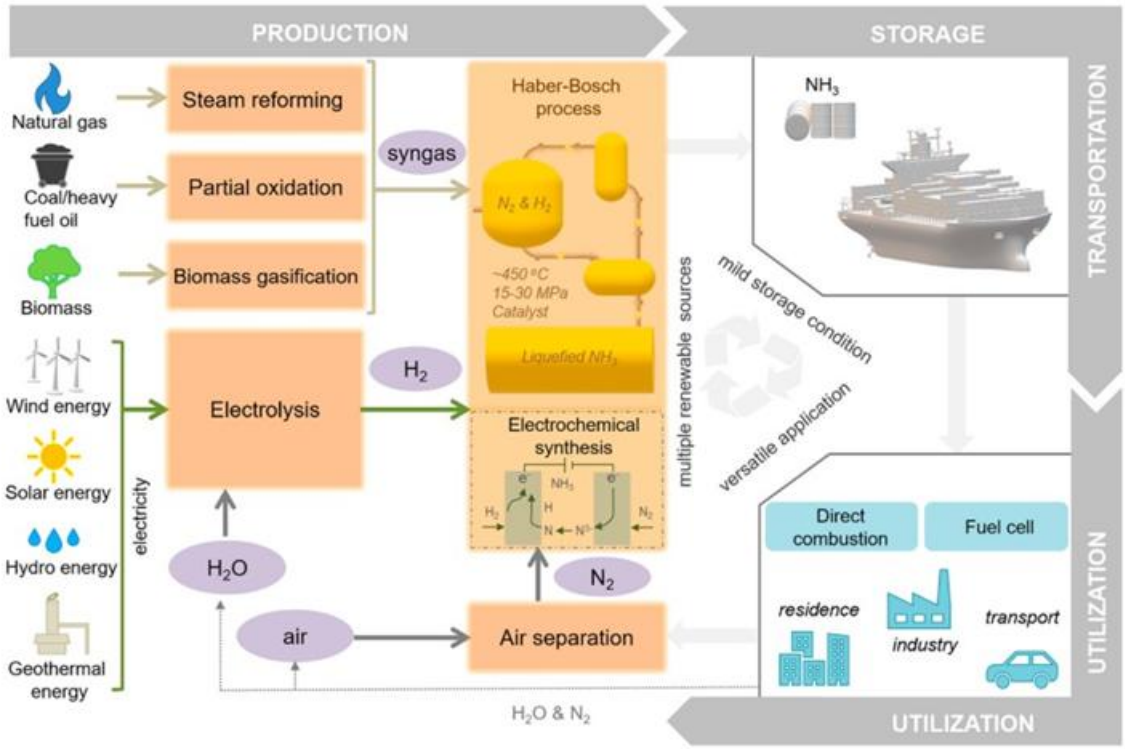


Figure 4: ammonia production and potential usage in power applications

1.3 Ammonia in internal combustion engines

Nowadays pollutions and greenhouse gases are the main problems related to the combustion of fossil fuels in internal combustion engines. Thus, it is crucial to find new fuels characterized by low emissions associated with the burning process. In fact, as stated in the Paris agreement the emissions of greenhouse gases must be under control to guarantees a mean global temperature increase of about 2°C. This decision is based on the global increase of greenhouse gases related to human activities thought the years, as shown in figure 5 [8,9]. Ammonia is a promising alternative to fossil fuels due to the zero-carbon impact during its combustion and, furthermore it can be used also as a hydrogen carrier [10,11]. Furthermore, if the production of ammonia follows a green process the global emission of this fuel can be considered without CO_2 impact. On the other hand, ammonia presents some disadvantages respect to conventional fuel, like low energy density, corrosive behaviour and worse combustion characteristics. In particular, the laminar flame speed of ammonia, as shown in figure 5, is much lower with respect to gasoline, as example considering stoichiometric conditions the laminar flame speed of ammonia is about 82% than those of gasoline. Again, like other alternative fuels such as ethanol, methanol, hydrogen and gasoline/diesel blends, ammonia is characterized by high octane number which can improve combustion properties and reduce undesirable effects such as knocking. The high-octane number also allows to use ammonia in engine characterized by high compression ratio. Regarding the allowable mixture strength of ammonia–air mixtures, the flame can propagate in mixture characterized by an equivalence ratio ranging between 0.63 and 1.4[12], even if available literatures research paper shrinks this range very close to the stoichiometric value. After the second world war the interest in ammonia as a fuel for internal combustion engine strongly decreased up to the last few years due to the current regulations about pollutants and greenhouse gases.

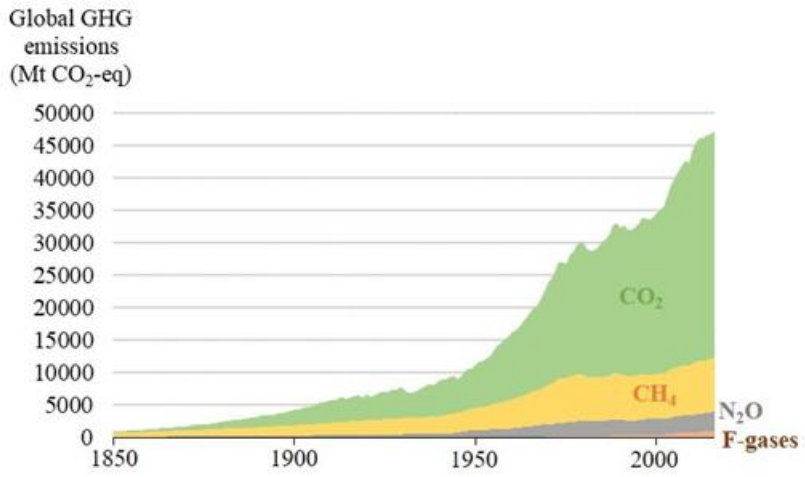


Figure 5: Worldwide greenhouse gases emissions related to human activities

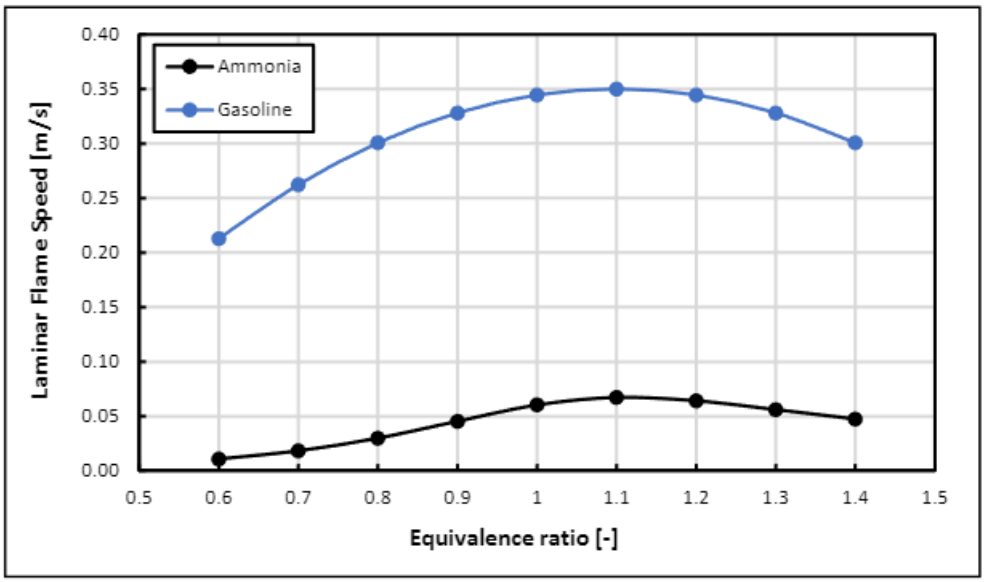


Figure 6: ammonia and gasoline laminar flame speed

The first use of ammonia as a fuel dates to 1878 [13], following that period due to the poor combustion performance of ammonia the research is mainly focused on the field of compression ignition engines, as example Gray et al [14] achieved a proper combustion of ammonia considering a compression ratio of 35:1 with an inlet temperature equal to 423K, while Pearsall et al. [15,16] tried to obtain stable combustion with a compression ratio of 30:1, without a proper ignition of the ammonia air mixtures.

Recently Lesmana et al. [17] stated that ammonia does not fit with low carbon real-world CI engines applications, due to unfavourable autoignition properties requiring very high compression ratios (CR), high intake temperatures or blending with hydrocarbon fuels to complete ignition, and because of that many studies focused their attention on a dual fuel approach to make ammonia adapt for compression ignition engine. Reiter and Kong [18,19] tested ammonia-diesel fuel mixtures in a multi-cylinder turbocharged diesel engine, reaching the maximum power outputs with low CO_2, soot and NO_x emissions, even if unburned ammonia emissions were high, therefore a specific after-treatments system is needed. Finally, Pochet et al. [20,21] experimentally investigated the potential of ammonia/hydrogen mixtures in Homogeneous-Charge Compression-Ignition (HCCI) engines and concluded that high compression ratios of about 22:1, as well as NO_x emission mitigation measures are required for satisfactory performances and emission compliance. Sahin et al. [22] investigated the behaviour of a small dual fuel CI engine running with premixed water–ammonia solutions. The addition of ammonia determined an increase in engine efficiency at all the investigated speed and load values. Even in this case, they found an increase in NOx related to the nitrogen present in NH3. The authors also pointed the attention on the damages of some elements of the carburetor used to add the fuel. Scharl et al. [23] investigated the mixture formation and spray combustion on a rapid compression–expansion machine. Combining 1D analyses and optical investigations, they found out that ammonia flames

do not appear stable after ignition. Zhang et al. [24] experimentally investigated the performance of a two-stroke low-speed engine powered by a dual-fuel direct injection mixture composed by ammonia and diesel. Varying the ammonia's amount, they discovered that diesel injection timing helps the regulation of the ignition in the early stage of combustion. The authors also claimed that this solution is important for the reduction in ammonia's combustion duration, and, consequently, the indicated thermal efficiency increases.

The autoignition properties of ammonia suggests the use of this fuel in spark ignition engine, also because the high-octane number allows to avoid knock phenomenon increasing the compression ratio. The usage of spark ignition engines running with neat ammonia has been studied firstly in the 1960's and the results showed that neat ammonia fuelling, considering both single-cylinder and multi-cylinder engines, guarantee lower engine performances in terms of indicated power, thermal efficiency and fuel consumption; furthermore, also the emissions were high respect to gasoline [25-27]. Recently many researchers widely investigated the usage of ammonia air mixtures in light duty spark ignition engines. Lhuillier et at. [28,29] experimentally investigated the combustion characteristics of ammonia in a modified GDI engine at 1500 rpm. They compared the combustion behaviour of ammonia with hydrogen-enriched ammonia and pure methane. The results showed that ammonia can be used in an SI engine, but to achieve proper engine operation, it was necessary to advance the spark timing. The efficiency was similar for each case studied, with pressure peaks lower for ammonia compared to those of other fuels. Cui et al. [30] experimentally analysed the effect of a pre-chamber with a jet flame to improve the ignition phase of ammonia and its combustion. They found that increasing the pre-chamber volume leads to an increase in jet duration and ignition energy. All these studies clarify ammonia can be used as a fuel for spark ignition engine, but due to the poor combustion properties it is better to consider the possibility of mixing ammonia with other fuels to solve these problems. Mounaim-Rousselle et al. [31] focused their attention on the operating limits of a small GDI engine modified to run with premixed ammonia–hydrogen–air mixtures (hydrogen content ranging from 0 to 10% by volume). Keeping the original spark plug device, they analyzed engine cycle variation and exhaust gas emissions when varying the intake air pressure (from about 0.55 bar up to 1 bar) at different engine speeds (from idle speed to 2000 rpm) for lean, stoichiometric and rich air–fuel mixtures. Running with pure ammonia, they found the engine could stably operate at up to 1500 rpm when the intake air pressure was equal to 1 bar, while the engine cycle variation limited low load operation. They indicated a coefficient of variation of IMEP higher than 5% when the intake air pressure was less than 0.75 bar. The engine was not able to operate at 2000 rpm for any of the air intake pressures. When the hydrogen percentage in the fuel mixture was 10%, the authors achieved proper engine operation for all considered cases. Guo et al. [32] investigated the combustion of lean gasoline–ammonia–air mixtures in an SI engine derived from a CI engine characterized by a glow plug and a sub-chamber. They found that increasing the ammonia concentration reduces the pressure peak, while NOx increases. The influence of the glow plugs on IMEP and thermal efficiency was negligible in almost all conditions. El

Fattah et al. [33] focused their research paper on the exhaust emissions and performance of an SI engine fuelled with water–ammonia–gasoline blends. They found that when adding water ammonia to gasoline, the engine thermal efficiency increased, but the CO formation also increased due to the occurrence of incomplete combustion. Additionally, NO_x emissions increased with the volume percentage of the water–ammonia solution. Zhang et al. [34] proposed a numerical study on the combustion characteristics of a spark-ignition engine fuelled by ammonia and hydrogen which is obtained from the reformation of the exhaust gas. The authors pointed out that by adding hydrogen, up to 10% by volume, the in-cylinder pressure increased, and the combustion duration decreased, leading to an improvement in combustion and thermal efficiencies. Frigo et al. [35,36] proposed a catalytic system for the hydrogen production able to produce 1.4 Nm^3/h from ammonia using a ruthenium-based catalyst reactor. They claimed that the whole system can work stand-alone or coupled with a spark ignition internal combustion engine and then they experimentally investigated a spark-ignition engine, used as a rang extender for electric vehicles, powered by ammonia and hydrogen where hydrogen is obtained by their ammonia cracking system. After defining the type of injector and its timings, they considered either full-load operations or half-load conditions, with the engine running from 2500 rpm to 5000 rpm and stoichiometric mixtures. The authors showed the amount of hydrogen necessary to increase the combustion velocity mainly depends on load and less on engine speed, and they considered a percentage of hydrogen of 6% (volume basis) at full load and 10% at partial load. Wang et al [37] proposed a numerical study on ammonia hydrogen blends compared them to methane, methanol and ethanol combustion. They proposed a 1D approach varying the equivalence ratio from 0.7 to 1.3, the hydrogen amount by volume (from 0 to 100%) and the compression ratio. They claimed that the laminar burning velocity needs an amount of 40–70% of hydrogen to reach the same level of hydrocarbon fuels unless the compression ratio increases. The ignition energy shows an opposite trend to laminar burning velocity. The authors also found that due to an incomplete oxidation, the combustion efficiency decreases if the amount of hydrogen and the equivalence ratio increase. Pyrc et al. [38] experimentally investigated an SI engine characterized by a variable pressure ratio and modified it to work as an engine fuelled with ammonia-hydrogen mixtures. Considering two different pressure ratios (8 and 10) and an amount of the energy shared by hydrogen from 0 to 70%, the results show that with about 12% of energy shared by hydrogen, the instability related to the ignition process disappears. With a compression ratio equal to 8, the authors observed that ignition delay decreases two times, while for a compression ratio equal to 10, it decreases almost three times; naturally, the specific energy consumption decreases as the compression ratio increases. Grannell et al. [39,40] experimentally investigated a stoichiometric ammonia-gasoline mixture in a laboratory research engine considering premixed port injection varying the compression ratio, loads and engine speeds. It was necessary to operate only with gasoline at idle in the premixed injection mode to achieve stable conditions, but a satisfying trade-off was found at full load considering 70 % ammonia and 30 % gasoline. Increasing the load allowed to reduce the required amount of gasoline but increasing the amount of ammonia it was necessary to advance the spark timing. Increasing the compression ratio between 8:1 and 10:1 improves the

thermal efficiency, especially at high loads, while increasing the engine speed led to more combustion promoter requirement. Very high NH_3 emissions were measured for pure ammonia fuelling at full-load and decreased with increasing gasoline content. Ryu et al. [41,42] analysed the direct injection of gaseous ammonia and partially dissociated ammonia in a research engine considering port fuel injection of gasoline as a co-fuel. They claimed that an injection pressure equal to 13.8 bar was suitable for direct injection at 40°C. Direct ammonia injection improve the power output in gasoline-ammonia blends at similar brake specific fuel energy consumptions, if the proper injection timing and duration were chosen.

1.4 Hydrogen production from ammonia

The usage of ammonia in blends is nowadays widely investigated, but in compliance with the current regulations only mixtures with other carbon-free fuels allows to achieve the objective of the carbon neutrality; in particular hydrogen is the main co-fuel considered especially for spark ignition engine, therefore it is important to define accurately the way in which this hydrogen can be produced. As for ammonia also hydrogen can be divided into different categories depending on the production process, and in particular it can be classified in grey hydrogen (the most polluting type), blue hydrogen (a process which use also carbon capture and storage) and green hydrogen (obtained by renewable energy sources) [43]. Among the different green processes there is one of particular interested because it is based on the use of ammonia which flows inside a catalytic or non-catalytic reactor to produce pure a hydrogen rich syngas, that can be purified by means of PSA and filters depending on the application required.

Reggetti et al. [44] investigated experimentally and by means of a simulation tool, the on-board hydrogen production by ammonia using the heat that can be obtained by the exhaust gas. In particular their activities are aimed to evaluate the hydrogen production capability and the allowable equivalent ratio considering the engine running with neat ammonia, varying intake pressure, inlet mass flow rate and temperature, equivalence ratio and spark timing and measuring both performance and emissions.

The authors assessed that increasing the equivalence ratio the amount of hydrogen produced rise up. The H_2 cracking efficiency was defined as the fraction of H2 fuel energy in the exhaust compared to total chemical energy in the exhaust gases (the ratio between the hydrogen mass flow multiplied by its lower heating value and the ammonia mass flow multiplied by its lower heating value and by a parameter which takes into account the equivalence ratio and the combustion efficiency).

Mercier et al. [45] focused their analysis on the upstream on-board hydrogen production to extend the allowable range of a spark ignition engine fuelled by ammonia. They investigated the performance of the engine testing different equivalence ratios, load conditions and dissociation rates. Their experiments showed that only a slight rate of ammonia's dissociation, about 10%, improves the engine range due to the better combustion stability. In the end they claimed the on-board cracking did not only improve the allowable range of the engine but can also help to reduce ammonia emissions. On the other hand, to reach the same engine work it was necessary to have a higher

ammonia consumption because of the lower cracking efficiency exploiting ammonia dissociation. Zhang et al. [46] investigated the on-board ammonia cracking to produce hydrogen for heavy-duty applications. They proposed an integrated system aimed to be a range extended electric powertrain. The authors said that the hydrogen produced by ammonia is enough to fuel the engine and the global consumption of the system is comparable to a diesel one, if the catalytic production ratio is below 6.5%. In the end they claimed that with a catalytic production ratio of 2.5% the system reaches an efficiency equal to 32.8%, consuming about 9% more energy with respect to diesel hybrid, but 5.1% less than neat diesel engine. Due to the low engine speeds that characterize the heavy-duty engines, ammonia could effectively be fired in applications such as marine engines, as reported in [47,48]. In addition, in [49], the authors theoretically investigated the behaviour of a diesel marine engine firing with ammonia–hydrogen blends and performing an HCCI combustion mode able to reduce the NO_X formation.

1.5 Ignition delay laminar flame speed and chemical kinetic approach to use ammonia in internal combustion engines

The knowledge of the combustion and ignition properties of a fuel is crucial to optimize its usage. While for laminar burning velocity there are some works which are useful to model the ammonia combustion in internal combustion engine, for ignition delay predictions there is much work that still needs to be done and there are few and partial results in the literature. Ammonia presents poor ignition properties; therefore, it is crucial to go deeper into the knowledge of this fuel to enhance stability and operability of it. The ignition delay time, which is the time needed to obtain a proper ignition of the fuel-oxidizer mixture considered, is a fundamental property not only to characterize the considered fuel but also to validate the chemical kinetic mechanisms. Considering ammonia, the autoignition temperature is about 84% higher than hydrogen, so it is clearly convenient to consider ammonias blend to improve its combustion characteristics. The effect of hydrogen addition, on the ignition delay of ammonia-air mixtures at high temperatures, was investigated in [11]. The authors considered a wide range of temperature (from 1020 to 1945 K), two different pressure levels (1.2 and 10 bar), and a hydrogen mole fraction varying from 0 to 0.7. They compared the experimental measurements to different chemical kinetic mechanisms to test their reliability. Also, Chen et al. [50] proposed a correlation for the calculation of ignition delay of both neat ammonia and ammonia slightly enriched with hydrogen, but only up to 95% NH_3, 5% H_2 by volume.

Laminar flame speed has been studied more than ignition delay for ammonia- air and ammonia's blends mixtures. Early and preliminary study date back to 1970' and 1982' [51,52], then further studies were proposed during the first decade of 2000' [53,54]. In the last few years further studies and correlations for laminar flame speed of ammonia and ammonia-hydrogen blends have been proposed. The research interest considered mainly hydrogen enrichment to keep the carbon neutrality of the fuel mixtures. Kumar and Meyer [55] proposed a study on the laminar flame properties of ammonia-hydrogen-

air mixtures considering ambient conditions using a Bunsen burner, paying particular attention to heat loss. The results they achieved presented significant discrepancies with the literature that could be related to uncorrected heat losses estimation and inaccurate initial conditions. Li et al. [56] conducted similar experiments on the same mixtures measuring the NO_x emissions at the combustor exhaust. In the end, for internal combustion engine's numerically investigation is fundamental to have a specific correlation for the estimation of the laminar flame speed. Starting from a chemical kinetic approach, Goldmann and Dinkelacker [57] proposed two different correlations able to calculate the laminar flame speed of ammonia-air and ammonia-hydrogen-air mixtures respectively. Lhuillier et al. [58] subsequently updated these relationships to allow turbulent combustion simulations with satisfactory accuracy and low computational cost for hydrogen contents in the fuel smaller than 50%.

Also, Pessina et al. [59] proposed a correlation for the calculation of the laminar flame speed of ammonia-hydrogen blends focusing on applications related to internal combustion engines. The correlations for laminar flame speed and ignition delay are very useful for 1D analysis of a spark ignition engine because they allow to couple the current one-dimensional tools with validated and specific values of these two parameters which are not available for fuels like ammonia that were not considered usable in engines until a few years ago. Furthermore, for the same reason, a chemical kinetic approach can be extremely helpful in 3D CFD analysis of engines fuelled by ammonia-air or ammonia blends.

Nitrogen and ammonia chemistry have firstly been studied only to understand the influence of fuel bound nitrogen and the NO_x formation pathways [60]. Recently, the growing interest in ammonia as a fuel has prompted researchers to define specific chemical mechanisms which are able to predict the burning of this substance. Detailed chemical kinetic mechanisms are useful in predicting and analyzing the combustion behaviour of air-fuel mixtures. However, mathematical relationships correlating overall parameters (such as laminar flame speed and ignition delay) to the main physical properties of the mixture (pressure, temperature, composition, etc.), could be very useful to define fast and efficient development tools for industrial purposes. In recent years, some authors investigated the combustion of ammonia-hydrogen-air mixtures proposing chemical kinetic mechanisms able to describe their oxidation pathways. Nakamura et al. [61] analyzed the ignition delay of ammonia-air mixtures in a micro flow reactor. They considered weak flames at different equivalence ratio (0.8; 1; 1.2) and proposed a chemical kinetic mechanism able to reproduce the measured data. Otomo et al. [62], starting from the work of Song et al [63], developed a chemical kinetic mechanism for ammonia-hydrogen-air mixtures. This model was able to reproduce both laminar flame speed and ignition delay time of different kinds of mixtures at three different levels of pressure (1.4; 11; 30 bar). Stagni et al. [64] carried out experimental tests on a jet stirred reactor under lean conditions ($0.01 \leq \Phi \leq 0.375$) in a range of temperature from 500 to 2000 K. They also modified a mechanism previously developed for methane [65] to predict the ammonia pyrolysis and oxidation. Shrestha et al. [66] proposed a detailed mechanism for ammonia oxidation including NOx formation. They considered both ammonia and ammonia-hydrogen blend. The same authors [67]

focused their attention also on the experimental determination of laminar flame speed for oxygen enriched ammonia and ammonia hydrogen blends at high pressure and temperature to define a specific kinetic model considering also nitrogen oxides formation. The usage of a chemical kinetic approach is also important to better estimate the emissions related to ammonia combustion. Ammonia's combustion produced an important amount of NO_x and NH radicals.

CHAPTER 2: The ammonia and hydrogen-enriched ammonia combustion: a numerical investigation

Combustion is a complex phenomenon in which thermodynamics, transport and chemical kinetic phenomena are involved together. To achieve proper combustion it is necessary to have a fuel, an oxidizer (which is commonly the air) brought into suitable conditions to start the process. Equation 2 and 3 presents the combustion reaction for stoichiometric mixture considering neat ammonia and ammonia hydrogen blends.

$$4NH_3 + 3O_2 \rightarrow 2N_2 + 6H_2O + heat \quad (2)$$

$$\left(1 - x_{H_2}\right)NH_3 + x_{H_2}H_2 + \frac{3 - x_{H_2}}{4}(O_2 + 3.76N_2) \rightarrow \frac{3 - x_{H_2}}{2}H_2O + \left(\frac{1 - x_{H_2}}{2} + \frac{3.76 * 3 - x_{H_2}}{4}\right)N_2 + heat \quad (3)$$

The stoichiometry allows to define the relationship between the fuel and the oxidizer which is defined as:

$$\frac{A}{F} = \left(\frac{m_{oxidizer}}{m_{fuel}}\right) \quad (4)$$

$$\left(\frac{\mathrm{A}}{\mathrm{F}}\right)_{st.} = \left(\frac{m_{oxidizer}}{m_{fuel}}\right)_{st.} = \frac{\frac{3-x_{H_2}}{4} \cdot 137.28}{\left(1-x_{H_2}\right) \cdot 17 + x_{H_2} \cdot 2} \quad (5)$$

$$\phi = \left(\frac{\mathrm{A}}{\mathrm{F}}\right)_{st.} \Big/ \frac{\mathrm{A}}{\mathrm{F}} \quad (6)$$

Where m_{fuel} and $m_{oxidizer}$ are respectively the mass for the considered blend. The reaction rate is highly influenced by the concentration of the reactants and by their temperature, and pressure, then during the combustion process the chain oxidation reaction are fundamental and globally the reaction rate strongly depends on the subproduct of combustion. The reaction velocity w_r is commonly described using the exponential factor of Arrhenius as described in the following equations:

$$w_r = C * p^n * exp\left(\frac{-E_a}{R * T}\right) \quad (7)$$

Where C and n are constants which depend by the considered reaction, E_a is the activation energy and the whole exponential part expresses the fraction of molecules that have an energy (due to thermal agitation) greater than the activation energy required to ensure the breaking of existing intermolecular bonds and their replacement with new ones. Also, the ignition phase is commonly described by an Arrhenius relationship (equation 8), and the ignition delay can be considered inversely proportional to the speed at which the oxidation reactions occur. Even in this case there is an exponential dependence on the temperature, this being a parameter that affects w_r.

$$\tau = A * p^{-n} * exp\left(\frac{E_a}{R * T}\right) \quad (8)$$

Where A, n and E_a are experimentally obtained. The ignition delay is a crucial parameter for internal combustion engine, and it is difficult to estimate due to lower order of magnitude (ms) related to engine operative conditions. Thus, it is necessary to bring the

studied mixture to the desired temperature and pressure conditions in times negligible with respect to the ignition delay to be detected. This can be done with shock tubes or rapid compression machines. For the spark ignition internal combustion engines, which are studied in this thesis, the combustion process is premixed, therefore it is crucial to study the flame front and its propagation in the end gas, considering also the turbulence inside the combustion chamber. To study the laminar premixed flame the theory of Mallard and Le chatelier [68] can be used. This model divided the flame in different zones: the reaction one characterized by a specific thickness δr where the exothermic reaction takes place; then there is the unburned gas zone which ignite thanks to the increase of the temperature related to the heat provided by the flame front considering the preheating zone equal to the flame thickness mentioned above. Assuming that the slope of the temperature curve is linear, the slope can be approximated by the equation $(T_f-T_i)/\delta$ where T_f and T_i are respectively the final flame temperature and the ignition temperature. The enthalpy balance then becomes:

$$\dot{m}c_p(T_i - T_0) = \lambda\left(\frac{T_f - T_1}{\delta}\right)A \qquad (9)$$

where λ is the thermal conductivity, $\dot{m}$ is the mass rate of the unburned gas mixture into the combustion wave, T_0 is the temperature of the unburned gases, and A is the cross-sectional area taken as unity. Since the problem as described is fundamentally one-dimensional, the mass rate is equal to $\rho*S_L*A$. This explains the relationship between the laminar flame speed S_L and the flame thickness δ.

In a spark ignition engine, the flow field does not allow to consider a laminar burning velocity, because the flame propagates in a turbulent flow field, which is generated by the high shear flows set up during the intake stroke and modified during the compression stroke. Considering a port fuel injection spark ignition engine, the fuel and the air are premixed inside the intake port, while the combustion process can be divided into two different stages: growth and development of the flame and then the flame propagation inside the combustion chamber. The main parameters which influence the turbulent combustion are the air to fuel ratio, in fact if the mixture is lean or rich the flame speed decreases; the compression ratio, which, if increased, determines an increase in temperature and therefore in the whole combustion process; the engine speed, the intake conditions and the turbulence. In particular, it is crucial to optimize the turbulence flow inside the engine to optimize the whole process, the interaction among the eddies of various scales is responsible of a transfer of energy sequentially from the larger eddies gradually to the smaller ones, through a process known as the turbulent energy cascade. Moreover, the cyclic variation must be considered, so mean velocity quantity needs to be considered coupled with turbulent velocity component. For the turbulence two different length scales can be considered, each coupled with a distinct time scale: the integral length scale (L_i), which reflects the greatest scale structure of the flow field, which is characterized by low frequency and significant fluctuations. It is defined as the integral of the autocorrelation coefficient of the variable velocity at two adjacent places in the flow in proportion to their separation, the Kolmogorov length scale (L_k), which is the lowest scale of turbulent motion, where turbulent kinetic energy dissipates into heat. The combustion regimes depend on the interaction between the

flame and the in-cylinder flow, and all these regimes are represented in the well-known Peters Borghi diagram. This diagram is based on three dimensionless number:

- ✓ the turbulent Reynold number: explains the ratio of inertial to viscous forces; $Re = \frac{u' * L_t}{\nu}$
- ✓ the Damkohler number: explain the relationship between turbulent and chemical time scales; $Da = \frac{\tau_t}{\tau_l} = \frac{\frac{L_t}{u'}}{\left(\frac{\delta_l}{S_L}\right)}$
- ✓ the Karlovitz number: is the ratio of the chemical time scale to the Kolmogorov time scale; $Ka = \frac{\tau_L}{\tau_K} = \frac{\left(\frac{L_t}{\delta_L}\right)^{-0.5}}{\left(\frac{u'}{S_l}\right)^{\frac{3}{4}}}$

The combustion zones of a Peters Borghi diagram are:

- Wrinkled flame in which the turbulence intensity is less than the laminar flame speed; hence, the turbulence lacks sufficient energy to corrugate the flame front.
- Corrugated flames which are characterized by the turbulence intensity surpasses the laminar velocity.
- Distributed reaction: a zone in which Ka becomes more than 1, and the tiniest eddies penetrate the pre-heat zone of the flame, but not the reaction zone, since the thickness of the reaction zone is still greater than the largest eddies.
- Well stirred reaction zone in which the combustion is governed by the chemical kinetic.

In the following figure is presented a typical Peter Borghi diagram in which are depicted all the combustion zones described above.

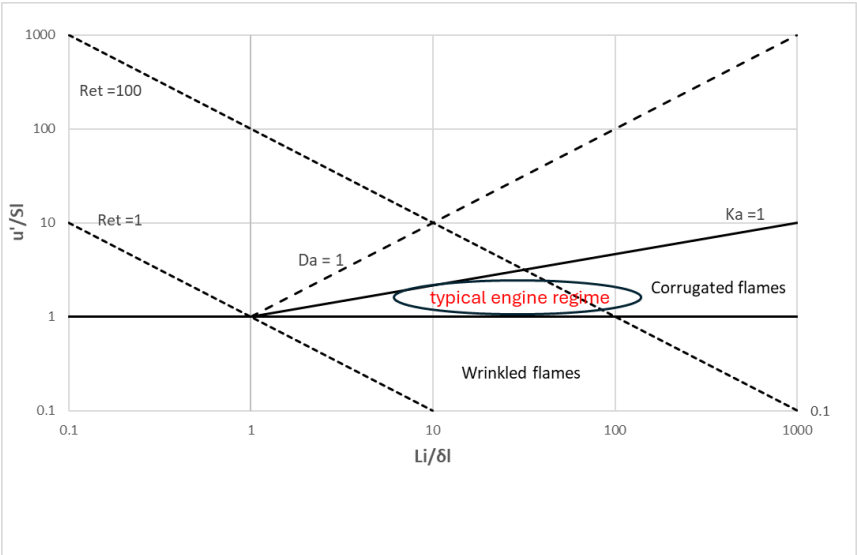


Figure 7: Peters Borghi diagram

Internal combustion engines, as shown in figure 7, are usually characterized by the corrugated flamelet regime. The entire reactive-diffusive flame structure is embedded

within eddies of the size of the Kolmogorov scale, where the flow is quasi-laminar. The chemical reaction zone thickness is smaller than the Kolmogorov scale and the flame appears as an ensemble of laminar flame sheets. Turbulent fluctuations wrinkle the flame, but do not perturb the flame structure. The boundary of the corrugated flamelet regime to the thin reaction zones regime is given by Ka = 1, i.e. the condition for which the flame thickness is equal to the Kolmogorov length scale. Also, the thin reaction zone regime has been observed in ICEs. In this regime, the smallest eddies can enter into the reactive-diffusive flame structure but are still larger than the reaction zone thickness.

The observation of combustion regimes determines the development of combustion models suitable for engines. The more common are based on the idea that fuel consumption is proportional to the laminar flame speed that characterizes the mixture, while flow field and turbulence influence how the fresh mixture enters the reaction zone.

For the 1D models, the eddy-burn-up model proposed by Keck, which will be described in the following subsections, is widely diffuse. The combustion phenomena are separated into two main steps. The first is the entrainment of fresh mixture into the turbulent flame zone depending on the flame surface, turbulence and laminar flame speed. In a subsequent phase the entrained mass is oxidized in a characteristic time scale depending on the ratio between the Taylor length scale and the laminar flame speed.

For 3d models, the coherent flamelet approach is the most common used for conventional engines and hydrocarbon fuels. It assumes the mass burning rate per volume unit is proportional to the laminar flame speed. The proportionality factor is represented by the flame surface density, determined via a balance equation. In this way, the CFM separates the treatment of the chemical problem, reassumed by the overall laminar flame speed, and the turbulent interactions described by the flame surface density.

Detailed chemical kinetic models coupled to the balance equations governing the flow can be also used. Today it appears as the most common choice for non-conventional fuel like ammonia characterized by very low laminar flame speed, i.e. Damkoler numbers lower than usual, detailed chemical kinetic have been also used.

The following sections will describe the engines under investigation and the model used to perform the analysis carried out. The engine investigated were simulated considering both neat ammonia and ammonia hydrogen blends propulsion (up to 15% of hydrogen by volume).

2.1 Cantera environment for ignition delay and laminar flame speed estimation

The ignition delay of stoichiometric ammonia-hydrogen-air mixtures has been investigated by means of the chemical mechanisms reported in Table 2. They have been mainly developed to reproduce the ammonia oxidation. However, they can also be used for hydrogen-enriched ammonia-air mixtures.

Table 2: chemical kinetic mechanism tested

Mechanism	Nakamura [61]	Otomo [62]	Stagni [64]	Shrestha [66]
Number of species	38	33	31	135
Number of reactions	232	213	203	> 1000
Validated for:				
Pressure [bar]	1	1	1	1.4-30
Temperature [K]	300-1400	1538-2000	650-1200 (500-2000)	1428-2857
Overall Air-fuel equivalence ratio [-]	0.8/1/1.2	0.5 - 2	0.5-2 (0.01-0.375)	0.5-2
Fuel blend H_2 content	0	0.2-0.3	0	-

Simulations have been carried out using Cantera environment [69] and imposing an ideal gas constant pressure reactor. The ignition delay has been evaluated by considering the inflection point of the temperature curve. The ignition delay is calculated as a function of the maximum derivative of the temperature curve [70].

The same approach has also been used to define the laminar flame speed and compare it with the correlation available in the literature.

2.2 Spark ignition engines investigated

The analysis presented in this thesis have been carried out considering two different light duty spark ignition engines. The first one is described in table 3. The engine features four cylinders: four valves per cylinder and a pent-roof combustion chamber. The intake ducts are shaped to produce a strong tumble motion able to generate high turbulence levels at the end of compression. The geometrical compression ratio is 9.8, quite high considering the usual gasoline engines. A waste-gate turbocharger group allows for performing a very high specific power. As usual in turbocharged SI engine, particularly rich mixtures must be used at high load levels to prevent knocking and to limit the exhaust gas temperature at the turbine inlet. This engine, which is in the laboratory of University of Cassino, has been modelled considering both 1D and 3D approaches to obtain operative maps for neat ammonia and ammonia hydrogen blends (15% of hydrogen by volume). Both these models have already been validated with respect to some experimental tests considering different fuels like gasoline or alcohols [71].

Table 3: First engine under investigation main characteristics

Model	Fiat Fire 1.4 T-Jet
Displaced volume	1368 cc
Stroke	84 mm
Bore	72 mm
Connecting Rod	129 mm
Compression ratio	9.8:1
Number of Cylinders	4
Number of Valves	4/cyl
Max Power	110.3 kW @ 5500 rpm
Max Torque	230 Nm @ 3000 rpm
Turbocharger group	IHI RHF3

The second engine investigated, which is located in the laboratory of the University of Orleans in France, has been modelled only by means of 3D CFD approach. This engine, which is presented in table 4, has been modelled thanks to a collaboration between university of Cassino, university of Orleans and UC Louvain university in Belgium. Starting from the experimental activities performed in France and widely described in [28,29,31,58] a mesh for this engine has been generated to obtain a validated model which can be useful also for the first engine tests. Unfortunately for this second engine there are no dynamic data available, obtained through experimentation or 1D modelling, which allow to fix the boundary conditions for the modelling of the engine intake stroke.

Table 4: second engine under investigation main characteristics

Model	PSA EP6DT
Displacement volume [cm^3]	399.5
Stroke [mm]	85.8
Bore [mm]	77
Connecting rod length [mm]	138.5
Compression ratio [-]	10.5:1
Number of valves	4

The two engines investigated are similar, therefore it can be acceptable to transfer the validation of the numerical models obtained for the engine for which experimental acquisitions are available on the engine for which they are not yet available. In particular, they present same field of application, similar valve lift, they generate similar tumble motion and also the shape of the head and the piston are close to each other.

2.3 1D model description

The engine described in Table 2 has been modelled considering both 1D and 3D CFD models. The one-dimensional model discretizes the in-pipe flow by means of the finite volume approach. Friction losses and heat flows towards the walls have been characterized according to the surface roughness using the "Sand Roughness" scale (Sand Roughness divided by the diameter of the pipe is "Relative Roughness", the friction

factor that is used in the Moody Diagram) and the Colburn correlation. Complex geometries, sharp changes in section and pipe joints were modelled using suitable discharge coefficients. The turbocharger has been modelled using the steady flow maps provided by the manufacturer. However, the turbine inlet scroll has been modelled as a duct to consider the propagation of pressure waves. To allow the boost pressure control, a part of the exhaust may bypass the turbine simulating the action of the wastegate valve. The burn rate is described by a quasi-dimensional predictive approach, considering the combustion chamber geometry, the spark location and timing, the air motion, and the fuel properties. A spherical flame propagates from the spark plug, while a turbulent entrainment process controls the combustion rate, as shown in the following equations:

$$\frac{dM_e}{dt} = \rho_e * A_f * (u' + S_L) \quad (10)$$

$$\frac{dM_b}{dt} = \frac{(M_e - M_b)}{\tau} \quad (11)$$

where M_e is the mass of the fresh gas mixture entering the flame front and M_b is the burned mass. A_f is the surface area at the edge of the flame front, ρ_e is the fresh gas density, u' is the turbulent intensity and S_L is the laminar flame speed. τ is a time constant depending on the ratio between the Taylor microscale of turbulence and the laminar flame speed. The Taylor scale, which is the intermediate length scale at which fluid viscosity significantly affects the dynamics of turbulent eddies in the flow, is calculated as a function of the integral length of turbulence and the kinematic viscosity of the unburned mixture. Following a hierarchical approach described in [72], both the integral length scale (li) and the turbulent intensity (u') have been imposed exploiting the flow field details provided by 3-D calculations. The heat transfer rate through the walls of the combustion chamber has been estimated by means of the well-known Woschni correlation, the friction losses have been estimated as a function of the engine speed.

To predict the knocking phenomena, Douaud and Eyzat's approach [73] was used. Knock occurs when the induction time calculated as in Equation (12) becomes higher than one, while its intensity is calculated as in [74] Equation (13).

$$I(t) = \int_0^t \frac{1}{\tau} dt \quad (12)$$

$$KI = \frac{(1 - x_b) * (cr - 1) * \sqrt{1 - \frac{\vartheta_k}{\theta ref}} * N}{N_{ref}} \quad (13)$$

where x_b is the mass of burned fuel, cr is the compression ratio, θ_k is the knock onset crank angle, N is the engine speed. θ_{ref} is the maximum crank angle for which knock is still audible and it is set to 50 CAD, while N_{ref} is a tuning parameter set equal to 3500 rpm.

This knock model has been coupled with a specific database of the ignition delay, which was estimated thanks to Cantera environment. All the ignition delay values (τ) obtained varying temperature and pressure to cover the whole range under investigation have been used in the relationship presented in equation 12. Furthermore, the model has

been used considering a specific correlation for the laminar flame speed of the ammonia and ammonia hydrogen blends considered, proposed by Goldmann and Dinkelacker [58] and presented in the following table (Table 5):

Table 5: Laminar flame speed correlation

Equation		Definition
$S_{L_{NH3}} = S_{L_0} * \left(\frac{T_u}{T_0}\right)^{\alpha} * \left(\frac{P}{P_0}\right)^{\beta} * k$	(14)	Ammonia laminar flame speed
$S_{L_0} = \frac{(a_1 + b_1 * \lambda)}{(1 + c_1 * \lambda + d_1 * \lambda^2)}$	(15)	Ammonia laminar flame speed at ambient condition
$\alpha = a_2 + b_2 * \lambda + c_2 * \lambda^2 + d_2 * \lambda^3 + e_2 * \lambda^4 + f_2 * \lambda^5$	(16)	Definition of α exponent of the temperature ratio
$\beta = a_3 + b_3 * \lambda + c_3 * \lambda^2 + d_3 * \lambda^3 + e_3 * \lambda^4 + f_3 * \lambda^5$	(17)	Definition of β exponent of the pressure ratio
$k = \begin{cases} k1 * k2^{\frac{P}{P_0}} * \left(\frac{P}{P_0}\right)^{ka} * \lambda^{k_4} \; \forall \; T_u \leq T_0 \wedge P < 0.5\ MPa \\ 1 \; \forall \; T_u \leq T_0 \wedge P > 0.5\ MPa \end{cases}$	(18)	Correction factor
$\alpha_2 = a_{2,P_3} + b_{2,P_3} * \lambda + c_{2,P_3} * \lambda^2 * \lambda^3$	(19)	Definition of α_2 parameter if $P \leq 0.5\ MPa \; \wedge T > 700\ K \; \wedge T \leq 900K$
$\beta_2 = a_{3,P_3} + b_{3,P_3} * \lambda + c_{3,P_3} * \lambda^2 + d_{3,P_3} * \lambda^3$	(20)	Definition of β_2 parameter if $P \leq 0.5\ MPa \; \wedge T > 700\ K \; \wedge T \leq 900K$
$S_{L_{0_2}} = a1 * b_{1,P_4}^{\lambda} * \lambda^{c_{1,P_4}}$	(21)	Ammonia laminar flame speed at ambient condition if P> $0.5\ MPa \; \wedge T_u > 800\ K \; \wedge T_u \leq 1000K$
$a_1 = a_{10} + (1 - a_{10}) * \left(1 - e^{-a_{11} * x_{H_2} - a_{12} * x_{H_2}^2 - a_{13} * x_{H_2}^3}\right)$	(22)	Definition of a_1 parameter if P> $0.5\ MPa \; \wedge T_u > 800\ K \; \wedge T_u \leq 1000K$

Equations from 14 to 18 refer to neat ammonia fuelling, and T_u and P are respectively the temperature and pressure of the unburned mixture. T_0 and P_0 are the reference conditions of temperature and pressure equal to 300 K and 0.1 MPa, respectively. λ is the air–fuel equivalence ratio and is equal to 1/ϕ. Coefficients a, b, c, d, e,f and k are

tabulated as a function of pressure and temperature ranges. For ammonia hydrogen blends the equation from 19 to 22 have been used, where T_n and P_n are the normalized temperature and pressure with respect to the reference conditions of T and P, respectively, equal to 300 K and 0.1 MPa. Even in this case the coefficients a, b, c, and d are tabulated as a function of temperature and pressure.

$$\begin{cases} T_n = \dfrac{T_u}{T_0} \\ P_n = \dfrac{P_u}{P_0} \end{cases}$$

Figures 8 presents a schematic overview of the 1D model used to assess the engine behaviour varying load and boost pressure considering the maximum brake torque condition (MBT) at knock limit for spark advance and the following constraints:

1. Maximum peak pressure [bar] = 100

2. Exhaust gas temperature [K] = 1173

3. Knock intensity [-] ≤ 0.5

4. Burned fuel fraction [%] ≥ 98

Furthermore, the cycle-to-cycle variations have been neglected, since the 1D model is unable to predict them.

For the points that did not respect all the constraints further analyses have been made to verify if they can be moved within the allowable operational range neglecting the maximum brake torque conditions. In these cases, starting from the maximum brake torque spark angle other ones close to this have been tested to verify that these points are effectively out of the allowable range of the engine. If the investigated point fall within the acceptable values of the considered constraints these have been added to the engine map for neat ammonia and for ammonia hydrogen blends. Furthermore, the 1D model used was also adopted to analyse the engine fuelled by an ammonia-syngas-air mixture, with the syngas obtained directly from the ammonia catalytic cracking system which was simulated by means of Aspen Plus tool.

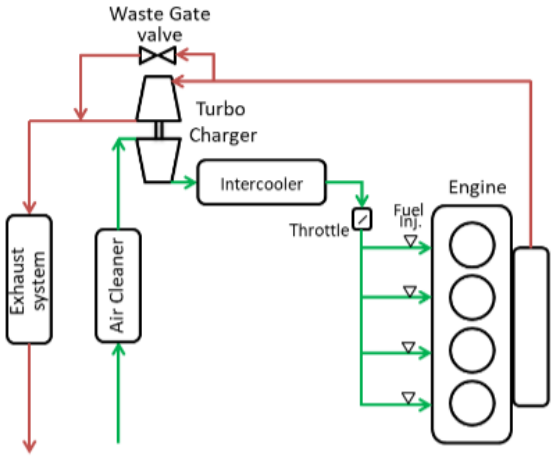


Figure 8: schematic layout of T-jet engine

2.4 3D CFD model description

To perform 3D CFD analysis the AVL Fire tool has been use coupled with a chemical kinetic approach. Calculations have been performed by means of a RANS approach [76-77], while the partial differential transport equations discretized according to the finite volume method and the well-known Simple/Piso algorithm have been solved. The RANS approach solves the following equations, and it is coupled with the chemical kinetic. In particular, the transport of the species and the reaction evolution are modelled following an Arrhenius law.

$$\rho \cdot \frac{DU_i}{Dt} = \rho \cdot \frac{\partial U_i}{\partial t} + \rho U_j \cdot \frac{\partial U_i}{\partial x_j} = \rho g_i + \frac{\partial(\tau_{ij} - \rho\overline{u_\iota \cdot u_j})}{\partial x_j} \tag{23}$$

$$\rho \cdot \frac{DH}{Dt} = \rho \cdot \left(\frac{\partial H}{\partial t} + U_j \cdot \frac{\partial H}{\partial x_i}\right) = \rho \cdot q_g + \frac{\partial P}{\partial t} + \frac{\partial\left(U_j \cdot \dot{\tau}_{\iota j}\right)}{\partial x_\iota} + \frac{\partial}{\partial x_j}\left(\lambda \cdot \frac{\partial T}{\partial x_\iota}\right) \tag{24}$$

$$\rho \cdot \frac{DC}{Dt} = \rho \cdot \left(\frac{\partial C}{\partial t} + U_j \cdot \frac{\partial C}{\partial x_j}\right) = \rho \cdot \dot{r} + \frac{\partial}{\partial x_j}(D * \frac{\partial C}{\partial x_j} - \rho \cdot \overline{c \cdot u_\iota}) \tag{25}$$

$$S_k = \frac{(\rho^{n+1} \cdot w_k^{n+1}) - (\rho^n \cdot w_k^n)}{\Delta t} \cdot V_{cell} \tag{26}$$

A first order, Euler, implicit differencing scheme has been used for time discretization, while for continuity and momentum equations second order schemes were used. For both turbulence and energy equations an upwind scheme was used. The k-z-f model [77] has been used for turbulent flow for the way it solves the flow near the wall according to a hybrid wall treatment [78], while the heat transfer through the walls has been modelled using a standard wall function. Furthermore, the k-z-f model has been preferred for the way it solves the flow near the wall according to a hybrid wall treatment. For both the engine investigated the thermodynamic fluid properties have been

calculated according to the ideal gas law and the ignition has been reproduced by releasing a certain amount of energy into a sphere with a diameter equal to 3 mm. This sphere is located considering the position of the spark-plug electrodes, while the energy release is modulated based on the ignition duration estimated in the laboratory. The initial and boundary conditions for the first engine investigated have been taken from the 1D model, considering the intake stroke and neglecting the exhaust one, while for the second engine, for which experimental data were available the intake stroke has been neglected and calculations start at intake valve closing (IVC) ending at exhaust valve opening (EVO). At IVC, a homogeneous charge has been considered. Both composition and temperature have been set according to the measured flows entering the cylinder (ammonia, hydrogen and air), the measured in-cylinder pressure and the instantaneous volume of the combustion chamber.

The first engine mesh, reported in Figure 9, reproduces only half geometry due to the symmetry of the engine geometry. The minimum number of the grid cells is about 50,000 (firing TDC), while the maximum number is approximately 350,000 (BDC during the intake stroke). For the second engine the mesh presented in Figure 10 h which presents about 220000 elements at TDC and 390000 elements at EVO has been used for the simulation. The combustion process has been modelled considering two different chemical kinetic mechanism: the Nakamura [61] and the Stagni ones [64]. The other ones did not guarantee a proper ignition for the engine conditions investigated therefore in this work they were not used. The main characteristics of the two mechanisms are summarized in the table 6. Firstly, the Nakamura mechanism has been chosen because it was the only one which provided proper ignition, then when the updated version of the Stagni one has been released it has been tested and it provides more accurate results so for the latter analysis this one has been preferred. Furthermore, the Stagni model considers ammonia decomposition, H-abstractions, the dissociation of the HNO intermediate and the formation of NO due to both the NH3 dissociation and the oxidation of N2 contained in the air. A complete overview of the conducted analyses is presented in the following flowchart.

Table 6: chemical kinetic mechanism used

Mechanism	Nakamura	Stagni
Number of species	38	31
Number of reactions	232	203
Validated for:		
Pressure [bar]	1	1
Temperature [K]	300-1400	350-1200 (500-2000)

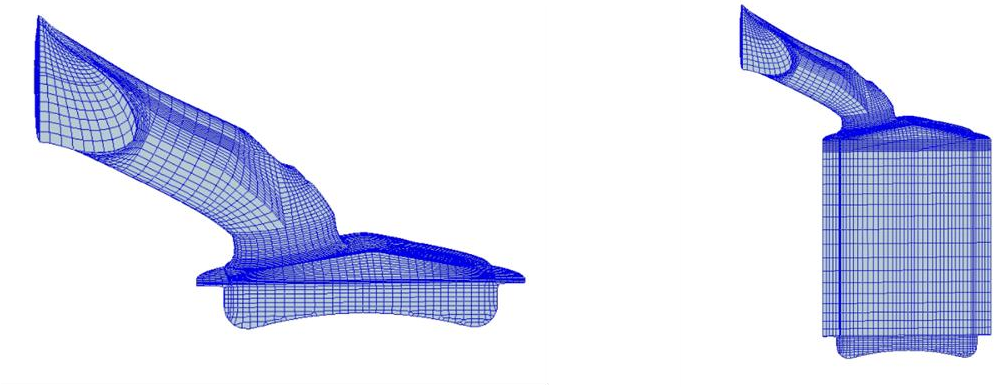


Figure 9: T-jet engine

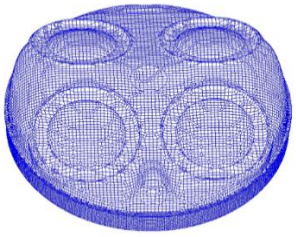
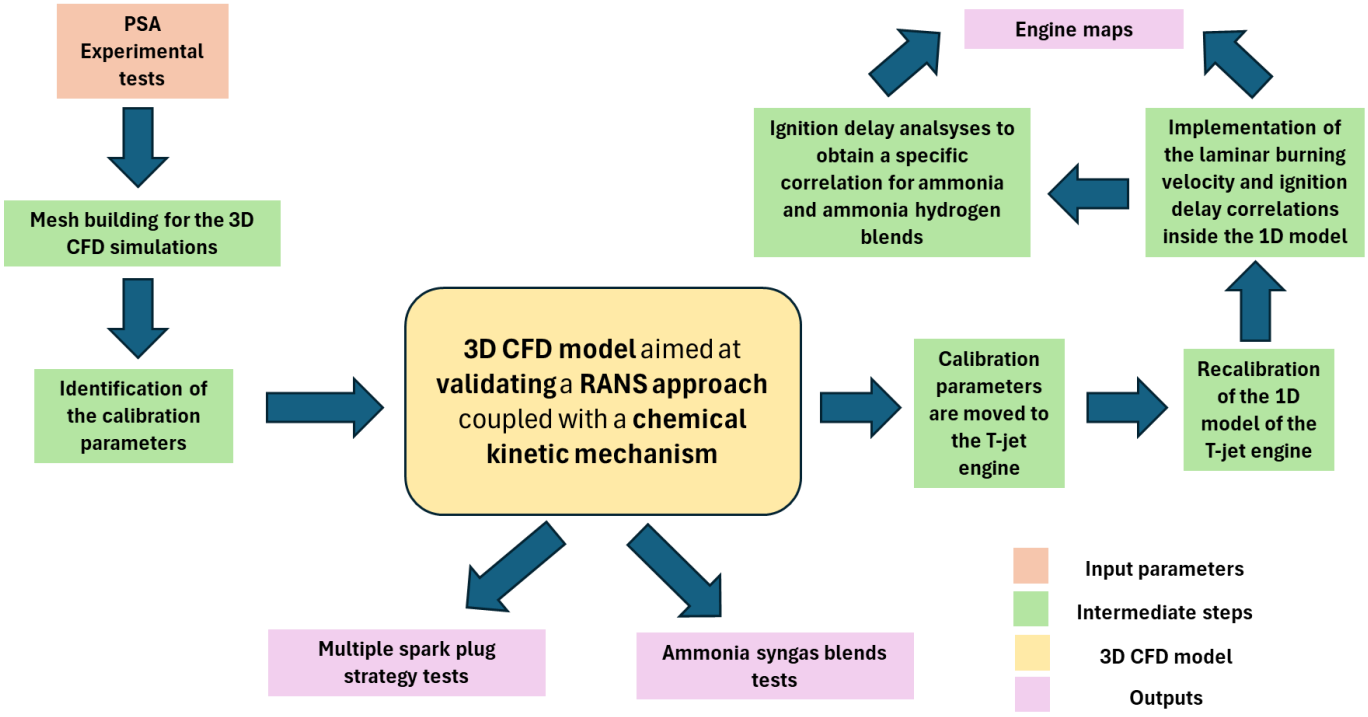


Figure 10: Mesh for PSA Engine


PSA Experimental tests
Mesh building for the 3D CFD simulations
Identification of the calibration parameters
3D CFD model aimed at validating a RANS approach coupled with a chemical kinetic mechanism
Multiple spark plug strategy tests
Ammonia syngas blends tests
Calibration parameters are moved to the T-jet engine
Recalibration of the 1D model of the T-jet engine
Implementation of the laminar burning velocity and ignition delay correlations inside the 1D model
Ignition delay analsyses to obtain a specific correlation for ammonia and ammonia hydrogen blends
Engine maps
Input parameters
Intermediate steps
3D CFD model
Outputs

Chapter 3: Results

3.1 Ignition delay estimation

Figure 11 presents the way in which the ignition delay has been evaluated referring to an ideal gas constant pressure reactor modelled by means of the Cantera environment. The ignition delay has been calculated by considering the inflection point of the temperature curve, i.e. the position of the maximum derivative of the temperature curve of the considered mixture, as also shown in [79]. At first, to validate the model used some calculated data have been compared to experimental data taken from [80]. Two ammonia-hydrogen blends have been evaluated: 5% of hydrogen by volume and 30% of hydrogen by volume. All the mixtures are stoichiometric, at 1.2 and 10 bar and different temperatures. Figures 12 and 13 report the comparisons for both 5% and 30% of hydrogen by volume.

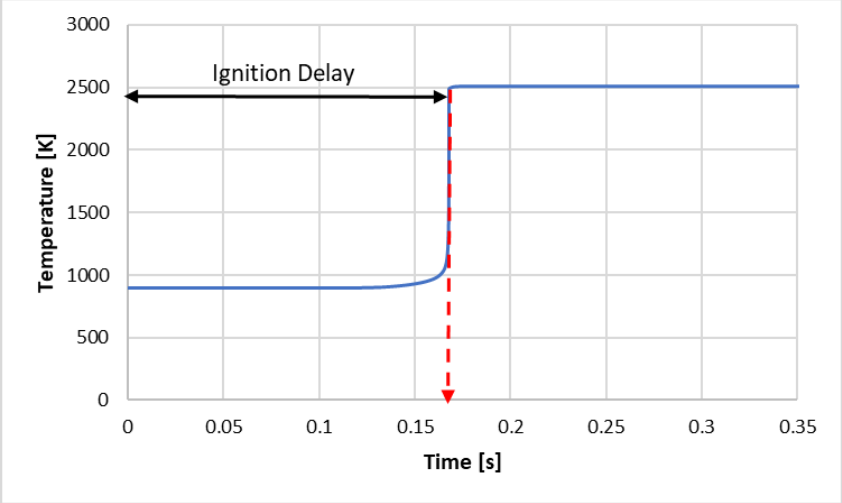


Figure 11: ignition delay estimation

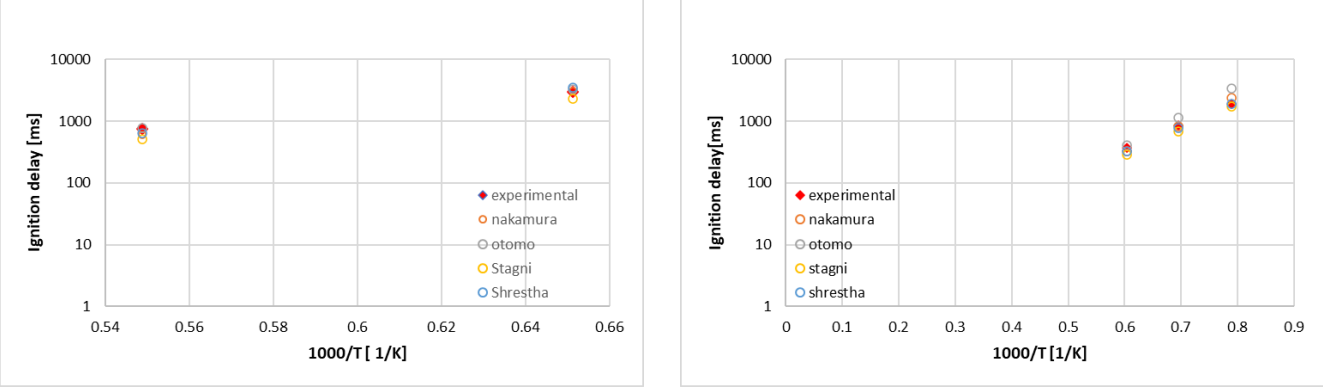
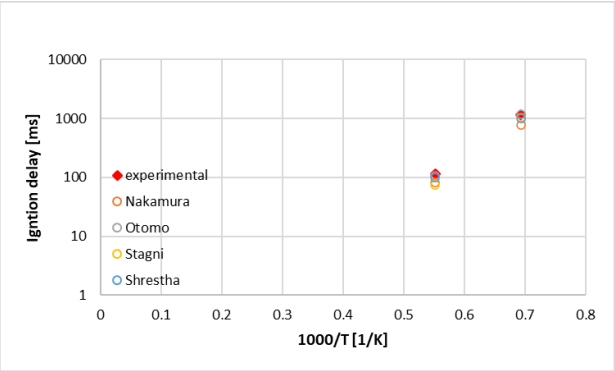


Figure 12: Comparison with experimental data at 1.2 bar. Fuel blend 5% hydrogen content (left) and 30% of hydrogen (right)



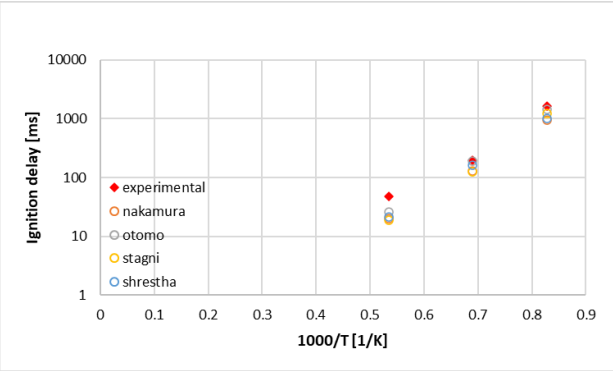
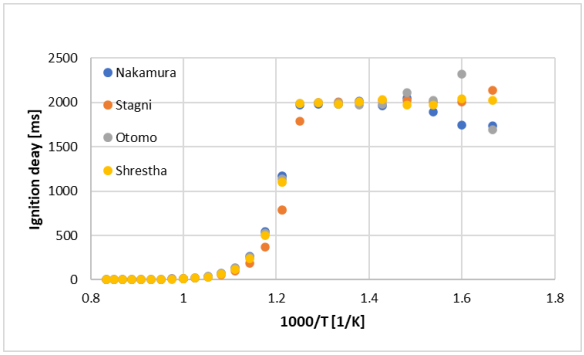


Figure 13: Comparison with experimental data at 10 bar for 5% hydrogen content (left) and 30% of hydrogen (right)

All the mechanisms reproduce quite well the measured ignition delays. Increasing the pressure, the calculated data tend to underestimate the measured ones. The calculated data scatter shows a coefficient of variation ranging from about 13.9% (30% H2 content, 1.2 bar, 1657 K) to about 27% (30% H2 content, 1.2 bar, 1270 K). Its averaged value of variation is 17.1%. At 1.2 bar, the difference between the average ignition delay calculated with the four mechanisms and the measured one varies approximately from a minimum of less than 1% (30% of H2 content at 1440 k) to a maximum of 22% (30% H2, 1270 K). At 10 bar, the same difference varies approximately from a minimum of 14% (5% H2, 1440 K) to a maximum of 30% (30% H2, 1870 K). After that, calculation have been carried out to obtain tabulated ignition delay values as a function of pressure, temperature and hydrogen content in the fuel mixture. In particular, pressure varies from 10 to 130 bar, temperatures from 600 to 1200 K and hydrogen content from 10 to 50% by volume. It is worth noting that all the mechanisms have been used at pressure levels higher than those for which they have been validated, as shown in table 4, but this is quite usual [60,80] due to the difficult to reach high pressure levels for the mechanism's validation.

Figures 14 and 15 show a comparison of the ignition delay prediction for some cases. All the mechanisms provide similar results at high and medium temperatures where the ignition delay varies with the temperature according to a classical Arrhenius law. Differences arise at low temperatures, approximately when the charge temperature is less than 700 K. This temperature is generally considered as the auto-ignition limit for ammonia-air mixtures. For every mechanism, there is a threshold temperature below which the ignition time tends to become constant. This threshold temperature decrease as the pressure increases.



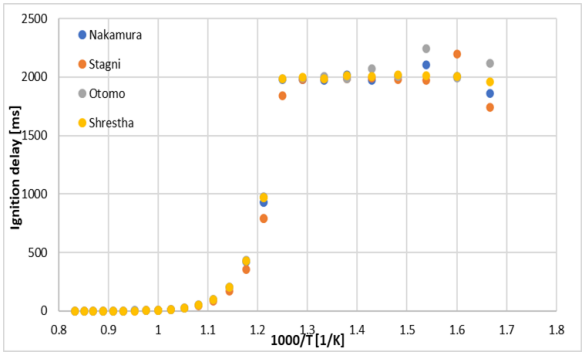
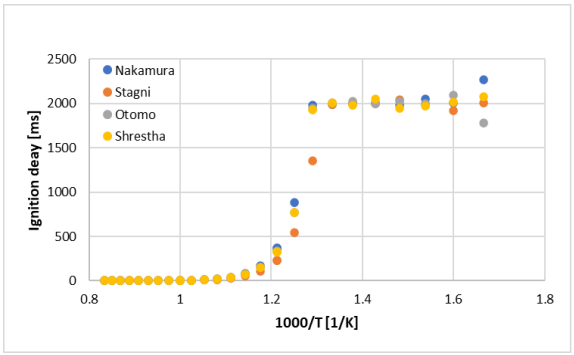


Figure 14: Calculated Ignition delays. 10 bar, 20% H2 content (left), 50% H2 content (right)



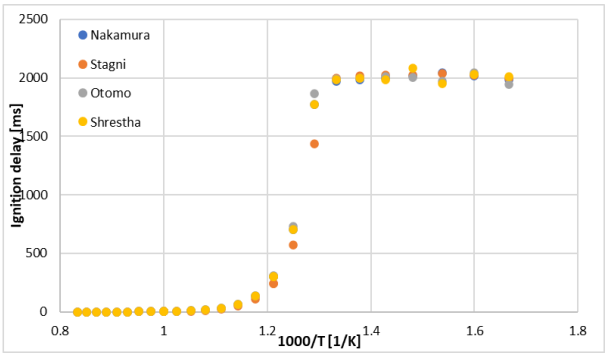


Figure 15: Calculated Ignition delays. 55 bar, 20% H2 content (left), 50% H2 content (right)

A correlation for ignition delay estimation has been obtained using a fitting procedure, in particular, the Curve Fitter tool, available in Matlab environment, has been used. A temperature limit ($TLIM$) has been found referring to the transition between an essentially constant value of the ignition delay (equal to 2000 ms, equation 27) and a trend well described by means of equation 28:

$$600K \leq T < T_{LIM}: \quad \tau = 2000\ ms \tag{27}$$

$$T_{LIM} \leq T < 1200K: \tau = a * p^m * \exp\left(b * p^n - \frac{1}{T}\right) \tag{28}$$

Where τ is expressed in ms, p is the pressure expressed in bar and T is the temperature expressed in K. The coefficients a,b,m and n are calculated as a function of the volumetric hydrogen content in the fuel blend (x_{H_2}, expressed in %), as reported in table 6, while T_{LIM}varies according to equation 29.

$$\begin{cases} T_{LIM} = 1023.15 \quad if\ P > 70\ bar \\ T_{LIM} = 1083.15 - 0.83 * (P - 10) \quad if\ P < 70\ bar \end{cases} \tag{29}$$

Table 7: Coefficients for equation 28

	$T_{LIM} \leq T \leq 825\ K$	$825\ K < T < 1000\ K$	$1000 \leq T \leq 1200\ K$
a	$2.947528E\text{-}11x_{H2}^4$ - $4.126567E\text{-}09x_{H2}^3$ + $2.094349E\text{-}07x_{H2}^2$ - $4.548702E\text{-}06x_{H2}$ + 3.551934E-05	$1.56415E\text{-}11x_{H2}^4$ - $2.25675E\text{-}09x_{H2}^3$ + $1.19344E\text{-}07x_{H2}^2$ - $2.74862E\text{-}06x_{H2}$ + 2.34252E-05	$-4.65000E\text{-}13x_{H2}^3$ + $9.18857E\text{-}11x_{H2}^2$ - $5.13864E\text{-}09x_{H2}$+ 1.17376E-07
b	$2.966667E\text{-}01x_{H2}^3$ - $3.541429E+01x_{H2}^2$ + $1.296190E+03x_{H2}$ + 7.112000E+03	$0.0408x_{H2}^3$ - $6.1964x_{H2}^2$ + $360.95x_{H2}$ + 13812	$8.54167E\text{-}03x_{H2}^4$ - $1.07750E+00x_{H2}^3$ + $4.74958E+01x_{H2}^2$ - $8.66750E+02x_{H2}$ + 2.65200E+04
m	$1.436667E\text{-}06x_{H2}^4$ - $1.247333E\text{-}04x_{H2}^3$ + $1.141333E\text{-}03x_{H2}^2$ + $1.008233E\text{-}01x_{H2}$ - 2.782000E+00	$-1.77250E\text{-}05x_{H2}^3$ + $1.77354E\text{-}03x_{H2}^2$ - $3.29321E\text{-}02x_{H2}$ - 1.45684E+00	$6.08704E\text{-}06x_{H2}^4$ - $7.87202E\text{-}04x_{H2}^3$ + $3.57175E\text{-}02x_{H2}^2$ - $6.68488E\text{-}01x_{H2}$ + 3.92785E+00
n	$-2.820833E\text{-}08x_{H2}^4$ + $1.235833E\text{-}06x_{H2}^3$ + $1.217208E\text{-}04x_{H2}^2$ - $7.171583E\text{-}03x_{H2}$ + 1.075400E-01	$-0.0009x_{H2}$ + 0.0521	$-3.61612E\text{-}07x_{H2}^4$ + $4.70157E\text{-}05x_{H2}^3$ - $2.15676E\text{-}03x_{H2}^2$ + $4.13011E\text{-}02x_{H2}$- 2.91454E-01

The correlation results have been compared with the mean tabulated data coming from the chemical-kinetic mechanisms, in the pressure range of 25-130 bar and for temperatures in the range 600-1200 K. Table 8 shows an overview of the errors of the proposed correlation.

Table 8: Errors of the proposed correlation

Mean absolute error [%]	**Points with absolute error greater than 15 % [%]**
5.7	9.5

Furthermore, figure 16 shows the percentage error maps obtained comparing the ignition delay provided by the proposed correlation and the mean tabulated data coming from the chemical-kinetic mechanisms, as a function of pressure and temperature for the different fuel mixtures considered.

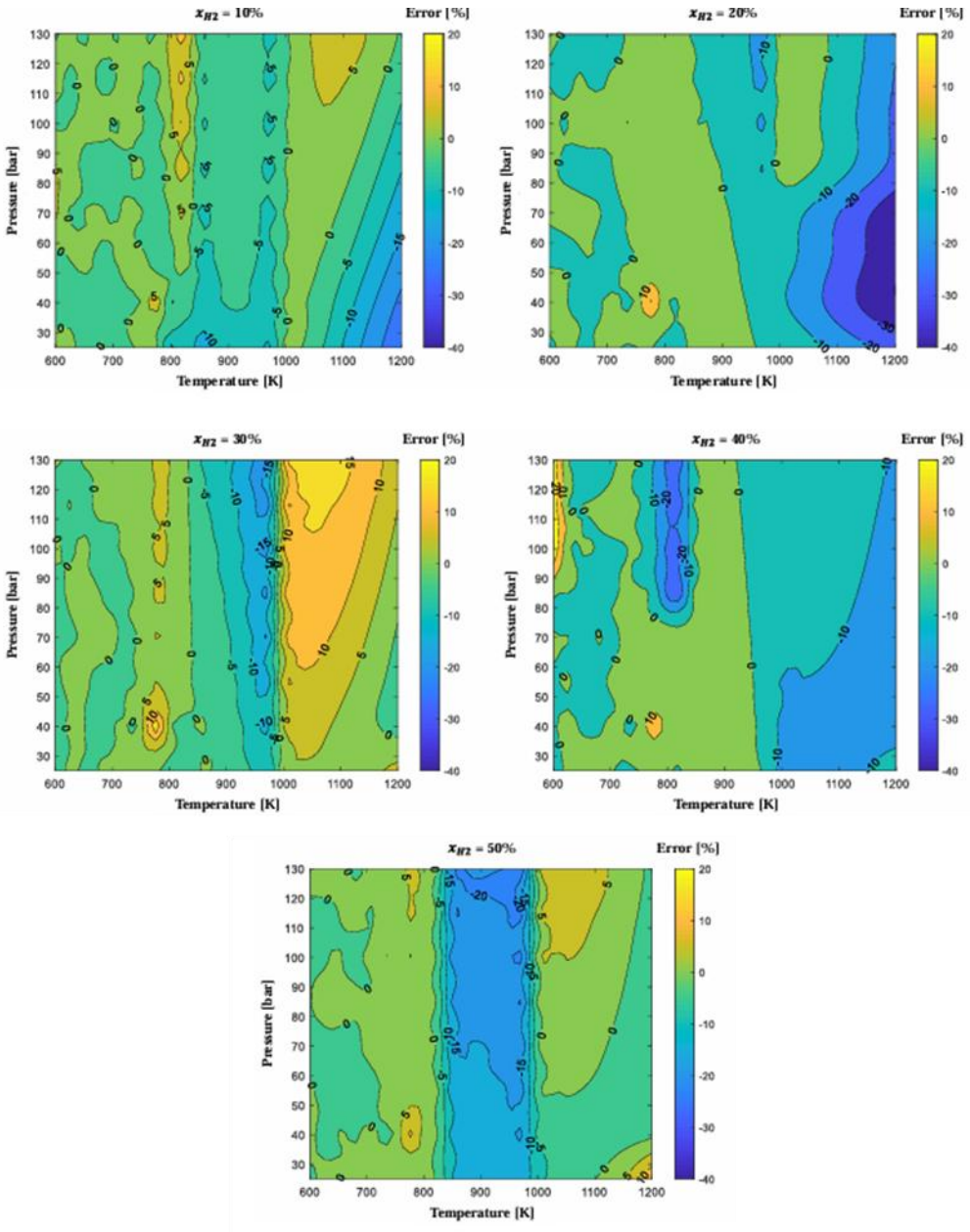


Figure 16: Percentage error maps of the proposed correlation as a function of pressure and temperature for the different fuel blends considered

Finally, referring to a spark ignition engine, which is the final usage of this result, the correlation found can be useful to estimate the knock onset, which depends on the evolution of the ignition delay in the "so called" end gas, i.e. the part of the charge not yet reached by the flame during the combustion phase. As an example, Figure 17 shows both pressure and temperature behaviours of the end gas region for a typical light duty, four cylinders, turbocharged spark ignition engine. Data have been calculated by means of the numerical approach described in chapter 2. In particular, the engine burns an ammonia-hydrogen blend (15% hydrogen by volume) running at 2000 rpm and delivering 260 Nm. Figure 18 depicts the pressure vs the unburned gases temperature conditions of the overmentioned operating point within the percentage error maps of the correlations found. Red circles show typical pressure vs temperature trends of unburned gas in a light duty SI engine fuelled with an ammonia-hydrogen blend. It is

important to underline that in these conditions the proposed correlations are within the 10% error with respect to the mean calculated data predicted by the mechanisms.

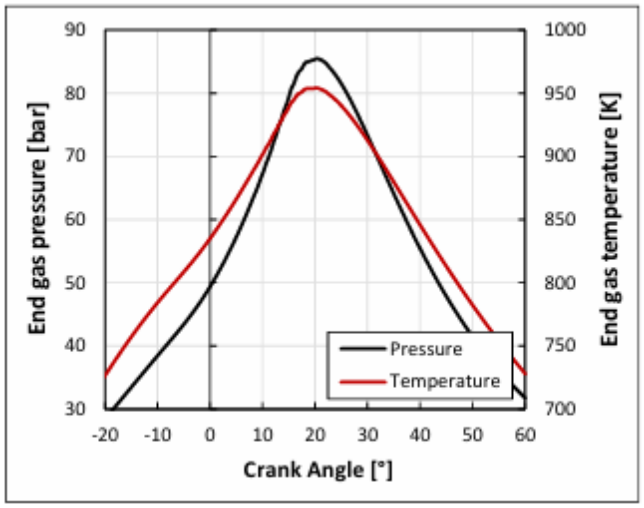


Figure 17: in-cylinder pressure and temperature of the unburned gases during the combustion evolution as a function of crank angle for a spark-ignition engine fueled with an ammonia-hydrogen blend

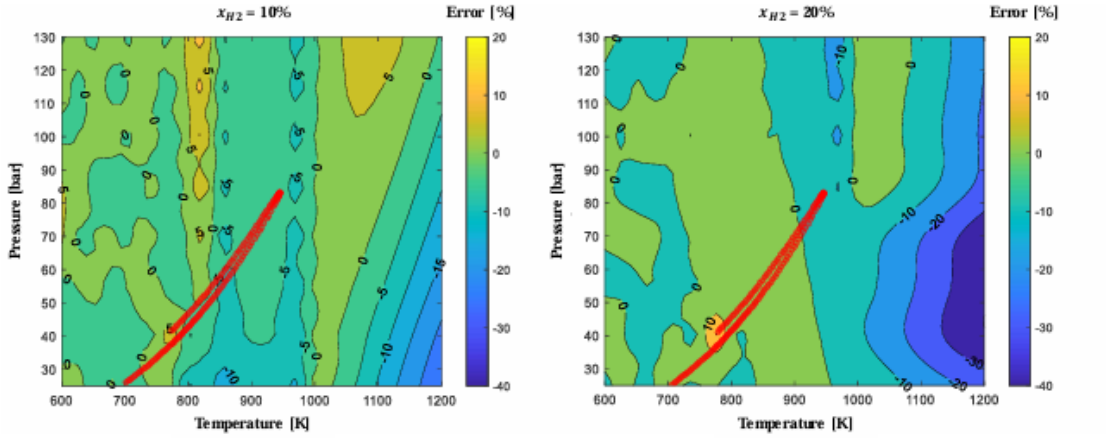


Figure 18: percentage error maps of the proposed correlation as a function of pressure and temperature for 10 and 20% of hydrogen by volume.

3.2 PSA EP6DT engine operating conditions considering different ammonia-hydrogen blends

Thanks to a collaboration which involves University of Cassino, UCLouvain and University of Orleans the analyses have been conducted to the PSA engine. Starting from the experimental results presented by Lhuillier et al. [30] and using the same 3D CFD approach already presented in chapter 2 some experimental points have been reproduced and also an in-depth analysis of flame development through the combustion chamber has been carried out. In particular, three different cases have been chosen, as reported in Table 8. The experimental setup is widely described in [30] Briefly, the engine is driven by an electric motor and the main shaft is equipped with a Kübler optical encoder for angular position monitoring with a 0.1 Crank Angle Degree

(CAD) resolution. In-cylinder pressure measurements are provided by a water-cooled AVL piezoelectric pressure transducer with a 0.1 CAD resolution and characterized by a measuring range of 0 – 25 MPa. Engine intake and exhaust temperature and pressure are monitored using type K thermocouples and piezo-resistive absolute pressure transducers, respectively. The fuel flow is measured and controlled using Brooks thermal mass flowmeters with ± 0.7% accuracy, preheated to the intake temperature of 323 K and premixed in an intake plenum before injection. The wet exhaust gases are analyzed using a Gasmet Fourier Transform Infrared (FTIR) spectrometer to assess H2O, NOx and NH3 concentrations, and after preliminary verifications, the authors estimated a maximum uncertainty on the species concentrations of about 10% of the full scale. Furthermore, an ADEV gas analyzer is used on a dry exhaust gas sample for H2 (thermal conductivity) and O2 (paramagnetic) measurement. The water vapor measurement done with the FTIR analyzer is used for wet correction. The accuracy of the H2 and O2 analyzers is ± 1 % (range 0 – 20 % H2, 0 – 21 % O2). For each test, 100 consecutive pressure cycles have been considered to quantify cycle-to-cycle variability.

Table 9: reference experimental tests

	Case 1	Case 2	Case 3
Engine speed [rpm]	1500	1500	1500
H_2 content in fuel mixture [vol. %]	0	5	15
Intake manifold Pressure [bar]	1	1	1
Intake manifold temperature [K]	323	323	323
Equivalence ratio [-]	1	1	1
Spark Angle [CADaTDC]	-43	-35	-27
Average P_{max} [bar]	38.4	39.6	40.7
Unburned NH_3 [ppm]	15288	13571	10410
COV_{IMEP} [%]	1.12	0.6	0.39

Also, for these analysis Stagni mechanism has been chosen and ignition has been reproduced by releasing a certain amount of energy into a sphere with a diameter equal to 3 mm. This sphere is located considering the position of the spark-plug electrodes, while the energy release is modulated based on the ignition duration estimated in the laboratory. For these simulations, due to the lack of time dependent data relating to the running duct inlet, the intake stroke has been neglected and calculations start at intake valve closing (IVC) ending at exhaust valve opening (EVO). At IVC, a homogeneous charge has been considered. Both composition and temperature have been set according to the measured flows entering the cylinder (ammonia, hydrogen and air), the measured in-cylinder pressure and the instantaneous volume of the combustion chamber. The charge motion has been initialized considering a single macro vortex reproducing the tumble motion characterizing pent-roof engines. The tumble index, as well as the integral length scale and the turbulent intensity, have been initialized according to preliminary investigations where the intake stroke has been modelled for a motored cycle carried out with constant conditions at the intake manifold. This is reasonable because dimensionless indices depend mainly on the engine geometry and are not strongly affected by the engine operation point. Finally, wall temperatures have

been set considering constant values based on literature data for similar engines. A complete overview of the initialized cases is presented in table 10. Calculated curves have been obtained considering 0.75 ms for the spark duration and 6.71 W/m^3 of power density provided by the spark. The latter parameter has been used as a tuning parameter.

Table 10: Case initialization

	Case 1	Case 2	Case 3
In cylinder pressure [bar]	1.06	1.06	1.06
Charge temperature [K]	403	396	399
Tumble index [-]	0.54	0.54	0.54
NH_3 mass fraction [-]	0.136	0.132	0.123
H_2 mass fraction [-]	0	0.00081	0.0025
Wall head temperature [K]	450	450	450
Wall piston temperature [K]	493	493	493
Wall liner temperature [K]	430	430	430

Figures 19 and 20 compares both the measured in-cylinder pressure curves and the rate of heat release curves with the simulated one, while figure 21 presents the whole combustion process for each case.

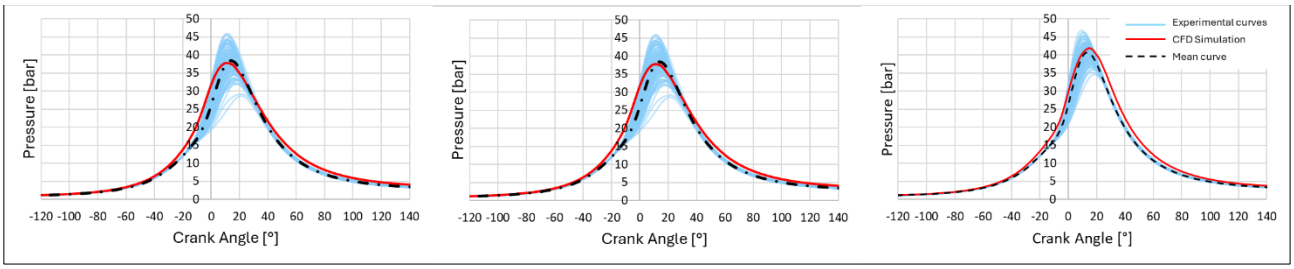


Figure 19: Measured in-cylinder pressure curves vs simulated ones

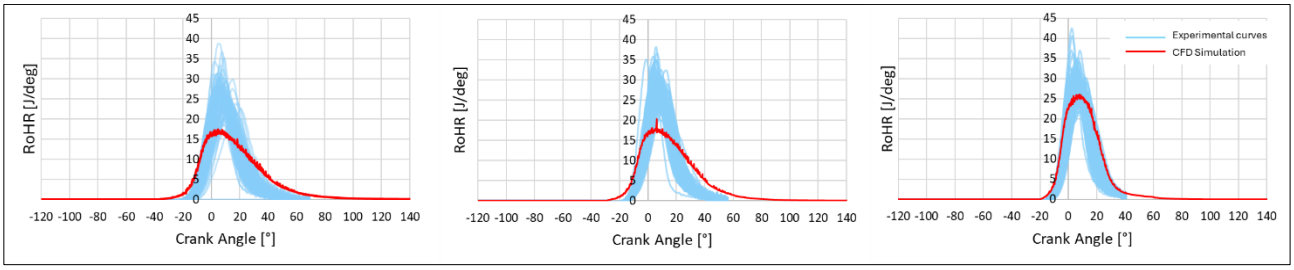


Figure 20: Measured rate of heat release curves vs simulated ones

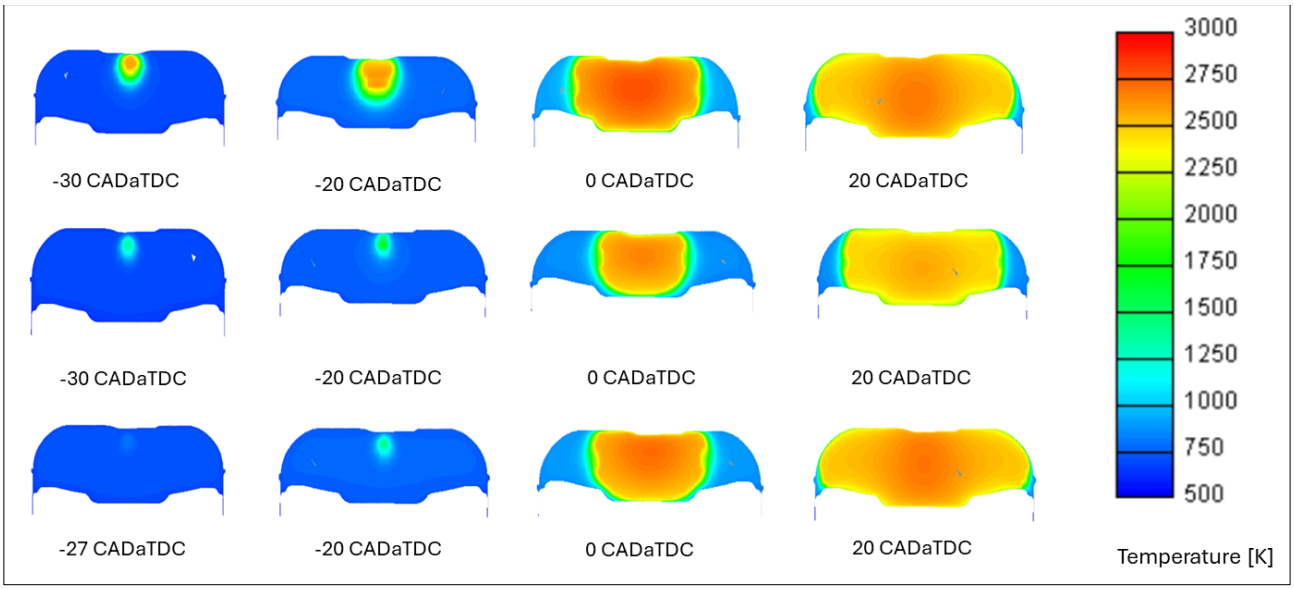


Figure 21: Calculated temperature field for Case 1 (top), Case 2 (middle) and Case 3 (bottom)

As shown, for the experimental data all the 100 curves are reported, while the dotted line represents the average calculated curve. The model well reproduces the investigated cases and table 10ù1 shows a comparison between the combustion duration Referring to case 3 and to the mean measured values, the difference between calculated ad measured CA50 is slightly larger than 1 CAD, while the combustion durations are estimated with an error equal to about 12% (CA0- 10) and about 4% (CA10-90). For neat ammonia (case 1) and 5% of hydrogen (case 2) by volume the model tends to overestimate the heat release during the first stage of the combustion development while it underestimates the rate of heat release peak and the final phase of combustion appears slower. This could be due to multiple factors. Firstly, it should be considered that the kinetic model was developed for pressures lower than those typical of the engine. Furthermore, the charge was considered perfectly homogeneous, while in real operation it is highly heterogeneous due to the imperfect mixing between air and fuel and due to the non-uniform distribution of hot residues coming from the previous cycle. Therefore, in the ignition region at the spark time the mixture composition and its temperature could be quite different from the average ones referring to the entire charge. That affects the local laminar flame speed value which determines the duration of the flame development stage.

Table 11: Comparison between mean measured values and calculated data

	Case 1		Case 2		Case 3	
	Measured	Calculated	Measured	Calculated	Measured	Calculated
CA0-10 [CAD]	40.0	36.1	32.5	29.2	24.5	21.4
CA10-90 [CAD]	31.6	52.6	29.7	46.3	26.9	28.1
CA50 [CAD]	9.0	12.5	8.6	12.3	7.7	9.0

During the rapid burning stage, which is the stage during which the fully developed flame spreads through the combustion chamber, it must be also considered that the turbulent flame speed also depends on the turbulence intensity produced by the flow field inside cylinder. The hypothesis of a single tumble macro vortex at IVC could influence this

aspect, resulting in a lower production of turbulence compared to that of the more complex flow field pattern existing in the chamber and therefore in a slower flame front propagation. However, the center of combustion is quite well estimated for all the investigated blends and the chemical kinetics model allows to reproduce the speeding up of the combustion process caused by enrichment with hydrogen. Comparing case 2 to case 1, the CA0-10 duration decreases by 19% according to both the average experimental data and the calculated data, while it decreases by 39% and 41% respectively if case 3 is compared with case 1. Besides, the calculated pressure curves fall within the measured dispersion band, so the model results can be considered acceptable. Furthermore, for all the investigated cases the end gas temperature increases with the hydrogen content in the fuel mixture.

The simulations allow to conduct an in-depth analysis of the combustion phenomenon, and in particular the conditions in which the flame front propagates and to estimate the turbulent flame speed. First, it is possible to determine the characteristic combustion regime for the investigated cases, in fact, ammonia has a rather low laminar flame speed which could lead to combustion regimes different from those that normally characterize engines. To do it, an iso-surface characterized by a mass fraction of O2 equal to the 90% of the initial value has been considered as the border between the end gas region and the flame front, which are depicted in figure 22 respectively with red and blue colours. The averaged values relative to the end gas have been considered to calculate the dimensionless parameters characterizing the combustion regime and presented in table 12.

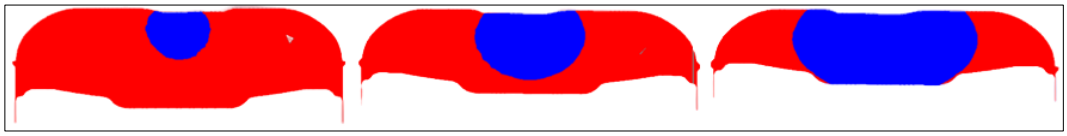


Figure 22: Flame front and end gas region for neat ammonia

Table 12: Average values calculated in the end gas region at peak pressure

	L_i	u'	T	P	S_l	δ_l	Re_T	Da
	[m]	[m/s]	[K]	[bar]	[m/s]	[m]	[-]	[-]
Case 1	0.0013	2.07	828.6	37.7	0.242	1.53E-4	75	1.03
Case 2	0.0012	1.87	879.5	36.8	0.312	1.23E-4	59	1.65
Case 3	0.0012	2.19	920.0	41.7	0.402	0.98E-4	68	2.30

Even in these cases the laminar flame speed has been calculated by means of Cantera environment, starting from the end gas composition, pressure and temperature, while the laminar flame thickness (δl) considering a Schimdt number equal to 1 as usual in Peters-Borghi diagram representations (figure 23).

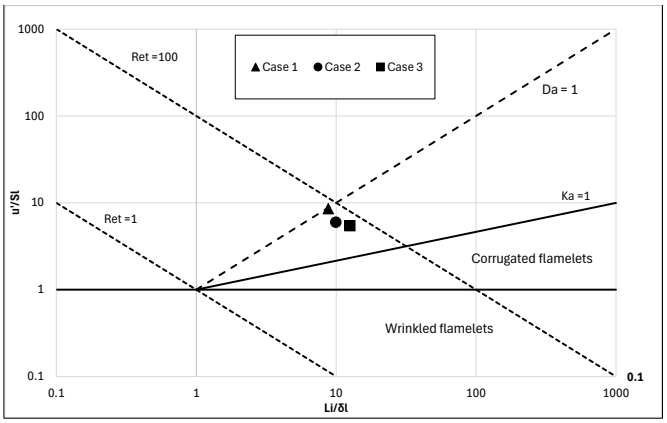


Figure 23: Peters Borghi diagram for the investigated mixtures.

Considering the peak pressure angle, the calculated integral length scale (L_i) is equal to about 1.2 mm, while the turbulent intensity (u') is about 50% of the mean piston speed. Despite the rather high temperatures, the laminar flame speed is rather low increasing from 0.24 m/s (neat ammonia) to 0.40 m/s (15% hydrogen enriched ammonia). Therefore, the characteristic chemical reaction time is comparable to the characteristic turbulent eddy turnover time and the Damkohler number ranges between 1.0 and 2.3. At the end, in the Peters-Borghi diagram the combustion regime falls between the lines at Damkohler number equal to 1.0 and Karlowitz equal to 1.0, i.e. slightly above the region that normally characterizes the operation of spark ignition engines.

Starting from these data the turbulent flame speed can be also calculated considering the growth of flame area, which is the blue area in the figure 23. An equivalent circle of radius R (calculated as shown in the equation (30)), and circumference length L (calculated with the formula presented in equation (31)), has been considered and the turbulent speed S_t has been calculated with the relationship presented in equation (32). This approach has been applied in the angular interval from the end of the development of the flame core until the flame is not too distorted by the interaction with the walls.

$$R = \sqrt{A/\pi} \tag{30}$$

$$L = 2 * \pi * R \tag{31}$$

$$S_t = \frac{\frac{dA}{dt}}{L} \tag{32}$$

In table 13 are reported the three turbulent flame speed calculated for the investigated cases. Data refers to a phase in which the calculated rate of heat release model generally tends to overestimate the heat release and therefore the calculated flame speeds are to be considered overestimated. However, they can be considered indicative for the process under investigation. In particular, the calculated values highlight that hydrogen enrichment strongly increases the flame speed, shortening the entire combustion process.

Table 13: Calculated mean turbulent flame speed

	Case 1	Case 2	Case 3
Mean S_t [m/s]	3.25	4.48	5.67

It is worth noting that due to the turbulent flow inside the combustion chamber these laminar speeds are an order of magnitude greater than the laminar flame speed calculated by means of Cantera libraries and reported in table 11.

Table 14 shows the concentration of unburned ammonia and pollutants detected in the wet exhaust gas at exhaust valve open, while figure 24 shows a comparison between the calculated ammonia consumption curves. Due to the higher burning rate of ammonia hydrogen blends the unburned ammonia concentrations decrease when the hydrogen content increases, while the NO concentrations increase. This suggests that a desired emissions trade-off could be found by optimizing the hydrogen content. Even if the model is not able to predict the measured quantities, it captures the same trend as the experimental data: adding 15% hydrogen decreases the ammonia emissions by 22% in the simulations and 30% in the experiments, while moving from neat ammonia to 5% of hydrogen, the unburned ammonia decreases 12% in the simulation and by 11% in the experiments. The unburned ammonia is localized mainly near the cylinder liner and in the crevices, as shown in figure 25.

Table 14: Unburned fuel and NOx concentrations in the wet exhaust gas

	NH_3 [ppm]		NO [ppm]		N_2O [ppm]		NO_2 [ppm]	
	Measured	Calculated	Measured	Calculated	Measured	Calculated	Measured	Calculated
Case 1	15288	6249	2734	1445	10	12	0	0
Case 2	13571	5464	2839	1569	10	10	0	0
Case 3	10410	4885	3836	1732	21	4	0	0

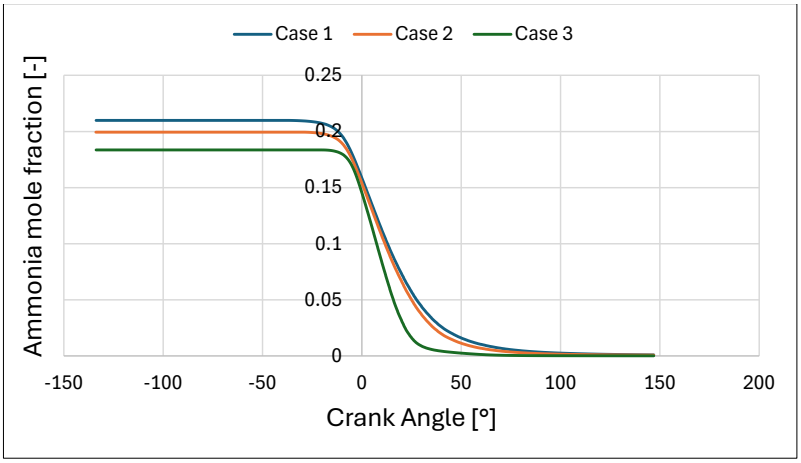


Figure 24: Ammonia consumption for the three cases investigated

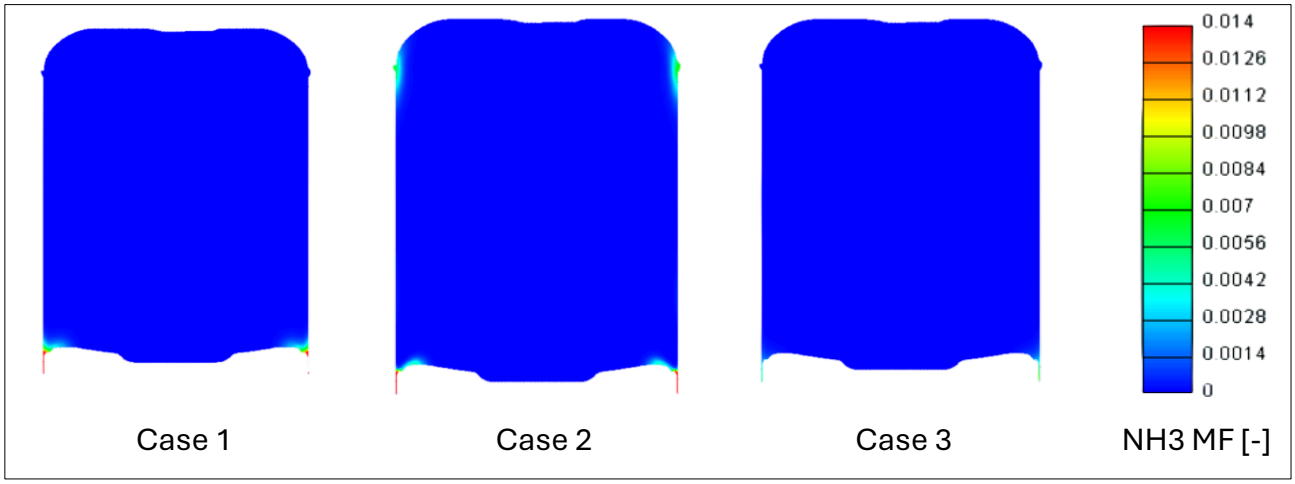


Figure 25: ammonia mass fraction distribustion at exhaust valve open

The increase in NO related to the higher temperatures in the combustion chamber is also captured by calculated data, even if the predicted growth rate is lower than the measured one. About the other NO_x, the amounts of calculated N_2O are small and very close to the measured ones. Both measured and calculated NO_2 are always equal to zero. By solving the chemical reaction pathways, the 3D model allows to analyse the behaviour of the considered chemical species inside the combustion chamber. The formation of the main combustion products, intermediates and pollutant emissions can therefore be investigated and are represented in figures 26-28. It is worth noting that the dissociation of ammonia produces H2, which is detected in the combustion chamber also for case 1, in which neat ammonia is burned. In this case, hydrogen begins to appear as heat release begins and it keeps a nearly constant concentration throughout the entire process. This can be explained by considering that hydrogen is produced and then consumed, at least until the flame extinguishes close to the walls. Here part of the ammonia dissociates but, at least according to the chemical mechanism used, not all the produced hydrogen oxidizes. The most common combustion intermediate is the OH radical which is completely consumed during the combustion development; NO is also produced. During the expansion stroke, it tends to dissociate due to the decrease in temperature. However, the expansion is too rapid and the NO freezes remaining far from chemical equilibrium conditions. This determines the strong presence of NOx in the exhaust. Among the other combustion intermediates directly attributable to ammonia, those with the highest concentration are shown in figure 28. It is interesting that their concentration is much lower than the other produced radicals (about two orders of magnitude). During the combustion, the species mostly produced are NH_2 and HONO. The latter tends to increase as the hydrogen content increases. However, all these intermediates are consumed during the expansion stroke and only very small quantities are calculated when the exhaust valve opens (Table 14ù5). These quantities decrease as the hydrogen enrichment increases.

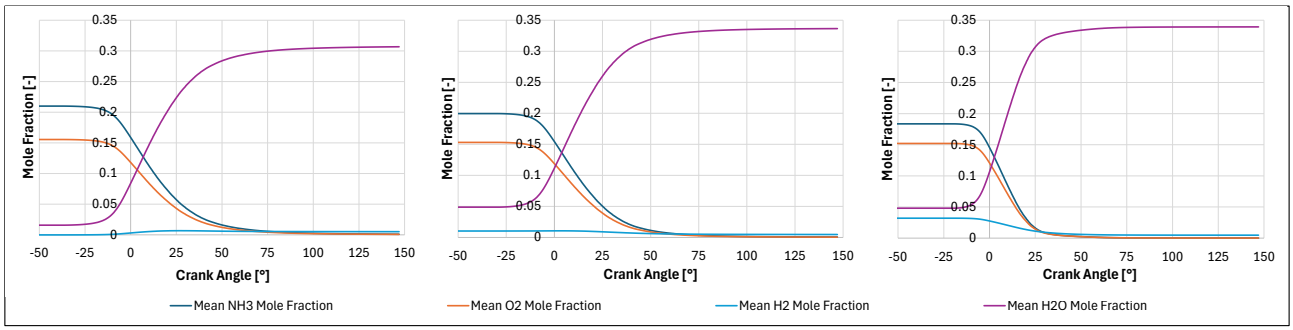


Figure 26: main species concentrations for the three cases investigated: Neat ammonia (left) 5% of hydrogen (middle) and 15% of hydrogen (right)

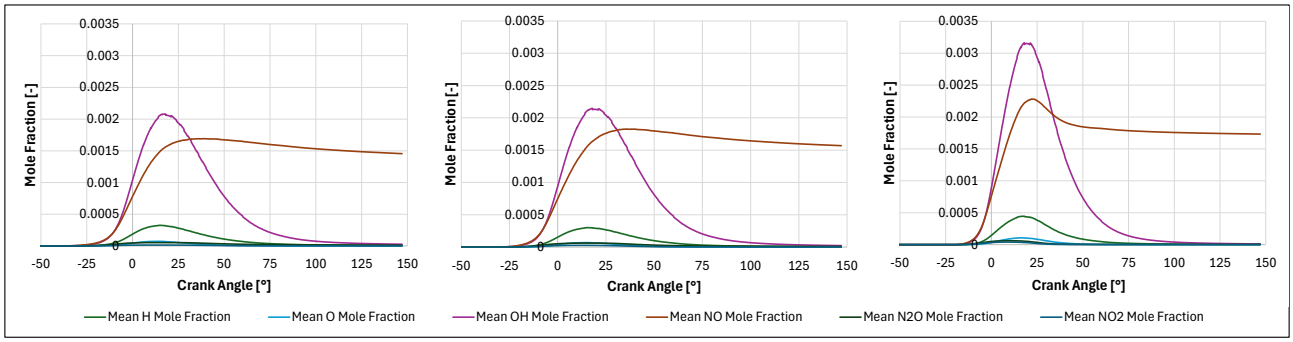


Figure 27: Main radical and NOx concentrations for the three cases investigated: Neat ammonia (left) 5% of hydrogen (middle) and 15% of hydrogen (right)

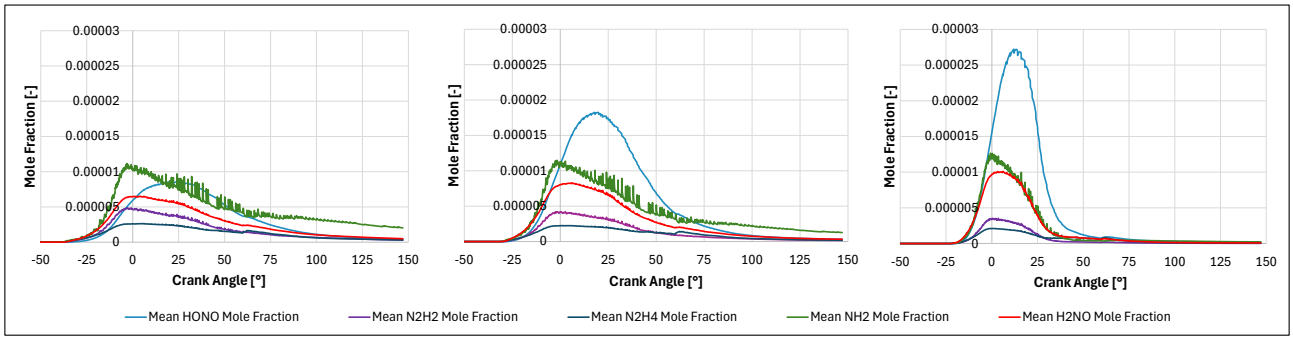


Figure 28: Concentrations of some species derived from NH_3 the three cases investigated: Neat ammonia (left) 5% of hydrogen (middle) and 15% of hydrogen (right)

Table 15: Calculated wet concentrations at exhaust valve opening

Species	Case 1	Case 2	Case 3
NH_2 [ppm]	2.0	1.3	0.2
N_2H_2 [ppm]	0.3	0.2	0.0
N_2H_4 [ppm]	0.3	0.2	0.0

To improve the combustion behaviour of this engine fuelled by ammonia and ammonia-hydrogen blends, simulations considering multiple spark plugs have been carried out. The modelling of the spark plugs has been made as in the previous described cases. Up to three spark plugs, as shown in Figure 29, have been considered. The spark plug S1 is placed at the center of the combustion chamber, while the spark plugs S2 and S3 are placed at the intake and exhaust side, respectively. For each case, three different configurations have been simulated: i) single spark (S1), which represents the same configuration used for the experimental tests, ii) twin spark (S1+S2) and iii) triple spark (S1+S2+S3). The multiple sparks plug analyses and the choice of testing the engine up to three spark plugs has been made because some research activities conducted on similar engines shows that this strategy can improve ammonia combustion.

In this preliminary analysis the spark angles remain the same of the experimental case to have a direct comparison between single and multiple sparks plugs strategy and to check if there is an improvement in ammonia combustion strongly enough to justify this choice. Further analyses will be carried out to define for each fuel blend the optimal spark plug and to optimize the whole process.

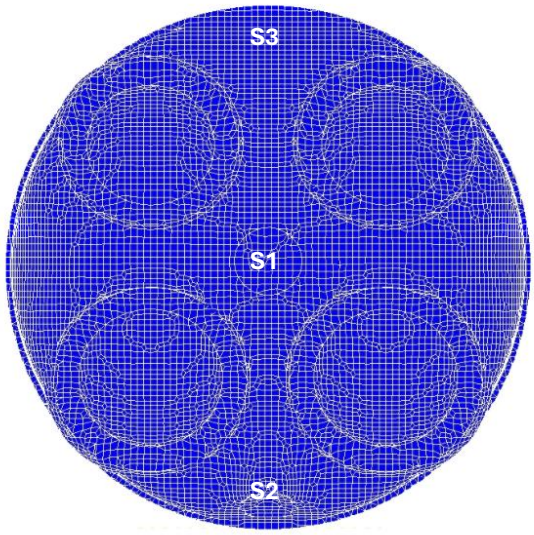


Figure 29: different spark plugs locations

Figures 30 and 31 compare both in-cylinder pressure and rate of heat release for each case investigated. With double spark plug the pressure peak increases of about 43% considering the engine running with neat ammonia, 28% with 5% of hydrogen by volume and 18% with hydrogen-enrichment equal to 15% by volume. The effect of multiple spark plugs seems to be very sensitive to the amount of hydrogen considered in the fuel mixture, therefore it might be useful to adopt this strategy with lower ammonia-hydrogen-enriched blends. Figure 31 shows the rate of heat release of each case investigated and the trends are the same for all the simulated points; furthermore for all the cases the in-cylinder temperature are within feasible values, as shown in Figure 32.

Finally, considering the $IMEP_H$ (Table 16), moving from single to twin spark strategy it increases respectively of 9%, 11% and 6.5% for neat ammonia, 5% and 15% of hydrogen by volume in the fuel mixture. These results confirm that multiple spark strategies better fit with lower amounts of hydrogen-enrichment considered.

Referring to the addiction of the third spark plug, the improvements are negligible in the case of ammonia-hydrogen blends (Cases 2 and 3). In the case of pure ammonia (Case 1), there is even a slight reduction in the calculated $IMEP_H$. This is probably due to the non-optimized position of the third spark plug. In fact, the images reported in Figures 33-35 show that the flame front developing in the squish zone located in the exhaust side tends to hinder the development of the front developing in the middle. This effect appears more evident when the engine runs on pure ammonia, where the ignition advance is higher, and the development of the fronts is slower.

Table 16: $IMEP_H$ comparisons

	Case 1 (neat ammonia)		Case 2 (5% of hydrogen by vol.)		Case 3 (15% of hydrogen by vol.)	
Spark strategy	Spark angle [CADaTDC]	$IMEP_H$ [bar]	Spark angle [CADaTDC]	$IMEP_H$ [bar]	Spark angle [CADaTDC]	$IMEP_H$ [bar]
Single spark	-43	7.94	-35	7.76	-27	8.25
Twin spark	-43	8.70	-35	8.64	-27	8.83
Triple spark	-43	8.68	-35	8.72	-27	8.86

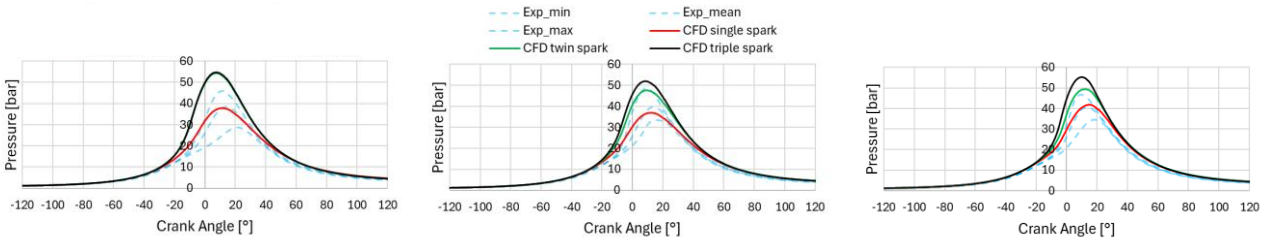


Figure 10: In-cylinder pressure. Case1 (left), Case 2 (middle), Case 3 (right).

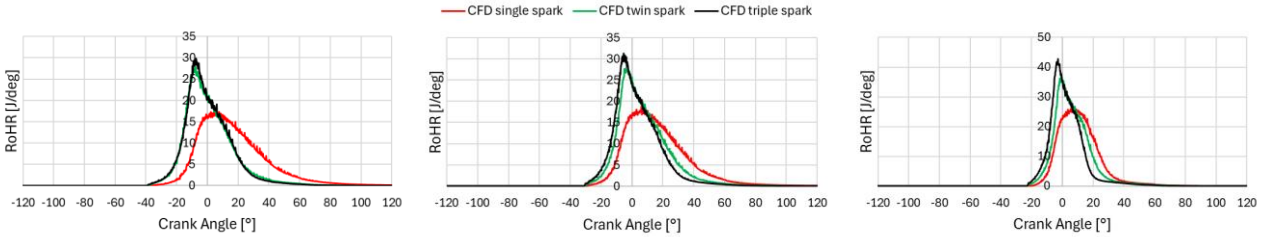


Figure 31: RoHR. Case1 (left), Case 2 (middle), Case 3 (right).

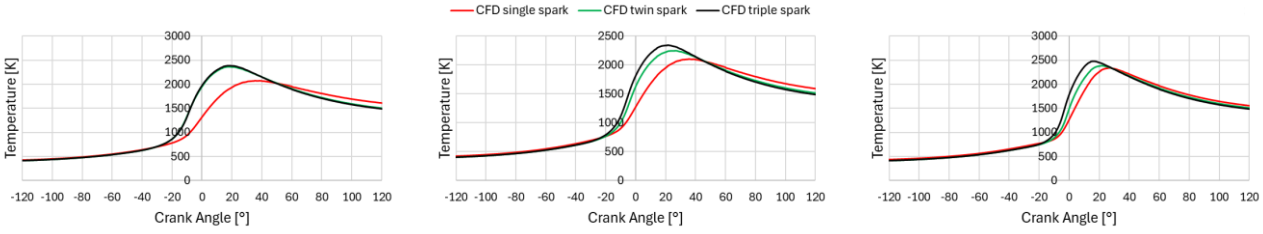


Figure 32: In-cylinder temperature. Case1 (left), Case 2 (middle), Case 3 (right).

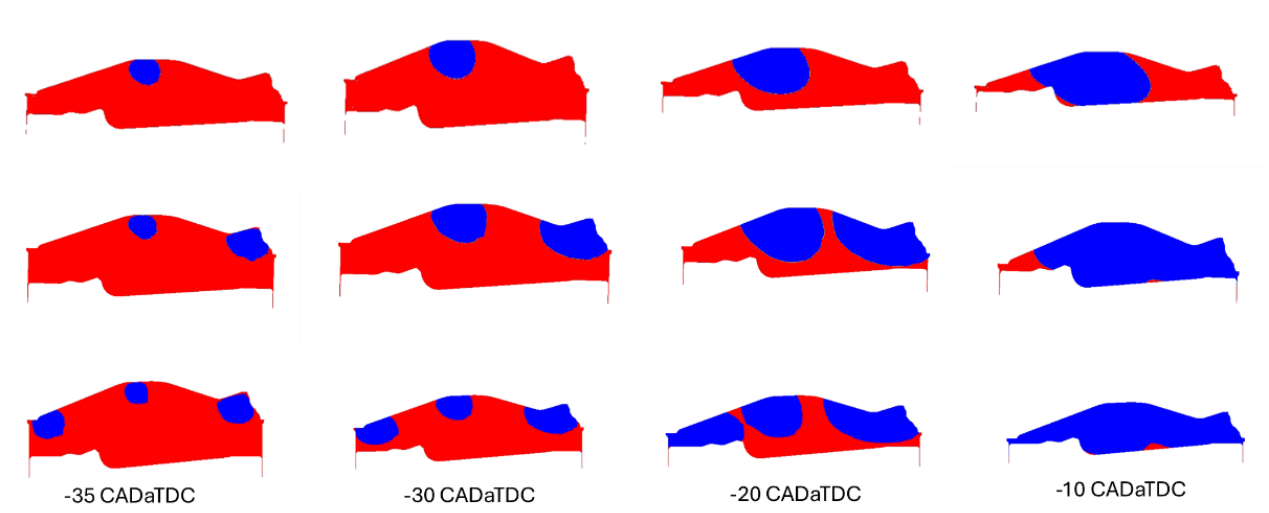


Figure 33: Flame propagation for Case 1. Single spark (top), twin spark (middle), triple spark (bottom).

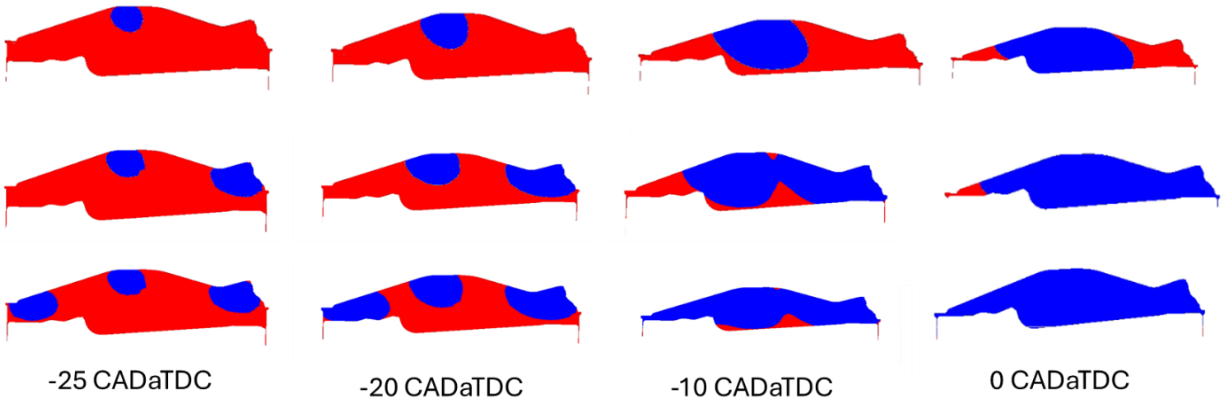


Figure 34: Flame propagation for Case 2. Single spark (top), twin spark (middle), triple spark (bottom).

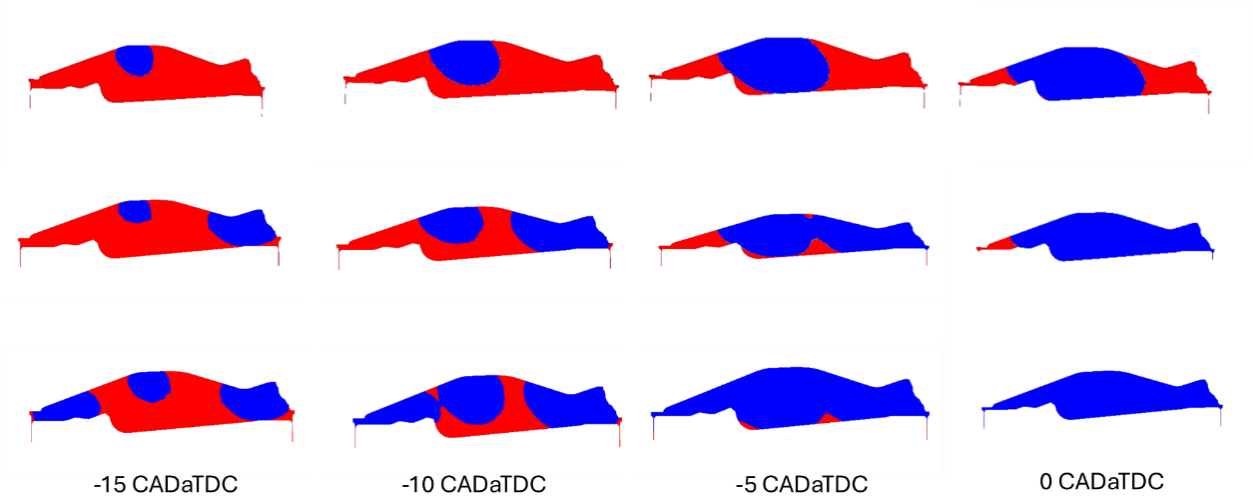


Figure 35: flame propagation for Case 3. Single spark (top), twin spark (middle), triple spark (bottom).

Table 17 presents a comparison related to the calculated combustion characteristics between the different cases investigated. It is worth noting that globally the adoption of the multiple sparks plugs strategy improve the combustion development leading to a

faster and better combustion with respect to the case with a single spark plug. As example the CA10-90 reduced of about 34%, 22% and 10% for the three cases investigated, as also shown in Figure 36, in which it is clearly represented that multiple spark plugs lead to an increase in the ammonia consumption curve's slope. Even these results show that the highest improvement is related to neat ammonia fuelling (Case 1), but, as also shown above, the higher is the amount of hydrogen the lower is the improvement in the combustion development.

Table 17: Calculated combustion characteristics.

	Case 1 (Neat ammonia)			Case 2 (5% of hydrogen by vol.)			Case 3 (15% of hydrogen by vol.)		
	Single spark	Twin spark	Triple spark	Single spark	Twin spark	Triple spark	Single spark	Twin spark	Triple spark
CA0-10 [CAD]	36.1	27.2	28.3	29.2	24.9	22.4	21.4	20.4	17.8
CA10-90 [CAD]	52.6	34.3	35.1	46.3	36.1	31.6	28.1	25.1	21.8
CA50 [CAD]	12.5	-2.3	-1	12.3	3.4	3.4	9	4.2	0.5

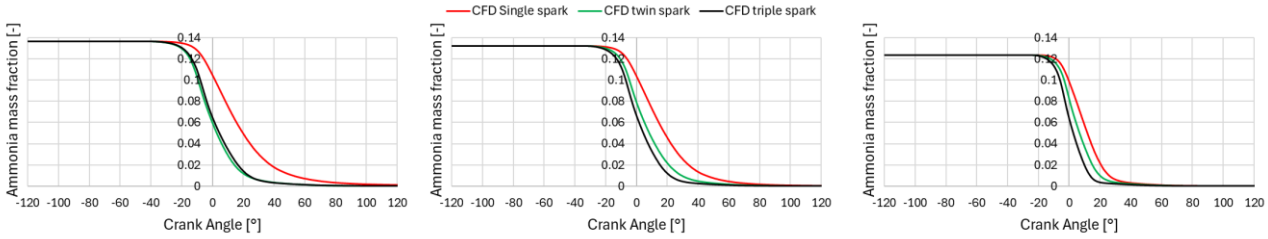


Figure 36: Ammonia consumption for all the investigated cases. Case 1 (left), Case 2 (middle), Case 3 (right).

Considering the main pollutants related to ammonia and ammonia-hydrogen blends, which are unburned NH_3, and NO_x, table 17 shows a comparison between single twin and triple spark strategy for these pollutants, considering wet exhaust gases.

Focusing on unburned ammonia, compared to the performance, the improvement in emission is smaller: in fact, for each mixture considered the reduction is respectively of about 13%, 8% and 3%. This is also confirmed for NOx emissions, and, in this case, the effect is less than unburned ammonia. As example the NO reduces only about 0.3% for neat ammonia and about 3% for the ammonia-hydrogen blends considered. This can be explained by the higher temperature peak reached in the combustion chamber. In fact, as explained by the well-known Zeldovich mechanism, the NOx formation is strongly influenced by the temperature and considering multiple sparks plug strategy, the peak increases respectively of 13%, 6% and 3% if the amount of hydrogen rises from 0 to 15% by volume.

Another aspect of interest is the amount of hydrogen which remains in the exhaust gas because, for the different fuel blends considered, hydrogen is also a subproduct of ammonia dissociation, as previously shown. In Figure 37, the consumption of hydrogen for all the investigated blends considering single, twin and multiple spark strategy is presented. From the plot on the left, it is clear that hydrogen is directly generated by

ammonia dissociation, in fact its amount rises from 0 and then start to consume. This happens in all the investigated cases and, as for ammonia, also hydrogen consumption benefits using multiple sparks plugs strategy. Similarly to the trends for ammonia, even for hydrogen the slope of the consumption curves is bigger with respect to single spark strategy and the amount of hydrogen in the exhaust gas reduces of about 1% (twin spark) and 0.5% (triple spark) for neat ammonia (Case 1), of about 1.43% (twin spark) and 2.1% (triple spark) considering 5% of hydrogen by volume (Case 2) and of about 1.5% (twin spark) and 1.7% (triple spark) considering hydrogen enrichment equal to 15% (Case 3).

The 3D CFD model, as expected, underestimate the amount of emission substances with respect experimental data, but the proposed model is able to follow the same variations if the quantity of hydrogen varies in the same way.

Table 18: Unburned fuel and NOx concentrations in the wet exhaust gas

	NH_3 [ppm]			NO [ppm]			N_2O [ppm]		
	Single spark	Twin spark	Triple spark	Single spark	Twin spark	Triple spark	Single spark	Twin spark	Triple spark
Case 1 (neat ammonia)	6249	5427	5401	1445	1443	1471	12	5	3
Case 2 (5% of hydrogen by vol.)	5464	5020	4890	1569	1513	1557	10	5	3
Case 3 (15% of hydrogen by vol.)	4885	4721	4665	1732	1675	1667	4	2	1

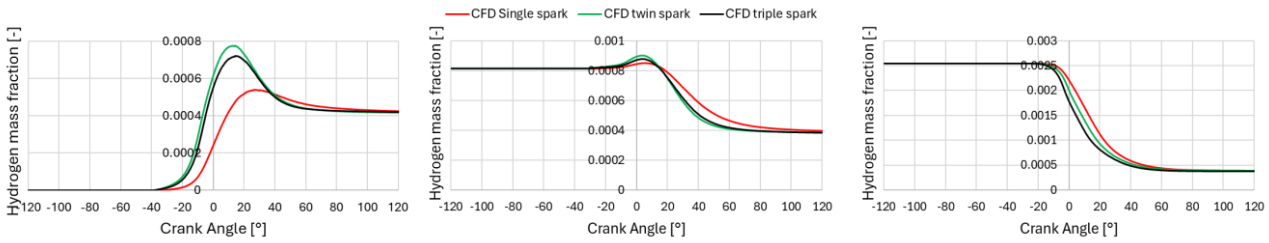


Figure 37: Hydrogen consumption for all the investigated cases. Case 1 (left), Case 2 (middle), Case 3 (right).

3.3 T-jet Engine operating conditions considering different ammonia hydrogen blends

To evaluate the potential of carbon free fuels applied to a typical automotive-derived light-duty engine, the engine described in Table 2 (T-jet engine) was considered. To evaluate its overall performance, its entire layout was modelled according to the 1D approach described in chapter 2. Not having experimental data relating to this engine operating with ammonia/hydrogen mixtures, the calibration of the combustion submodel was carried out considering a 3D-1D hierarchical approach starting from the results obtained for the engine described in the previous paragraph (PSA engine).

The two engines have identical fields of application and very similar geometry. In particular, both are characterized by pent-roof chambers with generation of tumble motions of comparable intensity. The ignition systems are also similar to each other. In this sense, it was decided to model the T-Jet engine with a 3D approach using the same sub-models used for the PSA. Then transfer the calibration carried out for the PSA engine

with the same discretization. Basically, this meant modelling the T-Jet's ignition timing by considering the same amount of energy released by the spark plug calibrated for the PSA engine. The pressure curves obtained from the 3D calculations were then used to calibrate the 1D model of the engine as shown in the following figures.

Two different fuel feeds have been considered:

- Neat ammonia
- Ammonia-hydrogen blends (15% of hydrogen by volume)

Figure 38 and 39 shows some comparison of in-cylinder pressure and heat release rate calculated by the 3D approach and the calibrated 1D model for both the mixtures investigated.

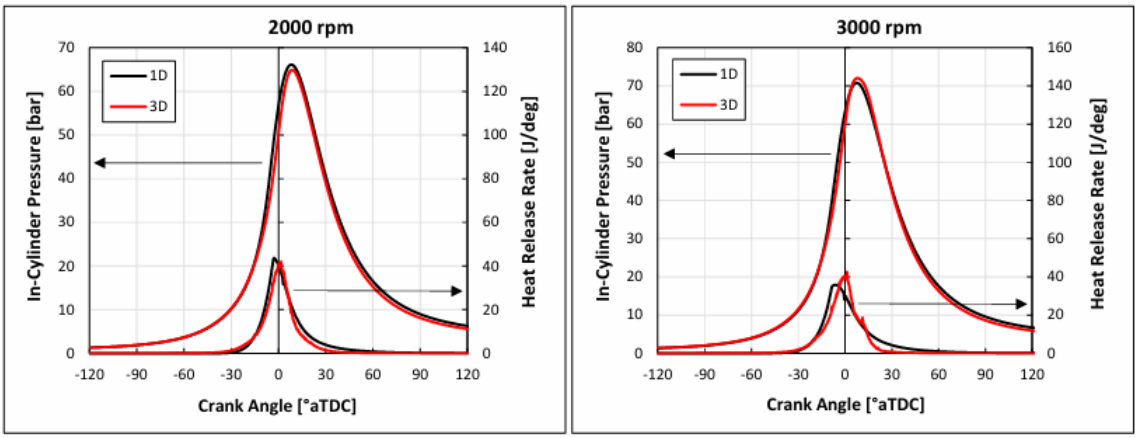


Figure 38: In-cylinder pressure and rate of heat release for both 1D and 3D CFD. Engine running with neat ammonia, stoichiometric mixture, WOT operation, no boost conditions, optimized spark angle at 2000 rom (left) and 3000 rpm (right).

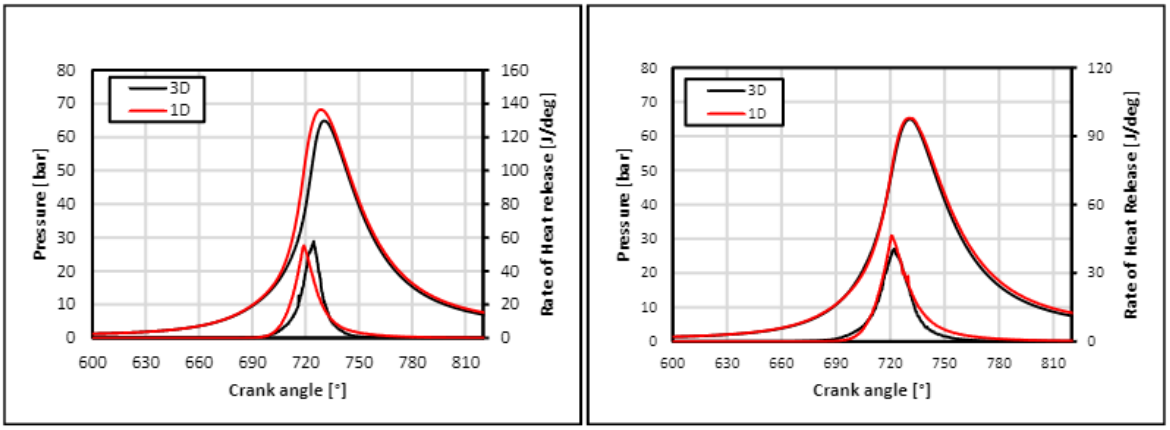


Figure 39: In-cylinder pressure and rate of heat release for both 1D and 3D CFD. Engine running with ammonia-hydrogen blend, stoichiometric mixture, WOT operation, no boost conditions, optimized spark angle at 1500 rpm (left) and 3000 rpm (right).

Furthermore, the calculated burned fuel fraction at exhaust valve open is presented in table 19. Unburned ammonia is overestimated by the 1D model which is not able to consider also the partial oxidation of ammonia. This causes, compared to the 3D results, an underestimation of the burned ammonia fraction less than 2%.

Table 19: Burned fuel fraction at exhaust valve open calculated by both 1D and 3D model

Engine Speed [rpm]	2000		3000	
	3D	1D	3D	1D
Burned fuel fraction at EVO [%]	99.95	98.84	99.99	98.42

Two different calibrations set have been obtained and since the 1D model is indirectly calibrated, it is fair to point out that the results obtained from the 1D analysis must be understood as qualitative. However, they are indicative and useful for the development of new engines that use carbon-free fuels.

3.3.1 Neat ammonia

To assess the behaviour of the analysed engine with ammonia fuelling, steady-state engine operating points were investigated by means of the 1-D approach considering both full throttle operation (WOT), with and without boost, and throttled operation were taken into consideration. As mentioned above, first, 1D calculations were carried out to reproduce some operating points and to compare the 1D calculations to the 3D results. Then, several analyses were performed using the 1D approach to assess both the performance and the operating limits of the ammonia engine. In the following sub-sections, the results of each analysis are described in detail. The constraints imposed remain the same presented in chapter 2.

At first, a parametric analysis of the effects of both equivalence ratio and spark timing in the engine performance and combustion have been done at a fixed engine speed equal to 1500 rpm. Then the spark angle was set considering maximum brake torque at knock limit condition for a stoichiometric mixture. The analyses have been carried out considering both throttled and unthrottled conditions. The effect of the different spark advances on the engine performance and combustion properties has been evaluated at a fixed engine speed equal to 1500 rpm, keeping also constant the equivalence ratio equal to one and no boost with wide open throttle conditions.

Figure 40 presents these results, and it is worth noting that higher spark advances lead to an increase in the combustion delay, (CA 0-2) and furthermore also a reduction in the combustion duration (CA 10-90) has been found, as shown in table 19. The CA 10-90 reduction is higher than the CA 0-2 increase, and when the spark advance grows both the in-cylinder pressure peak and the burned fuel fraction at exhaust valve open increases. The optimized spark advance considering the maximum brake torque condition at knock limit was equal to 699° bTDC with a break specific fuel consumption equal to 420 g/kWh.

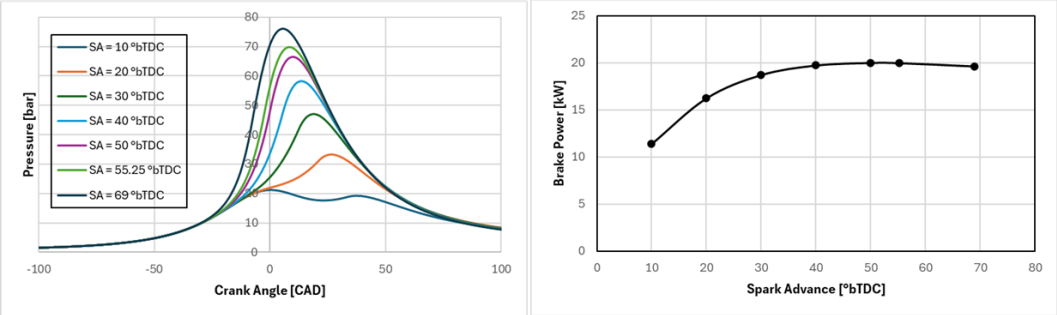


Figure 40: In-cylinder pressure (left) and brake power (right) for different spark angle considering the equivalence ratio equal to 1, no boost conditions, engine speed equal to 1500 rpm and wide open throttle conditions.

Table 20: Combustion characteristics and engine performance

Spark Advance [°bTDC]	30	40	50	60	69	80
CA0-2 [CAD]	29.3	33.3	38.5	44.2	49.7	56.5
CA10-90 [CAD]	101.9	50.1	35.8	30.5	28.1	26.8
Burned Fuel Fraction at EVO [%]	91.3	95.7	97.7	98.6	99.1	99.4
Brake Efficiency [%]	29.7	34.4	36.8	37.9	38.2	38.0
BSFC [g/kWh]	539.9	465.8	435.1	422.6	419.5	421.7

After that the effect of the fuel mixture composition has been evaluated fixing the optimal spark angle found. The obtained results are presented in figure 41 and table 21.

It is important to underline that both the combustion delay and the combustion efficiency decrease if the equivalence ratio increases leading to a higher value of the burned fuel fraction. In particular, at stoichiometric conditions the burned fuel fraction is equal to 99.1 % while at equivalence ratio equal to 0.9 it falls down below the 90%. The faster combustion of the rich mixture leads to a higher in-cylinder pressure peak and a consequence of that also the engine power is higher. On the other hand, the maximum engine efficiency and the minimum brake specific fuel consumption was reached considering an equivalence ratio equal to 0.9, but the overall combustion duration is higher with respect to stoichiometric conditions. For these reasons all the further analysis related to this engine were conducted considering only stoichiometric conditions. This choice was made since, at higher engine speeds, a too slow combustion could not allow a proper engine operation. On the other hand, rich mixtures were avoided since they lead to ammonia emissions which are not acceptable due to the higher unburned ammonia emissions.

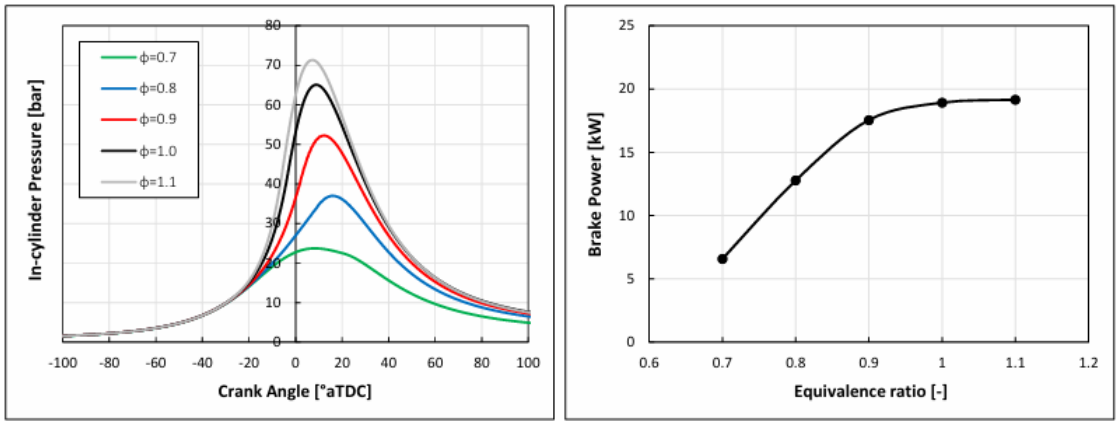


Figure 41: In-cylinder pressure (left) and brake power (right)

Table 21: Combustion characteristics and engine performance

Equivalence ratio [-]	0.7	0.8	0.9	1.0	1.1
CA0-2 [CAD]	66.3	59.3	53.9	49.7	47.7
CA10-90 [CAD]	/	/	41.2	28.1	24.6
Burned Fuel Fraction at EVO [%]	61.7	87.4	96.5	99.1	91.0
Brake Efficiency [%]	18.0	31.1	38.6	38.2	35.9
BSFC [g/kWh]	889	516	415	420	446

Then the performances of the engine fuelled by neat ammonia were investigated varying the engine speed and the boost levels. Results are presented in the following figures and in each operating point, the mixture was set to be stoichiometric, and the spark angle was adjusted to the optimal value. It is worth highlighting that spark timings more advanced than typical ones of SI engines are needed to obtain a proper combustion with ammonia fuelling due to its low laminar flame speed. Naturally, the more the engine speed increases, the more the optimal spark timing will advance. The combustion duration increases with increasing engine speed, while it decreases with increasing boost pressure and the optimal spark advance consequently varies, reaching the imposed constraint at the highest engine speeds. It is worth noting that the increase in the angular combustion duration (CA0-90) with increasing the engine speed is typical of SI engines, but it can be critical in the case of ammonia fuelling due to the low laminar flame speed of ammonia–air mixtures and at medium and high rotation speeds, the engine could not properly operate. The engine efficiency rises with the rising of the boost pressure showing very high values at low engine speed, while when the engine speed increases it decreases due to the slowdown of the combustion. However, the engine efficiency always remains over 32%. The BSFC consequently varies from a minimum value of about 380 g/kWh to a maximum value of about 500 g/kWh. Furthermore, the engine power also reached interesting values, close to the ones of a gasoline engine, as example at 6000 rpm with a boost pressure equal to 1.4 the engine can deliver about 100 kW. Unfortunately, higher engine speeds appear unsustainable considering the trends of both the unburned ammonia content and the temperature of the exhaust gas leaving the cylinders. Indeed, increasing combustion durations lead to an incomplete fuel

combustion and to higher temperatures of the exhaust gases which leave the cylinders. It is worth noting that when increasing the boost level, the burned ammonia fuel fraction improves, while the exhaust gas temperature increases at a given engine speed. In the end, the maximum allowable engine speed is about 3000 rpm both at no boost operation (due to the unburned fuel constraint) and at BP = 1.4 bar (due to the exhaust gas temperature constraint). The boost level 1.8 is unacceptable, since the maximum in-cylinder pressure exceeds the maximum allowable value in each operating point.

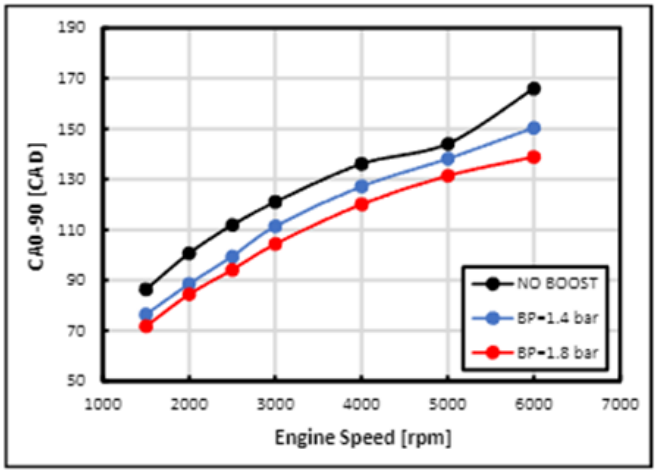


Figure 42: combustion duration for different boost levels

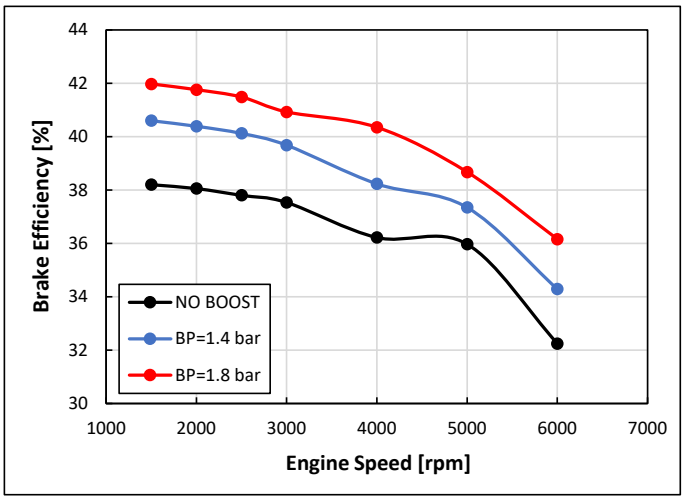


Figure 43: Brake efficiency at different boost levels

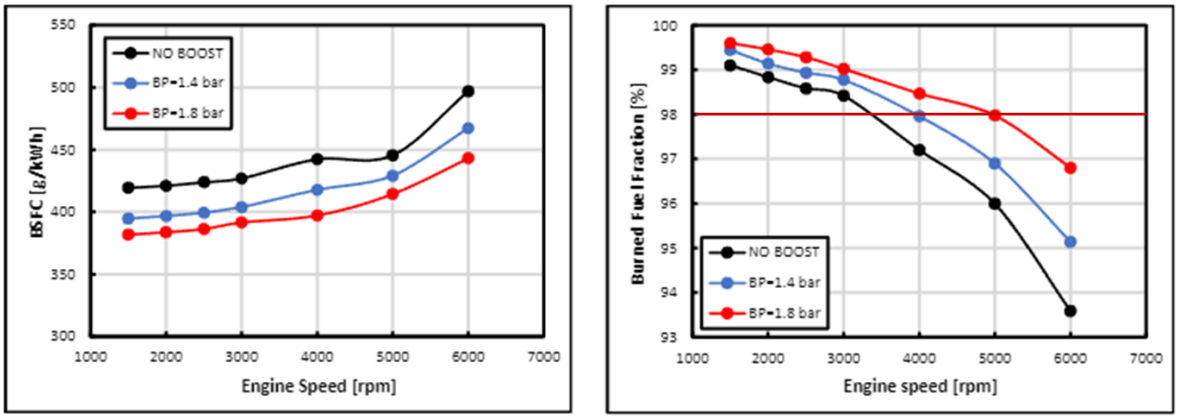


Figure 44: Brake specific fuel consuption (left) and burned fuel fraction (right)

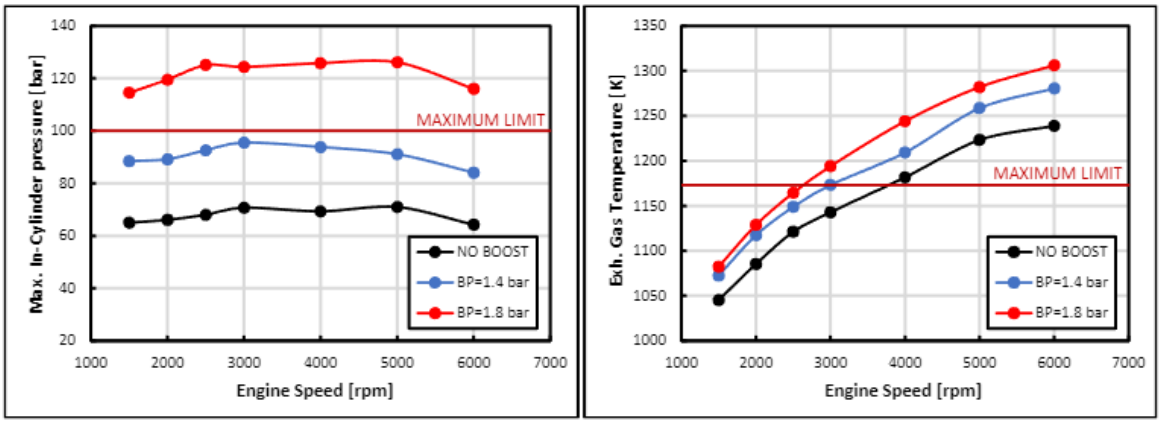


Figure 45: maximum in-cylinder pressure (left) and exhaust gas temperature (right)

The effects of increasing geometrical compression ratios (from 9.8 to 11.0) on the engine behaviour were evaluated at wide throttle operation, no boost condition. As in the previous analysis, the spark angle was adjusted to the optimal value. For all the engine speed considered, the increase in the combustion ratio leads to a reduction in the combustion. This happens because during the compression ratio the pressure in the cylinder is higher than the one of the cylinder with the standard geometrical compression ratio and this increase determines also an increase in the charge temperature and therefore in the flame speed. The better thermodynamics effect, caused by both the increase in the geometrical compression ratio and the faster combustion, determines a not negligible improvement in the engine efficiency and in the engine power, even if for the engine power the improvement is less than for the engine efficiency (figure 44). Increasing the geometrical compression ratio creates benefits for both the quantity of the unburned ammonia at exhaust valve opening and for the exhaust gas temperature, as presented in figure 47 right; this improvement depends mainly by the faster combustion which makes the combustion process more complete. Furthermore, the temperature of the exhaust gas leaving the cylinder decreases due to the increasing expansion phase. Contrariwise the in-cylinder pressure peak increase

while remaining below the maximum limit. Finally, for no boost conditions, with the increased compression ratio, even at 4000 rpm operating point complies with the operating limits, guaranteeing proper engine operation.

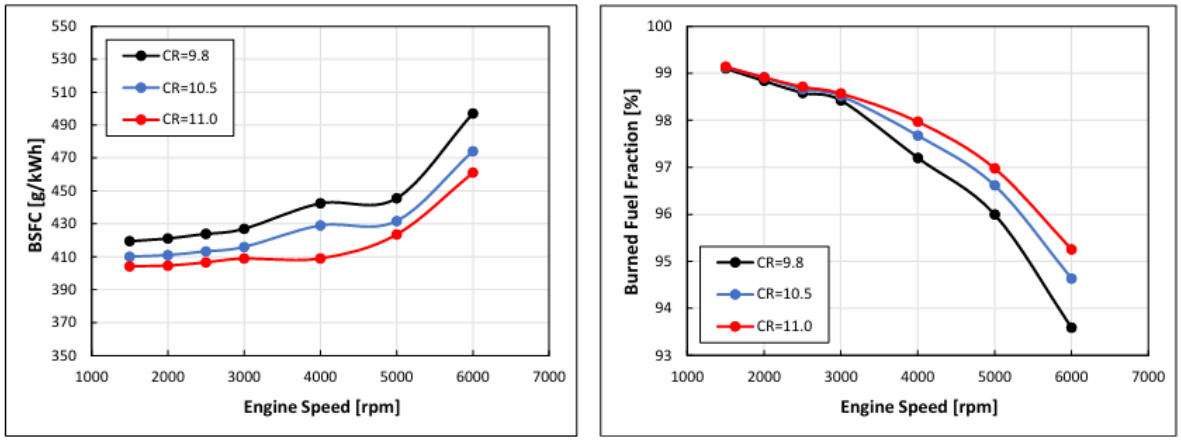


Figure 46: Brake specific fuel consumption (left) and burned fuel fraction (right) for different compression ratio

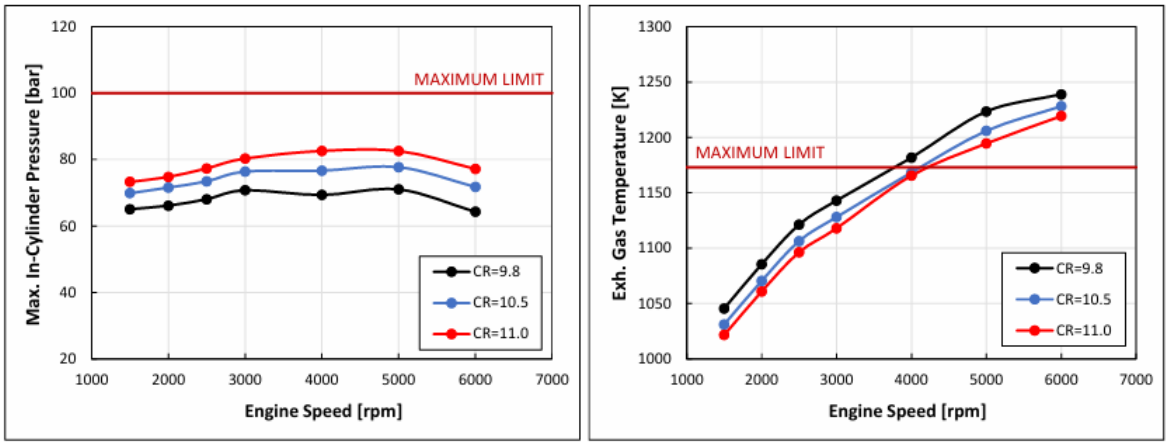


Figure 47: maximum in-cylinder pressure (left) and exhaust gas temperature(right) for different compression ratio

Considering no boost conditions, the standard compression ratio of the engine, stoichiometric ammonia-air mixtures and optimal spark angle, the effect of different throttle openings on the engine behaviour was evaluated. The analyses have been carried out only at 1500 and 3000 rpm and the results are presented in figure 48. As typical in port fuel injection spark ignition engine, when throttling the engine, the brake efficiency decreases due to the growing of the pumping losses. Furthermore, as shown in figure 49, the combustion duration increases due to the higher dilution of the charge which reduces the laminar flame speed. Indeed, higher CA 0-90 values at decreasing engine loads lead to a reduction of the burned fuel fraction which is amplified for the highest engine speed. These results clearly show that at 3000 rpm the load regulation can be critical in terms of unburned ammonia emissions. In the end using a numerical approach, the cycle-by-cycle variations cannot be evaluated therefore the operating range could be further reduced due to an excessive value of the coefficient of variation

IMEP. All the results presented agree with [29], therefore it can be considered acceptable for this engine.

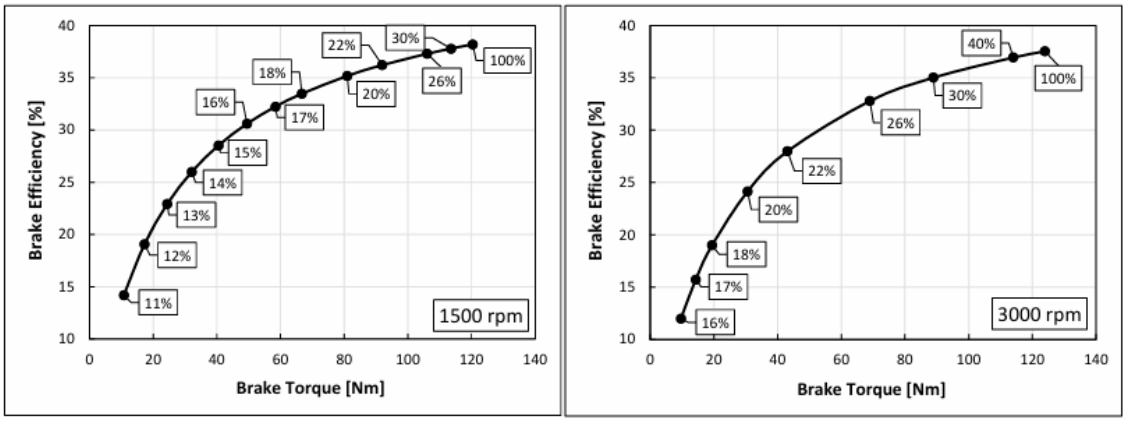


Figure 48: brake efficiency as a function of the brake torque for 1500 and 3000 rpm. The labels highlight the different throttle opening values

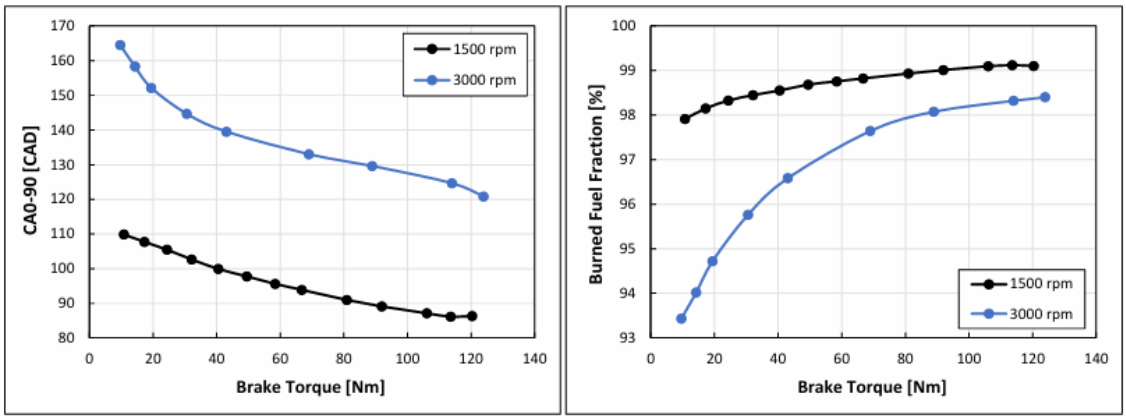


Figure 49: CA 0-90 (left) and burned fuel fraction (right) versus engine torque for 1500 and 3000 rpm

3.3.2 Ammonia-hydrogen blends

To overtake the problems related to ammonia combustion, and to keep the whole process without carbon's emissions ammonia hydrogen blend (15% of hydrogen by volume) are tested in the same engine. Basing on the results for neat ammonia only stoichiometric mixtures are investigated by means of 1D simulations considering both high load conditions and low load conditions. Also, for these analyses the constraints imposed remain the same presented in chapter 2.

To assess the engine behaviour at partial load conditions a parametrical analysis was carried out varying the throttle opening until a minimum torque of about 10 Nm was reached. The whole analyses were performed considering different engine speeds (from 1500 to 6000 rpm), no boost conditions and spark angle set to the optimum value

considering maximum brake torque at knock limit. Figure 50 highlights the engine efficiency considering an engine speed equal to 3000 rpm when the throttle opening change. As for neat ammonia, even in this case due to the pumping losses when the engine load decreases also the engine efficiency falls. Moreover, as shown in figure 51 right, the increasing in the combustion duration (CA 0-90) related to the increase of the engine speed became critical for the lowest load at medium regime and for almost all the loads at high regimes. In fact, as presented in figure 51 left, in the latter cases the minimum acceptable burned fuel fraction was not reached, and these points cannot be considered operative points for the engine. On the other hand, partial load conditions were sustainable for the whole considered range at engine speed equal to 1500 and 2000 rpm, with the lower values of the burned fuel fraction at minimum load equal to 98.8% and 98.9% respectively. Considering 3000 and 4000 rpm the entire map was not exploitable since the lowest loads did not respect the imposed constraints. At 5000 rpm only wide-open throttle and very low throttling conditions guarantee a proper engine operation, while for 6000 rpm the 98% of burned fuel fraction was never reached. It is worth noting that for these analyses only the constraint for burned fuel fraction was critical, while the others were always respected, therefore they were not presented.

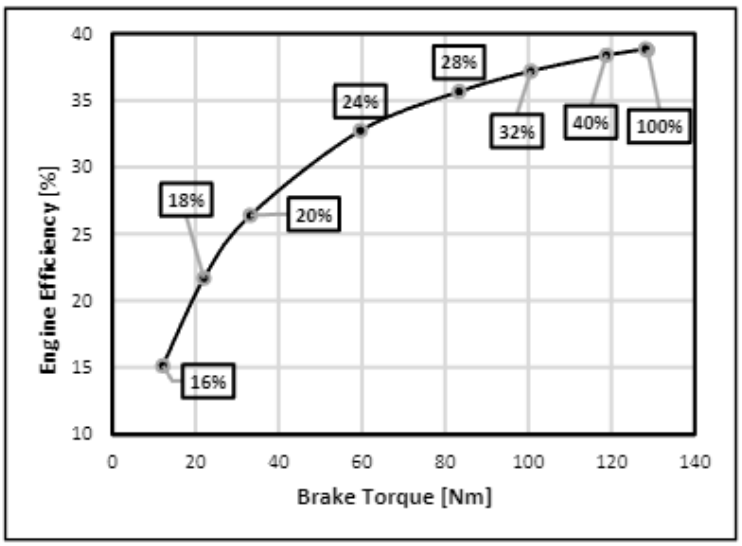


Figure 50: Engine efficiency as a function of engine torque at 3000 rpm for different loads

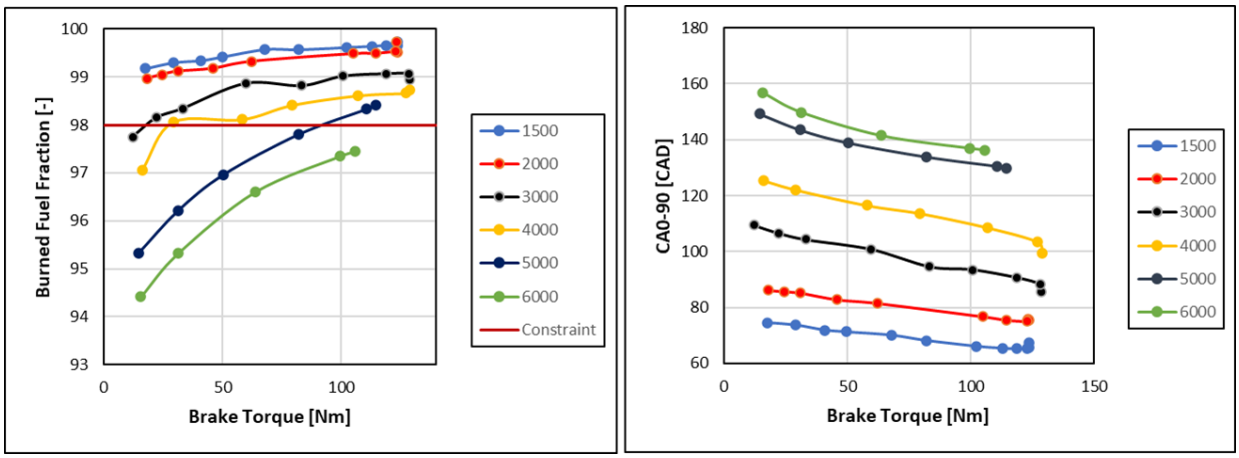


Figure 51: Burned fuel fraction (left) and CA 0-90 (right) for different loads

The same engine speeds have been considered for high load analyses. Even in these cases the equivalence ratio was always equal to 1 and the boost pressure levels varies from 1 (no boost conditions) to 2.

Figure 52 left shows the calculated engine torque delivered by the engine with the spark angle sets to the maximum torque at knock limit. Obviously, the engine torque increased when the boost pressure level grew. The combustion duration CA 0-90 follows the same trend of the spark angle, and in particular it increases when the engine speed increase, while it decreases when the boost pressure increase. Even these results, as for neat ammonia, are in good agreement with some experimental results presented in [30].

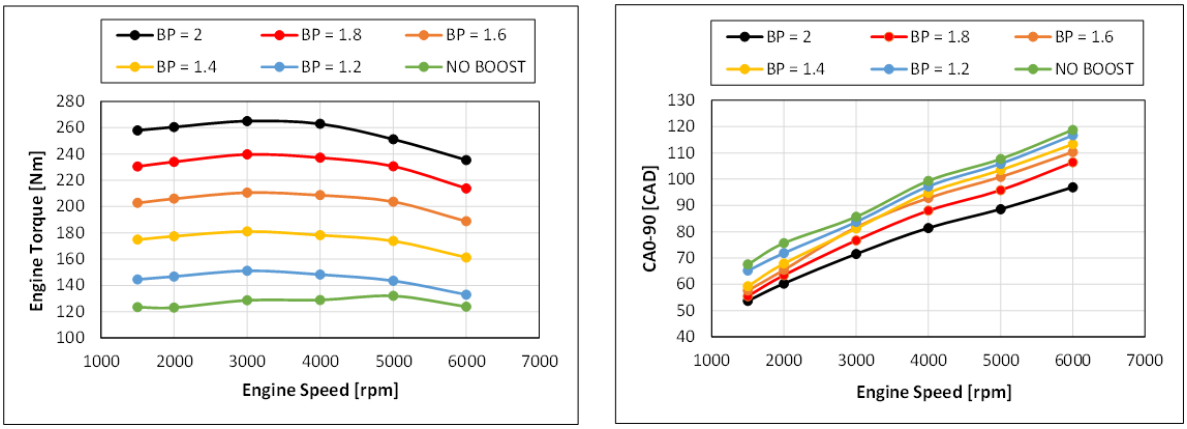


Figure 52: Engine torque (left) calculated at maximum brake torque at knock limit spark advance and relative combustion duration (right) for different boost levels

Unfortunately, not all the points presented in figure 53 respect the imposed constraints and therefore, they cannot be considered acceptable. In particular, the engine running with the optimal spark advance reached an unacceptable in-cylinder pressure peak for boost levels equal or greater than 1.6 for each engine speed. Furthermore, for 5000 rpm also the exhaust gas temperatures were outside the acceptable range for any boost

level. The exhaust gas temperature did not limit the engine operative range only below 3000 rpm, while in an engine speed range from 3000 to 5000 it determined a maximum allowable boost pressure. Finally, above 5000 rpm and at low boost pressure the engine also showed unacceptable unburned fuel fraction at exhaust valve open.

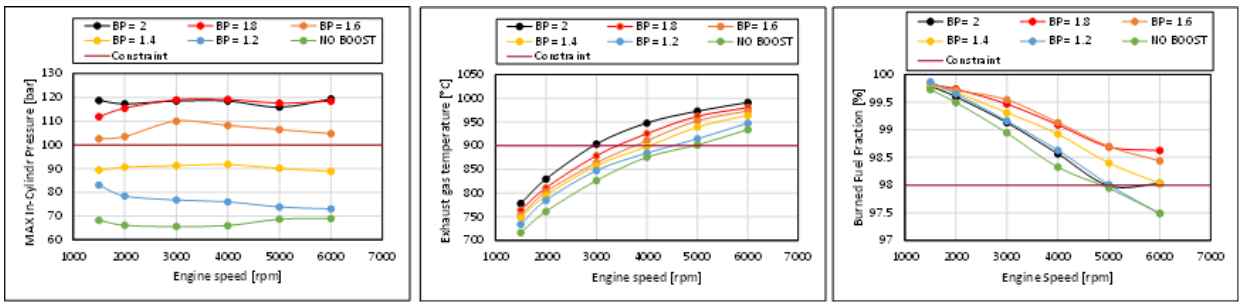


Figure 53: Maximum in-cylinder pressure (left), exhaust gas temperature (middle) and burned fuel fraction (right) calculated for the engine running at the maximum torque knock limit spark advance

These results show that the engine operation is strongly limited by the imposed constraints. However, it is possible for some of the points which are out of the allowable range to vary the spark angle from the optimal one to extend the operating range of the engine. For example, at 3000 rpm and boost level equal to 1.6 delaying the spark angle allow to reach a lower in-cylinder pressure peak which is acceptable respect to the imposed constrain. On the other hand, both exhaust gas temperature and unburned fuel fraction increased, but they still remained within the allowable limits. This result was achieved and only lost about 3% of engine efficiency, as presented in table 22.

Table 22: Engine recalibration at 3000 rpm and boost level equal to 1.6

	Maximum Torque Operating Point	Recalibrated Operating Point
Max. In-Cylinder Pressure (bar)	111.7	96.5
Engine Torque (Nm)	213.3	209.7
Engine Power (kW)	67	65.9
Engine Efficiency (%)	41.7	41.1
Spark advance (°bTDC)	44.3	35
Exhaust Gas Temperature (°C)	866.4	882.2
Burned Fuel Fraction (%)	99.9	99.7

Therefore, it was possible to identify an operating area where all parameters fall within the acceptable limits for many engine operating points that have been previously excluded. The results of this constrained optimization are presented in figure 54 where various engine parameters are reported as a function of the engine speed and engine torque. The feasible region was large at low engine speed where good engine operation

was possible. Between 1500 rpm and 3000 rpm, the engine could be regulated, delivering a torque ranging from a minimum value around 15 Nm to a maximum value greater than 200 Nm. The maximum engine torque was about 240 Nm; it was delivered at 1500 rpm, where a boost pressure equal to 2 bar could be achieved. This boost level could be kept only up to 2000 rpm. Above 3000 rpm, the engine could run with an average maximum boost pressure of 1.4 bar, and the maximum delivered toque decreased almost linearly with the engine speed. In addition, the minimum load achievable by the engine reduces significantly as the engine speed increased. The combination of these two effects reduced the operating capacity of the engine as the speed increased. It could not run at 6000 rpm. The engine efficiency was higher than 33% for almost all points; it never fell below about 19%. The maximum efficiency was very high: it was about 42% when the engine ran at low speed and the load was slightly less than the allowable maximum. Correspondingly, the specific consumption turned out to vary from about 350 g/kWh to about 750 g/kWh. Spark advances are always very high. They ranged from a minimum of 25 CAD at 1500 rpm, maximum load, to a maximum of 110 CAD at 5000 rpm, low load.

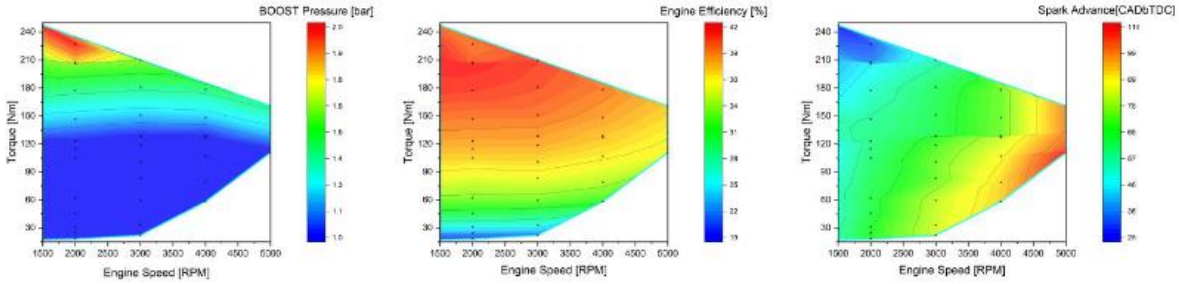


Figure 54: Boost level, engine efficiency and spark advance as a function of engine speed and torque

3.3.3 Ammonia and ammonia-hydrogen comparison

Finally, the engine running with ammonia-hydrogen-air mixture has been compared to the one running with neat ammonia and from figure 55 to figure 57 the in-cylinder pressure curves and rate of heat release curves are presented considering fixed engine speed equal to 3000 rpm and different load conditions. For each load level, due to the low laminar flame speed, the spark advances for neat ammonia fuelling are higher compared with the ammonia-hydrogen blend ones. In fact, the combustion duration values are always higher for pure ammonia operation. For the lower load (figure 56) the low combustion rate leads to a too high reduction of the burned fuel fraction for neat ammonia and, consequently, the analyzed operating point is not suitable, while at the medium load (figure 57) the engine can achieve proper operative conditions for both the mixtures considered. In the end, considering the highest load (figure 58), the operation with pure ammonia is again critical since both maximum in-cylinder pressure and exhaust gas temperature constraints are not respected. These results clearly show that the addition of hydrogen to the fuel mixture improves the combustion characteristics leading to a wider load regulation flexibility of the engine.

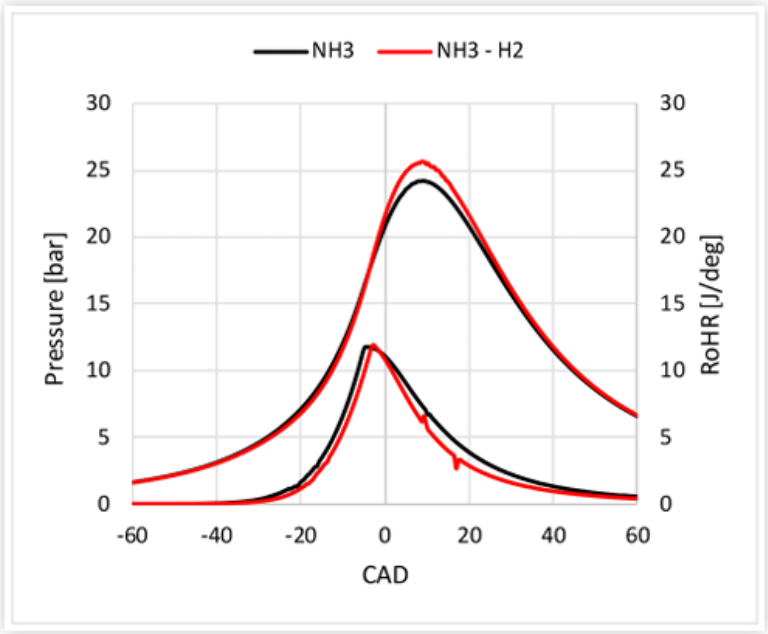


Figure 55: In-cylinder pressure and rate of heat release for ammonia and ammonia hydrogen blend considering an engine speed equal to 3000 rpm and throttle opening equal to 20%

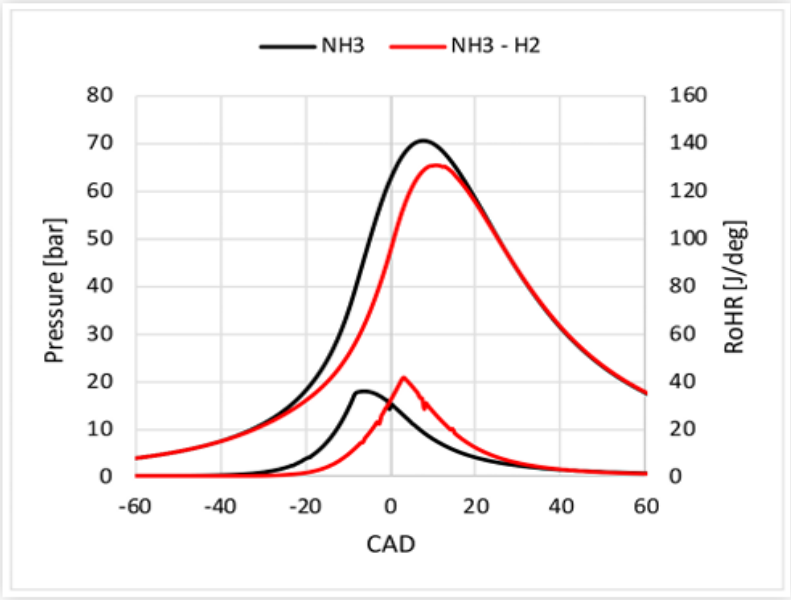


Figure 56: In-cylinder pressure and rate of heat release for ammonia and ammonia hydrogen blend considering an engine speed equal to 3000 rpm and wide open throttle conditions

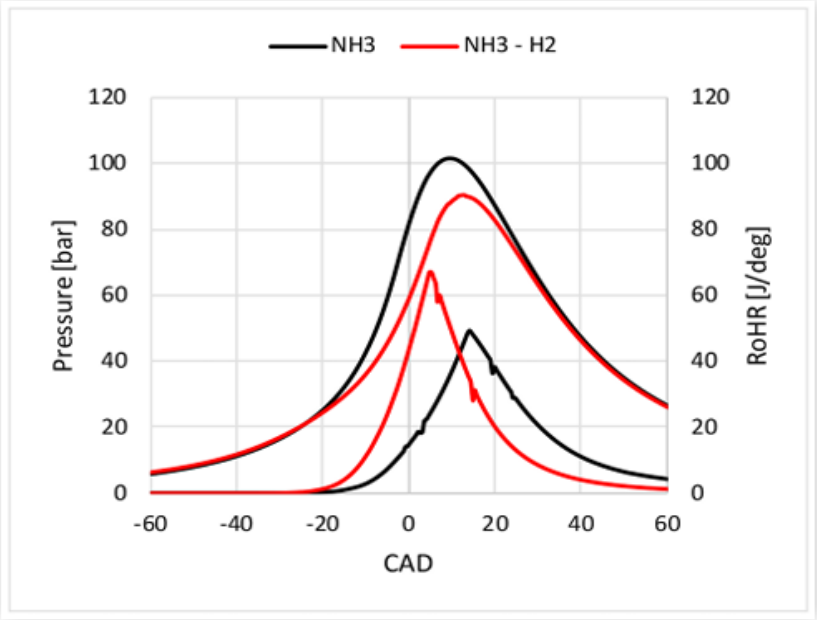


Figure 57: In-cylinder pressure and rate of heat release for ammonia and ammonia hydrogen blend considering an engine speed equal to 3000 rpm and boost pressure equal to 1.6 bar

To better clarify the differences between the engine running with neat ammonia and the engine running with ammonia hydrogen blends in the following figures is presented a comparison between the engine maps obtained for these two fuel mixtures. Ammonia fuelling shows a narrowed exploitable region with respect to the ammonia-hydrogen blend; in fact, while with the second mixture engine can run up to 5000 rpm, with the first one it can run only up to 3000 rpm. This is related to the lower laminar flame speed of ammonia with respect to ammonia hydrogen blends, which strongly limits the engine speed reachable. Furthermore, also load regulation is much more critical for ammonia fuelling. The engine fuelled by pure ammonia achieves a boost pressure equal to 2 bar only at 1500 and 2000 rpm, while for 3000 rpm the maximum reachable boost is equal to 1.4 bar. On the other hand, for the ammonia hydrogen-blend a boost pressure equal to 1.6 bar can be reached up to 3000 rpm, while for 4000 and 5000 rpm the maximum boost exploitable is equal to 1.4 bar. The brake efficiency is also affected by the addition of hydrogen. Considering 3000 rpm, which is the maximum regime for ammonia propulsion, the maximum engine efficiency increases from about 39% (pure ammonia) to about 41% (hydrogen-ammonia).

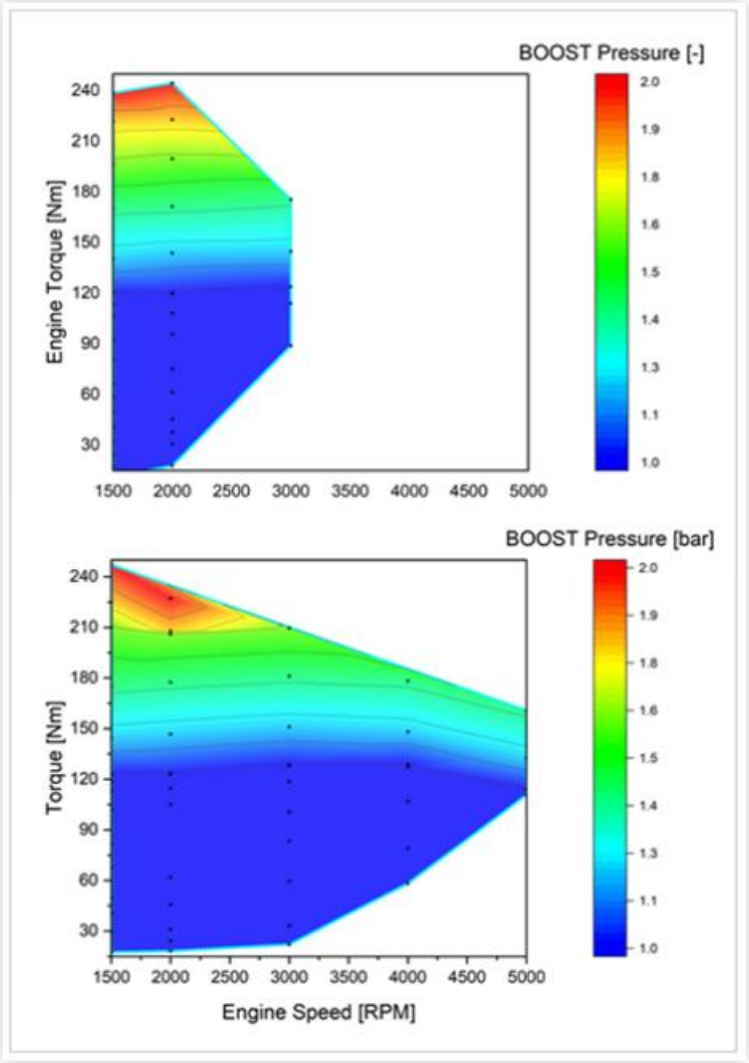


Figure 58: maps for boost pressure for ammonia and ammonia hydrogen blend

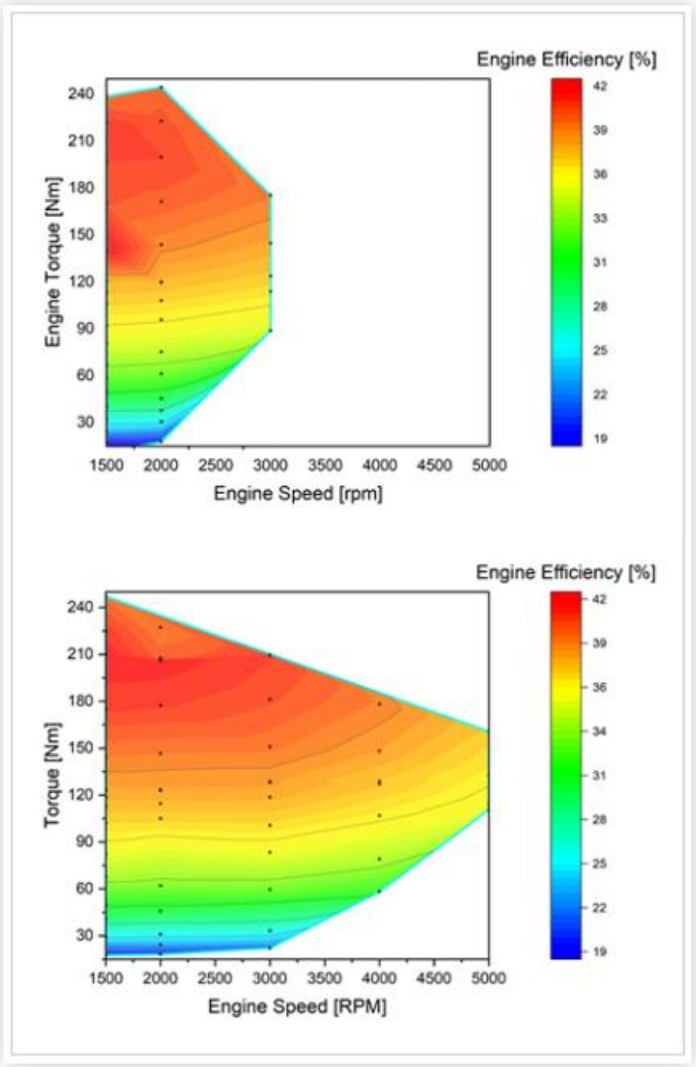


Figure 59: maps for engine efficiency for ammonia and ammonia hydrogen blend

The maps shown so far describe the engine behaviour predicted by the 1D code in accordance with the limits reported in chapter 2. As already underlined, the calculation model does not allow to evaluate the cyclic variation. Given the low laminar flame velocity of ammonia, when using conventional ignition systems, it is expected that the engine will not be able to operate stably at many of the points that the model considers acceptable. Indeed, considering light-duty engines and conventional ignition systems, the few experimental data available in literature for ammonia engines are presented for speeds up to 2000 rpm and medium-high loads. For engines running on ammonia/hydrogen there are data up to 3000 rpm.

Therefore, these maps were then recalculated focusing the attention on high load conditions and very small parzialization, as presented in [30].

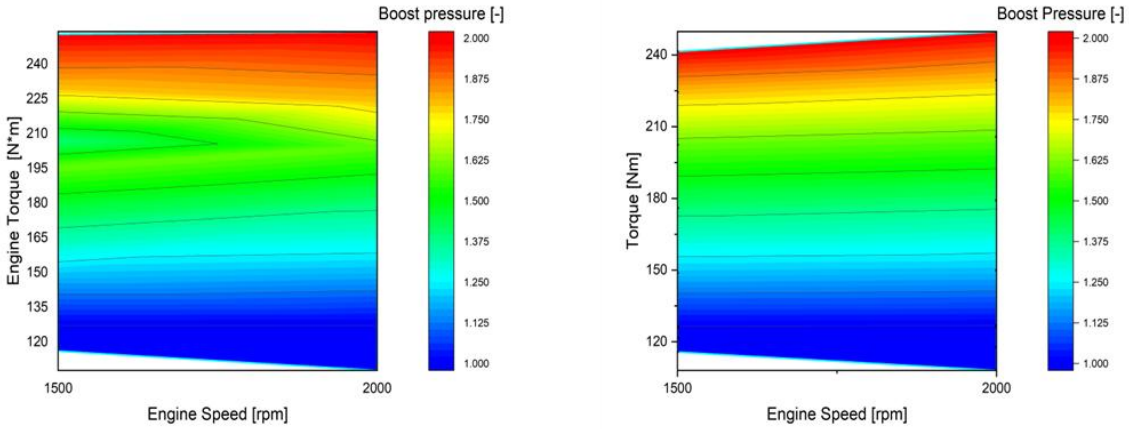


Figure 60: Ammonia map vs ammonia hydrogen map for boost pressure

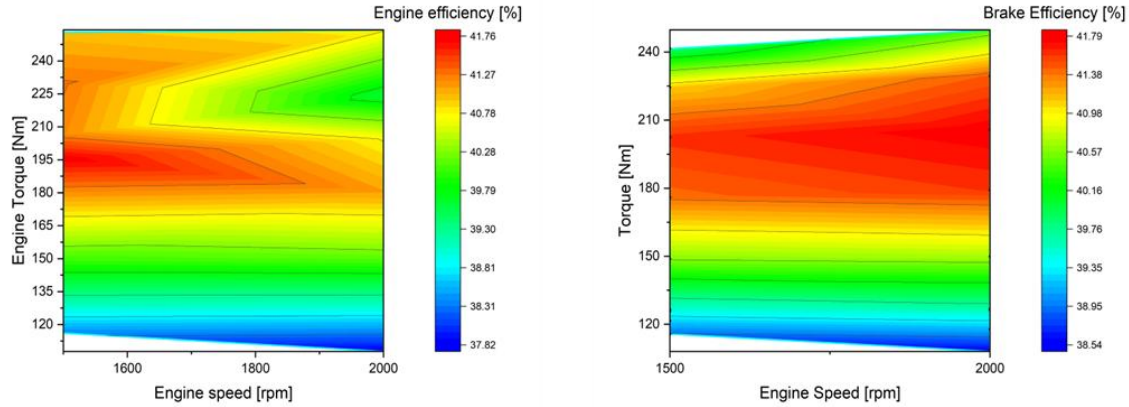


Figure 61: Ammonia map vs ammonia hydrogen map for engine efficiency

3.4 Ammonia cracking system and ammonia-syngas blends analyses

Hydrogen is very useful to enhance the combustion behaviour of the engine and to extend the operational range with respect to neat ammonia fuelling. On the other hand, the usage of ammonia-hydrogen blends requires the availability of the hydrogen necessary for the combustion process. This hydrogen can be stored considering specific tanks or can be directly produced by ammonia considering a catalytic cracking system which is able to convert ammonia into a syngas mainly composed by hydrogen and nitrogen, as shown in the following equation.

$$2NH_3 \rightarrow N_2 + 3H_2$$

A cracking system has been simulated in ASPEN plus considering different ammonia conversion efficiencies, respectively equal to 98%, 90%, 75% and 60%. The range from 98 to 60% has been chosen according to the typical efficiency values for these systems. The catalytic cracking system exploits the residual heat of the exhaust gases exiting the turbine to keep the cracking reactor temperature equal to 500°C, while during the system startup electric heaters must be used. The syngas obtained by the process has been used in blend with ammonia substituting the hydrogen. For these analyses the PSA

EP6DT engine has been used and the 15% of hydrogen by volume in the fuel blend has been considered. Therefore, the inlet mass flow rate of ammonia in the catalytic cracking system has been chosen considering the necessary amount of hydrogen by mass to keep the volume ratio between hydrogen and ammonia equal to 15% varying the conversion efficiency. The syngas is just composed by hydrogen, nitrogen and unconverted ammonia, neglecting the other subproducts.

For the CFD analyses, the conditions remain the same presented in the subparagraph 3.2 (case 3). Only the mass fraction of the mixture has been changed considering the presence of more nitrogen with respect to the initialization presented for the ammonia-hydrogen blend. Globally the air to fuel ratio was kept stoichiometric for each conversion efficiency considered, thus the amount of ammonia taken from the tank is calculated considering also the amount of unconverted ammonia in the syngas.

Figure 62 shows a comparison of the pressure curves for the different conversion efficiency considered, while figure 63 presents the temperature curves. It is evident that the variation of the conversion efficiency has no effect on the combustion process in fact, figures 62-63 shows that the maximum deviation among the cases is less than 2%. The highest curve, for both pressure and temperature, is the one corresponding to the 60% of efficiency because in this case the amount of nitrogen in the syngas is less than the other cases, while the amount of unconverted ammonia increases.

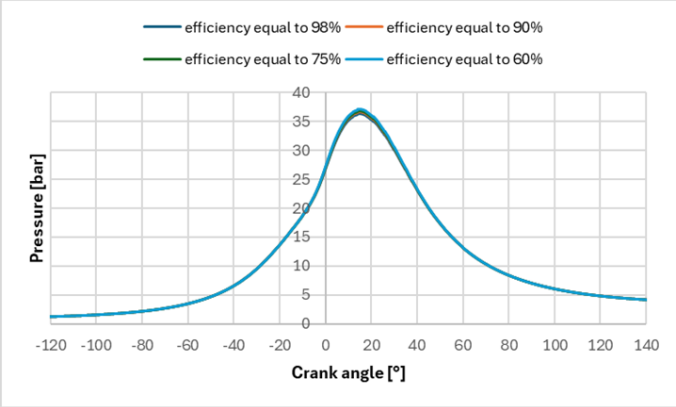


Figure 62: pressure curves at different conversion efficiencies

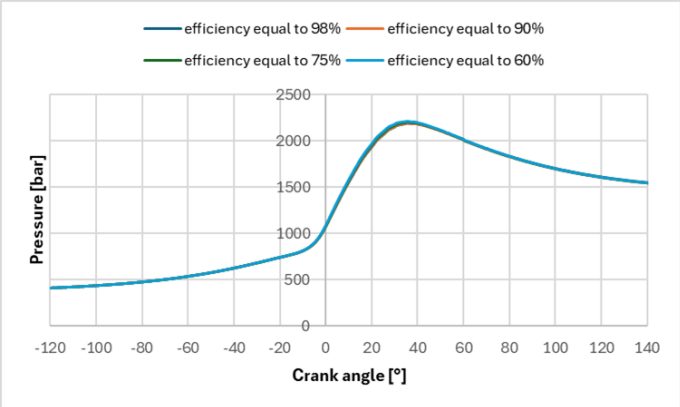


Figure 63: temperature curves at different conversion efficiencies

The combustion durations which are presented in table 23 allow to consider completely negligible the effect of the conversion efficiency on the combustion process, in fact the deviations between all the calculated values fall within the 2%. This is confirmed by the results presented in Figure 64, in which the rate of heat release curves considering different conversion efficiencies are presented. It is worth noting that the combustion center for all the cases falls within the same crank angle which is about 5 degrees later than the ammonia-hydrogen blend case.

Table 23: Combustion durations at different ammonia conversion efficiency

98% efficiency		90% efficiency		75% efficiency		60% efficiency	
CA0-10	26	CA0-10	25.9	CA0-10	25.9	CA0-10	25.7
CA10-90	37.2	CA10-90	36.9	CA10-90	36.5	CA10-90	36.3
CA50	14.8	CA50	14.6	CA50	14.4	CA50	14.2

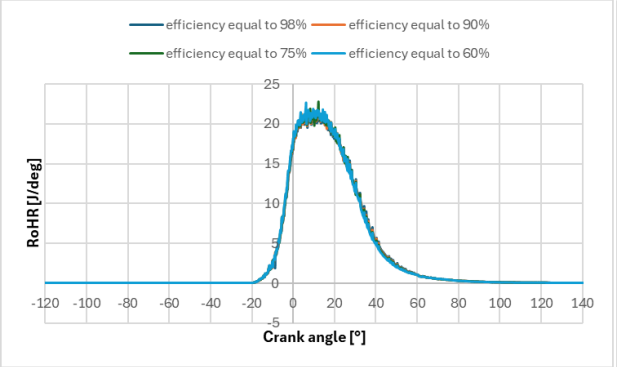


Figure 64: Rate of heat release curves considering different conversion efficiency

Table 24 shows that, considering the different conversion efficiencies, even emissions are not strongly affected. Moreover, the amount of unburned ammonia decreases if the conversion efficiency decreases (with a maximum deviation equal to 4%), while the NO amount slightly increases (0.4%). This happens due to the higher temperatures which are reached in the combustion chamber when the conversion yield reduces its values; as a matter of fact, the higher temperature improves the combustion process, but on the other hand favours the NO_x formation following the well-known Zeldovich mechanism.

Table 24: emissions comparison considering different conversion efficiencies

Ammonia conversion efficiency [%]	NH_3 [ppm]	NO [ppm]	N_2O [ppm]	NO_2 [ppm]
98	1973	2048	7	0
90	1952	2049	7	0
75	1942	2053	7	0
60	1890	2058	7	0

The results presented above clearly show that the conversion efficiency does not strongly affect the process, therefore only the case with and efficiency equal to 98% is considered for the comparison with the ammonia-hydrogen engine. Using the same approach presented in [15] the turbulent flame speed has been assessed for the engine running with ammonia-syngas blend and it was compared to the one of the ammonia-hydrogen blends. Furthermore, also $IMEP_H$, center of combustion, combustion durations and emissions were compared to better define the operational limits and the potential of the ammonia-syngas blend compared with ammonia-hydrogen blend. Table 25 summarize all the parameters comparison.

Table 25: comparison of different parameters between ammonia-hydrogen and ammonia-syngas fuelling

	Ammonia-hydrogen	Ammonia-syngas	Deviation [%]
Turbulent flame speed [m/s]	5.67	4.58	-19.22
$IMEP_H$ [bar]	8.25	8.38	1.58
CA 0-10 [CAD]	21.4	26	21.50
CA 10-90 [CAD]	28.1	37.2	32.38
CA 50 [CAD]	9	14.8	64.44
NH_3 unburned at EVO [ppm]	4885	1973	-59.61
NO at EVO [ppm]	1732	2048	18.24
NO_2 at EVO [ppm]	4	7	75.00
N_2O at EVO [ppm]	0	0	0.00
Pressure Peak [bar]	41.91	36.42	-13.10
Max Temperature [K]	2337.54	2187.7	-6.41

The presence of a higher amount of nitrogen in the combustion chamber causes greater dilution during the combustion process which explain the reduction of the turbulent flame speed, the pressure peak and the maximum in-cylinder pressure (Figures 65-66). In particular the pressure peak reduces by about 13%, while the maximum temperature is 6% less considering ammonia-syngas blend instead of ammonia-hydrogen blend. Moreover, the combustion process is slower if the engine is fueled by ammonia-syngas blend, in fact, both the CA 0-10 and the CA 10-90 are higher than the case of ammonia-hydrogen. In particular, the CA 0-10 is 21% higher, while the CA 10-90 is about 32% higher. Even in this case the deviations can be explained considering the dilution effect related to the higher presence of nitrogen in the fuel-air mixture. In the end, considering the reference case, it is worth noting that the syngas instead of hydrogen worsen the combustion process, but overall, the deviations are not too large.

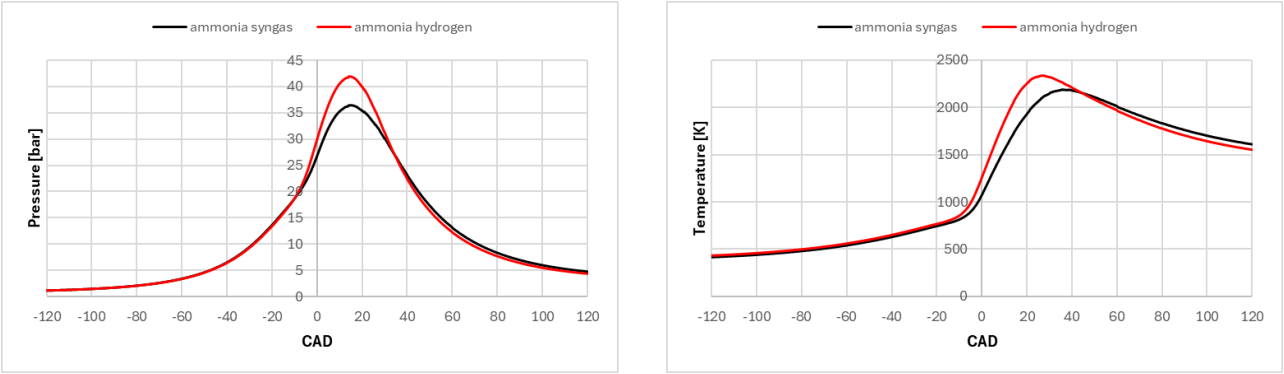


Figure 65: Pressure (left) and temperature (right) curves for ammonia hydrogen and ammonia syngas blends

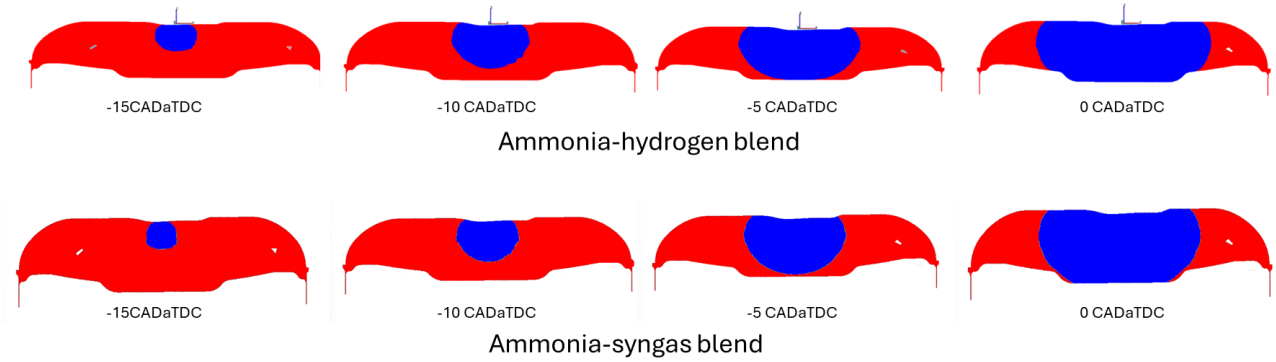


Figure 66: Turbulent flame speed assessment for ammonia-hydrogen and ammonia-syngas blends

On the other hand, emissions change considerably with respect to ammonia-hydrogen fuelling, in fact, as shown in Table 24, the amount of unburned ammonia decreases while the NO_x increases. This is probably related to the highest quantity of nitrogen when the engine is fuelled by ammonia-syngas blend. In fact, the nitrogen has a good chemical affinity with oxygen therefore when there is a great availability of both these substances the global amount of NO_x increases. Furthermore, considering that when ammonia molecules break down among all the substances that are generated there are radicals but also nitrogen, and if the engine is fueled by an ammonia-hydrogen blend this nitrogen partially reacts with oxygen to generate nitrogen oxides, part is one of the main combustion products. If the engine is fueled by an ammonia-syngas blend the total amount of nitrogen increases therefore the total amount of nitrogen oxides increases and this also led to a lower amount of unburned ammonia, because in that case the quantity of the combustion subproducts related to the partial oxidation increases due to the dilution effect. Globally the unburned ammonia, which neglect the NO_x formation reduced its amount because part of this fuel, after the dissociation reacts to produce nitrogen oxides, so in the end it can be inferred that globally the process produces about the same quantity of pollutants, but when the engine runs with ammonia-syngas blend change the types of these ones.

Conclusion

In this thesis work, the potential of ammonia and ammonia-hydrogen blends has been numerically investigated to define their usability in spark-ignition internal combustion engines instead of conventional fuels to reduce the CO_2 emissions related to the combustion process. The purpose of this work is to explore the potential of ammonia as a fuel for internal combustion engines, aiming to address the complications arising from the use of conventional fuels that produce CO_2 due to their carbon molecules. The current literature does not provide an in-sight knowledge about the simulation models of ammonia in spark ignition internal combustion engine. In this thesis specific 1D and 3D CFD models have been regulated to define a specific procedure to numerical investigated the combustion of ammonia as a neat fuel and in blends with hydrogen. The simulations have been carried out using both 1D and 3D-CFD models with the aim of building specific engine maps for the blends investigated.

First of all, starting from experimental data, the 3D-CFD model, coupled with a chemical kinetic approach, has been validated reproducing the different engine operating points (neat ammonia, 5% of hydrogen and 15% of hydrogen by volume) of a light-duty spark ignition engine. Then, an in-depth analysis aimed at the estimation of the turbulent flame has been carried out. The model well predicts the combustion behaviour of the engine, it catches the global phenomenon providing a good accuracy for all the investigated engine points, considering both combustion and emissions trends. In particular, the combustion center is quite well estimated, and the chemical kinetics model allows to reproduce the speeding up of the combustion process caused by enrichment with hydrogen. In particular, comparing 5% of hydrogen by volume to neat ammonia, the CA0-10 duration decreases by 19% according to both the average experimental data and the calculated data, while it decreases by 39% and 41% respectively if 15% of hydrogen is compared with neat ammonia. For emissions the model captures the same trend as the experimental data: adding 15% hydrogen decreases the ammonia emissions by 22% in the simulations and 30% in the experiments, while moving from neat ammonia to 5% of hydrogen, the unburned ammonia decreases 12% in the simulation and by 11% in the experiments.

Then multiple spark strategy has been tested on the same engine to improve the combustion behaviour of this engine fuelled by ammonia and ammonia-hydrogen blends.

Considering double spark plug the pressure peak increases of about 43% considering the engine running with neat ammonia, 28% with 5% of hydrogen by volume and 18% with hydrogen-enrichment equal to 15% by volume. The effect of multiple spark plugs seems to be very sensitive to the amount of hydrogen considered in the fuel mixture, therefore it might be useful to adopt this strategy with lower ammonia-hydrogen-enriched blends. The $IMEP_H$, moving from single to twin spark strategy increases respectively of 9%, 11% and 6.5% for neat ammonia, 5% and 15% of hydrogen by volume in the fuel mixture. These results confirm that multiple spark strategies better fit with lower amounts of hydrogen-enrichment considered. The improvement in emission is smaller: in fact, for each mixture considered the reduction is respectively of about 13%,

8% and 3%. This is also confirmed for NOx emissions, and, in this case, the effect is less than unburned ammonia

The validated 3D combustion model has been used to calibrate a 1D model of a second spark-ignition engine. The aim has been to simulate the operation of this engine in case of ammonia and ammonia-hydrogen fuelling. This choice can be justified by the fact that the two engines are very similar from a geometrical point of view, the application range for both is the same and the turbulent motions inside the combustion chamber are very close to each other. Thus, the 1D model has been used to obtain specific engine maps considering neat ammonia and hydrogen-enriched ammonia (15% by volume) blends. The whole analyses shows that the engine fuelled with ammonia required a spark advance bigger than gasoline engine and globally the combustion process is slower, however the engine can provide proper engine conditions also if it is fuelled with ammonia. The maps clearly show that ammonia can be used instead of conventional fuel in engine, but the allowable range is very narrow if compared to the one of gasoline engine, on the other hand the results allow to define the optimal engine operating range for these blends. In particular, the engine provided stable engine conditions at the lowest engine speed tested, suggesting that ammonia can be an optimal fuel for heavy duty and marine engines. The results related to the second engine investigated can be improved with experimental tests to enhance the 1D predictive model.

Finally, a cracking system has been considered to produce hydrogen directly from ammonia and the use of the syngas which exits the system, in blends with ammonia instead of hydrogen, has been assessed by means of 3D simulations. Results clearly indicate that using the syngas instead of hydrogen determines a reduction in the combustion velocity, due to the dilution related to the higher amount of nitrogen in the fuel mixture, but the engine still reach stable conditions. On the other hand, considering emissions, the unburned ammonia decreases, while the NO_x amount increases; this suggests that the engine fuelled by ammonia-syngas blend requires the presence of a dedicated pollutant abatement system.

The main outcome of this thesis can be summarized as:

- The low laminar flame speed of ammonia–air mixtures lead to increased combustion durations and to optimal spark timings more advanced than typical ones of SI engines. On the other hand, no knock occurrence was detected.
- Considering unthrottled engine operation and stoichiometric conditions, the combustion duration decreases for increasing boost pressure. Due to the operating limits of both in-cylinder pressure and exhaust gas temperature, the maximum regime which guarantees a proper engine operation is 3000 rpm, except for the highest boost level (BP=1.8 and 2 bar).
- A small amount of hydrogen (by mass) improved the combustion behaviour with respect to pure ammonia fuelling, leading to reduced combustion durations and extending the operating range of the engine.
- With ammonia-hydrogen fuelling, the engine can theorically run up to 5000 rpm, while with neat ammonia fuelling it can run only up to 3000 rpm

- Between 1500 rpm and 3000 rpm, the engine could be properly regulated. The engine could not reach 6000 rpm.
- The maximum engine torque (about 240 Nm) was delivered at 1500 rpm. The engine efficiency ranged between 42% and 19%. Correspondingly, the specific consumption varied from about 350 g/kWh to about 750 g/kWh.
- Partial load operation became critical for the lowest loads at medium regimes and for almost all the loads at high regimes, due to unacceptable values of the burned fuel fraction. Low regimes (1500 and 2000 rpm) were sustainable for the whole considered throttling range. Medium regimes (3000 and 4000 rpm) were not sustainable at the lowest loads. At high regimes (5000 and 6000 rpm), a proper engine operation was not reachable, except for WOT and very low throttling conditions at 5000 rpm.
- The calculated mean flame speeds are an order of magnitude greater than the calculated laminar flame speeds, highlighting the effect of hydrogen addition on the acceleration of the combustion process. Moving from neat ammonia to 15% of hydrogen by volume the mean turbulent flame speed increases of about 75%.
- The dissociation of ammonia produces H_2, which is detected in the combustion chamber by the 3D CFD model also if neat ammonia is burned and, at least according to the chemical mechanism used, not all the produced hydrogen oxidizes.
- Multiple sparkplugs strategy allows to improve the $IMEP_H$ of the engine, but the presence of the third spark plug does not affect considerably the engine. Furthermore, the multiple sparks plug strategy also permits to reduce the emissions related to the combustion process.

This work shows that ammonia can be used as a fuel for spark ignition internal combustion engines, especially if it is used in blends with hydrogen. Up to now it is just a research field, but following the results presented it can be used especially in heavy duty engine. In fact, ammonia shows more stable conditions at the lower engine speed investigated and therefore chiefly in the naval sector it can be a good alternative to the conventional fuel. In this field also the problem related to the essential adjustments to the engine system can be readily addressed due to the diminished requirement for compact systems.

Bibliografy

[1] Stančin H, Mikulčić H, Wang X, Duić N. A review on alternative fuels in future energy system. Renew Sustain Energy Rev 2020;128. doi:10.1016/j.rser.2020.109927.

[2] Bae C, Kim J. Alternative fuels for internal combustion engines. Proc Combust Inst 2017;36:3389–413. doi:10.1016/j.proci.2016.09.009.

[3] Valera-Medina, A., Xiao, H., Owen-Jones, M., David, W. I., & Bowen, P. J. (2018). Ammonia for power. *Progress in Energy and combustion science*, *69*, 63-102.

[4] Kojima, Y. (2013). A green ammonia economy. *Proceedings of the 10th Annual NH*, *3*.

[5] Gezerman, A. O. (2022). A critical assessment of green ammonia production and ammonia production technologies. *Kemija u industriji: Časopis kemičara i kemijskih inženjera Hrvatske*, *71*(1-2), 57-66.

[6] Health Protection Agency "Ammonia: health effects, incident management and toxicology. HPA 2014. Available online https://www.gov.uk/government/ publications/ammonia- properties- incident- management- and- toxicology.

[7] Xue M, Wang Q, Lin B Le, Tsunemi K. Assessment of Ammonia as an Energy Carrier from the Perspective of Carbon and Nitrogen Footprints. ACS Sustain Chem Eng 2019;7:12494–500. doi:10.1021/acssuschemeng.9b02169

[8] Gütschow J, Jeffery ML, Gieseke R, Gebel R, Stevens D, Krapp M, et al. The PRIMAP-hist national historical emissions time series. Earth Syst Sci Data 2016; 8:571–603. doi:10.5194/essd-8-571-2016.

[9] Gütschow J, Jeffery L, Gieseke R. The PRIMAP-hist national historical emissions time series v2.0 (1850 2016). 2019. doi: 10.5880/PIK.2019.001.

[10] Kojima, Y.; Yamaguchi, M. Ammonia as a hydrogen energy carrier. Int. J. Hydrogen Energy 2022, 47, 22832–22839

[11] CMørch, S.; Bjerre, A.; Gøttrup, M.; Sorenson, S.C.; Schramm, J. Ammonia/hydrogen mixtures in an SI-engine: Engine perfor-mance and analysis of a proposed fuel system. Fuel 2011, 90, 854–864.

[12] Kobayashi, H.; Hayakawa, A.; Somarathne, K.K.A.; Okafor, E.C. Science and technology of ammonia combustion. Proc. Combust.Inst. 2019, 37, 109–133

[13] Thurston, R.H. A History of the Growth of the Steam-Engine. Nature 1972, 19, 381–382.

[14] Gray, J.T., Jr.; Dimitroff, E.; Meckel, N.T.; Quillian, R.D., Jr. Ammonia Fuel-Engine Compatibility and Combustion. In Proceedings of the Automotive Engineering Congress & Exposition. 1966. Available online: https://www.researchgate.net/publication/296646977_Ammonia_Fuel_-_Engine_Compatibility_and_Combustion (accessed on 20 January 2022).

[15] Pearsall, T.J.; Garabedian, C.G. Combustion of Anhydrous Ammonia in Diesel Engines; SAE Technical Paper 670947; SAE International: Warrendale, PA, USA, 1967.

[16] Pearsall, T.J. Ammonia Application to Reciprocating Engines. Volume 1. 1967. Available online: https://www.researchgate.

net/publication/235199347_AMMONIA_APPLICATION_TO_RECIPROCATING_ENGINES_VOLUME_1 (accessed on 20 January 2022).
[17] Lesmana H, Zhang Z, Li X, Zhu M, Xu W, Zhang D. NH3 as a transport fuel in internal combustion engines: A technical review. J Energy Resour Technol Trans ASME 2019;141. doi: 10.1115/1.4042915.
[18] Reiter AJ, Kong SC. Combustion and emissions characteristics of compression-ignition engine using dual ammonia-diesel fuel. Fuel 2011;90:87–97. doi:10.1016/j.fuel.2010.07.055.
[19] Reiter AJ, Kong SC. Demonstration of compression-ignition engine combustion using ammonia in reducing greenhouse gas emissions. Energy and Fuels 2008;22:2963–71. doi:10.1021/ef800140f.
[20] Pochet M, Truedsson I, Foucher F, Jeanmart H, Contino F. Ammonia-Hydrogen blends in Homogeneous Charge Compression-Ignition Engine. SAE Tech Pap 2017. doi:10.4271/2017-24-0087.
[21] Pochet M, Jeanmart H, Contino F. A 22:1 Compression Ratio Ammonia-Hydrogen HCCI Engine: Combustion, Load, and doi:10.3389/fmech.2020.00043. Emission Performances. Front Mech Eng 2020;6:43.
[22] Sahin, Z.; Akcanca, I.Z.; Durgun, O. Experimental investigation of the effects of ammonia solution (NH3OH) on engine performance and exhaust emissions of a small diesel engine. Fuel 2018, 214, 330–341.
[23] Scharl, V.; Lackovic, T.; Sattelmayer, T. Characterization of ammonia spray combustion and mixture formation under high-pressure, direct injection conditions. Fuel 2023, 333, 126454.
[24] Zhang, Z.; Long, W.; Dong, P.; Tian, H.; Tian, J.; Li, B.; Wang, Y. Performance characteristics of a two-stroke low speed engineapplying ammonia/diesel dual direct injection strategy. Fuel 2023, 332, 126086.
[25] Starkman ES, Newhall HK, Sutton R, Maguire T, Farbar L. Ammonia as a Spark Ignition Engine Fuel: Theory and Application. SAE Tech Pap 1966:660155. doi:10.4271/660155
[26] Cornelius W, Huellmantel LW, Mitchell HR. Ammonia as an engine fuel. SAE Tech Pap 1965;650052. doi:10.2307/44460524.
[27] Sawyer RF, Starkman ES, Muzio L, Schmidt WL. Oxides of Nitrogen in the Combustion Products of an Ammonia Fueled Reciprocating Engine. SAE Tech Pap 1968;680401. doi:10.4271/680401.
[28] Lhuillier, C.; Brequigny, P.; Contino, F.; Rousselle, C. Combustion Characteristics of Ammonia in a Modern Spark-Ignition Engine. In Proceedings of the Conference on Sustainable Mobility, Catane, Italy, 14–15 October 2019
[29] Lhuillier, C.; Brequigny, P.; Contino, F.; Rousselle, C. Performance and Emissions of an Ammonia-Fueled SI Engine with Hydrogen Enrichment. In Proceedings of the 14th International Conference on Engines & Vehicles, Capri, Italy, 15–19 September 2019.
[30] Cui, Z.; Tian, J.; Zhang, X.; Yin, S.; Long, W.; Song, H. Experimental Study of the Effects of Pre-Chamber Geometry on theCombustion Characteristics of an Ammonia/Air Pre-Mixture Ignited by a Jet Flame. Processes 2022, 10, 2102.
[31] Mounaïm-Rousselle, C.; Bréquigny, P.; Dumand, C.; Houillé, S. Operating Limits for Ammonia Fuel Spark-Ignition Engine. Energies 2021, 14, 4141.

[32] Guo, B.; Ichiyanagi, M.; Kajiki, K.; Aratake, N.; Zheng, Q.; Kodaka, M.; Suzuki, T. Combustion Analysis of Ammonia Fueled High Compression Ratio SI Engine with Glow Plug and Sub-Chamber. Int. J. Automot. Eng. 2022, 13, 1–8.

[33] AbdElFattah, S.F.; Ezzat, M.F.; Mourad, M.A.; Elkelawy, M.; Youssef, I.M. Youssef Experimental Investigation of the Performance and Exhaust Emissions of a Spark-Ignition Engine Operating with Different Proportional Blends of Gasoline and Water Ammonia Solution. J. Eng. Res. 2021, 5, 38–45.

[34] Zhang, H.; Li, G.; Long, Y.; Zhang, Z.; Wei, W.; Zhou, M.; Belal, B.Y. Numerical study on combustion and emission characteristicsof a spark-ignition ammonia engine added with hydrogen-rich gas from exhaust-fuel reforming. Fuel 2023, 332, 125939.

[35] Comotti M, Frigo S, Hydrogen generation system for ammonia e hydrogen fuelled internal combustion engines, International Journal of Hydrogen Energy (2015), http://dx.doi.org/10.1016/j.ijhydene.2015.06.080

[36] Stefano Frigo, Roberto Gentili,Analysis of the behaviour of a 4-stroke Si engine fuelled with ammonia and hydrogen,International Journal of Hydrogen Energy,Volume 38, Issue 3,2013,Pages 1607-1615,ISSN 0360-3199,https://doi.org/10.1016/j.ijhydene.2012.10.114.

[37] Wang, D.; Ji, C.; Wang, S.; Yang, J.; Wang, Z. Numerical study of the premixed ammonia-hydrogen combustion under engine-relevant conditions. Int. J. Hydrogen Energy 2021, 46, 2667–2683

[38] Pyrc, M.; Gruca, M.; Tutak, W.; Jamrozik, A. Assessment of the co-combustion process of ammonia with hydrogen in a researchVCR piston engine. Int. J. Hydrogen Energy 2022, 48, 2821–2834

[39] Grannell SM, Assanis DN, Bohac S V., Gillespie DE. The Fuel Mix Limits and Efficiency of a Stoichiometric, Ammonia, and Gasoline Dual Fueled Spark Ignition Engine. J Eng Gas Turbines Power 2008;130:042802: 1-8. doi:10.1115/1.2898837.

[40] Grannell SM, Assanis DN, Gillespie DE, Bohac S V. Exhaust emissions from a stoichiometric, ammonia and gasoline dual fueled spark ignition engine. Proc. Spring Tech. Conf. ASME Intern. Combust. Engine Div., Milwaukee, Wisconsin, USA: 2009, p. 135–41. doi:10.1115/ICES2009-76131.

[41] Ryu K, Zacharakis-Jutz GE, Kong SC. Performance enhancement of ammonia-fueled engine by using dissociation catalyst for hydrogen generation. Int J Hydrogen Energy 2014;39:2390–8. doi:10.1016/j.ijhydene.2013.11.098

[42] Ryu K, Zacharakis-Jutz GE, Kong S-C. Effects of gaseous ammonia direct injection on performance characteristics of a spark-ignition doi:10.1016/j.apenergy.2013.11.067. engine. Appl Energy 2014;116:206–15.

[43] Dawood, F., Anda, M., & Shafiullah, G. M. (2020). Hydrogen production for energy: An overview. International Journal of Hydrogen Energy, 45(7), 3847-3869.

[44] Shawn A. Reggeti, Seamus P. Kane, William F. Northrop,Hydrogen production in ammonia-fueled spark ignition engines,Applications in Energy and Combustion Science,Volume 14,2023,100136,ISSN 2666-352X,https://doi.org/10.1016/j.jaecs.2023.100136.

[45] A. Mercier, C. Mounaïm-Rousselle, P. Brequigny, J. Bouriot, C. Dumand,Improvement of SI engine combustion with ammonia as fuel: Effect of

ammonia dissociation prior to combustion,Fuel Communications,Volume 11,2022,100058,ISSN 2666-0520,https://doi.org/10.1016/j.jfueco.2022.100058.

[46] Hao Zhang, Nuo Lei, Zhi Wang, Ammonia-hydrogen propulsion system for carbon-free heavy-duty vehicles,Applied Energy,Volume 369,2024,123505,ISSN 0306-2619,https://doi.org/10.1016/j.apenergy.2024.123505.

[47] Rodríguez, C.G.; Lamas, M.I.; Rodríguez, J.D.; Abbas, A. Possibilities of Ammonia as Both Fuel and NOx Reductant in MarineEngines: A Numerical Study. J. Mar. Sci. Eng. 2022, 10, 43.

[48] Liu, L.; Tan, F.; Wu, Z.; Wang, Y.; Liu, H. Comparison of the combustion and emission characteristics of NH3/NH4NO2 andNH3/H2 in a two-stroke low speed marine engine. Int. J. Hydrogen Energy 2022, 47, 17778–17787.

[49] Wang, Y.; Zhou, X.; Liu, L. Theoretical investigation of the combustion performance of ammonia/hydrogen mixtures on a marinediesel engine. Int. J. Hydrogen Energy 2021, 46, 14805–14812

[50] Chen, Jundie, et al. "Effect of hydrogen blending on the high temperature auto-ignition of ammonia at elevated pressure." Fuel 287 (2021): 119563. DOI:10.1016/j.fuel.2020.119563

[51] Ronney PD. Effect of Chemistry and Transport Properties on Near-Limit Flames at Microgravity. Combust Sci Technol 1988;59:123–41. doi:10.1080/00102208808947092.

[52] Ronney PD. Effect of Chemistry and Transport Properties on Near-Limit Flames at Microgravity. Combust Sci Technol 1988;59:123–41. doi:10.1080/00102208808947092.

[53] Jabbour T, Clodic DF. Burning Velocity and Refrigerant Flammability Classification. Trans - Am Soc Heat Refrig Air Cond Eng 2004;110:522–33

[54] Takizawa K, Takahashi A, Tokuhashi K, Kondo S, Sekiya A. Burning velocity measurements of nitrogen containing compounds. J Hazard Mater 2008;155:144–52. doi:10.1016/j.jhazmat.2007.11.089.

[55] Kumar P, Meyer TR. Experimental and modeling study of chemical-kinetics mechanisms for H2-NH3-air mixtures in laminar premixed jet flames. Fuel 2013;108:166–76. doi:10.1016/j.fuel.2012.06.103.

[56] Li J, Huang H, Kobayashi N, He Z, Nagai Y. Study on using hydrogen and ammonia as fuels: Combustion characteristics and NOx formation. Int J Energy Res 2014;38:1214–23. doi:10.1002/er.3141.

[57] Goldmann, Andreas, and Friedrich Dinkelacker. "Approximation of laminar flame characteristics on premixed ammonia/hydrogen/nitrogen/air mixtures at elevated temperatures and pressures." Fuel 224 (2018): 366-378. DOI:10.1016/j.fuel.2018.03.030

[58] Lhuillier, Charles, et al. "Experimental investigation on laminar burning velocities of ammonia/hydrogen/air mixtures at elevated temperatures." Fuel 263 (2020): 116653. DOI:10.1016/j.fuel.2019.116653

[59] Pessina, V., et al. "Laminar flame speed correlations of ammonia/hydrogen mixtures at high pressure and temperature for combustion modeling applications." International Journal of Hydrogen DOI:10.1016/j.ijhydene.2022.06.007

[60] Glarborg P, Miller JA, Ruscic B, Klippenstein SJ. Modeling nitrogen chemistry in combustion. Prog Energy Combust Sci 2018;67:31–68. doi:10.1016/j.pecs.2018.01.002.

[61] Nakamura, Hisashi, Susumu Hasegawa, and Takuya Tezuka. "Kinetic modeling of ammonia/air weak flames in a micro flow reactor with a controlled temperature profile." Combustion and Flame 185 https://doi.org/10.1016/j.combustflame.2017.06.021. (2017): 16-27.

[62] Otomo, Junichiro, et al. "Chemical kinetic modeling of ammonia oxidation with improved reaction mechanism for ammonia/air and ammonia/hydrogen/air combustion." International Journal of Hydrogen Energy 43.5 (2018): 3004-3014. https://doi.org/10.1016/j.ijhydene.2017.12.066.

[63] Song, Yu, et al. "Ammonia oxidation at high pressure and intermediate temperatures." Fuel 181 (2016): 358-365. https://doi.org/10.1016/j.fuel.2016.04.100.

[64] Stagni, Alessandro, et al. "An experimental, theoretical and kinetic-modeling study of the gas-phase oxidation of ammonia." Reaction Chemistry & Engineering 5.4 (2020): 696-711. DOI:10.1039/C9RE00429G

[65] Song, Y., et al. "The sensitizing effects of NO2 and NO on methane low temperature oxidation in a jet stirred reactor." Proceedings of the Combustion Institute 37.1 (2019): 667-675. https://doi.org/10.1016/j.proci.2018.06.115.

[66] Shrestha, Krishna P., et al. "Detailed kinetic mechanism for the oxidation of ammonia including the formation and reduction of nitrogen oxides." Energy & fuels 32.10 (2018): 10202-10217.

[67] Shrestha, Krishna Prasad, et al. "An experimental and modeling study of ammonia with enriched oxygen content and ammonia/hydrogen laminar flame speed at elevated pressure and temperature." Proceedings of the Combustion Institute 38.2 (2021): 2163-2174.

[68] Glassman, I., Yetter, R. A., & Glumac, N. G. (2014). Combustion. Academic press.

[69] Goodwin, D.G.; Moffat, H.K.; Speth, R.L. Cantera: An Object-Oriented Software Toolkit for Chemical Kinetics, Thermodynamics, and Transport Processes, Version 2.2. 1.; Cantera Developers: Warrenville, IL, USA, 2017

[70] Schiffner, Michael, Michael Jud, and Thomas Sattelmayer. "Reaction Kinetics Analysis of Dual Fuel Internal Combustion Engines Based on Ignition Delay Times Using n-Heptane/Methane Fuel Blends." Proceedings of the 8th European Combustion Meeting, Dubrovnik, Croatia. 2017.

[71] Scala, F.; Galloni, E.; Fontana, G. Numerical analysis of a downsized spark-ignition engine fueled by butanol/gasoline blends at part-load operation. Appl. Therm. Eng. 2016, 102, 383–390.

[72] Bozza, F.; Fontana, G.; Galloni, E.; Torella, E. 3D-1D Analyses of the Turbulent Flow Field, Burning Speed and Knock Occurrence in a Turbocharged SI Engine. SAE Trans. J. Engines 2007, 116, 1495–1507.

[73] Douaud, A.; Eyzat, P. Four-Octane-Number Method for Predicting the Anti-Knock Behavior of Fuels and Engines. SAE Trans.1978, 87, 294–308.

[74] Richard, S.; Bougrine, S.; Font, G.; Lafossas, F.-A.; Le Berr, F. On the Reduction of a 3D CFD Combustion Model to Build a Physical0D Model for Simulating Heat Release, Knock and Pollutants in SI Engines. Oil Gas Sci. Technol.—Rev. IFP 2009, 64, 223–242.

[75] Ó Conaire, M.; Curran, H.J.; Simmie, J.; Pitz, W.; Westbrook, C.K. A comprehensive modeling study of hydrogen oxidation. Int. J.Chem. Kinet. 2004, 36, 603–622

[76] Girimaji, S. (2006): Partially-Averaged Navier-Stokes Model for turbulence: A Reynolds-Averaged Navier-Stokes to Direct Numerical Simulation bridging method. J. of Applied Mechanics, 73, 413-421.

[77] Girimaji, S., Jeong, E. and Srinivasan, R. (2006). Partially-Averaged Navier-Stokes Model for turbulence: Fixed point analysis and comparison with unsteady Partially Averaged Navier-Stokes. J. of Applied Mechanics, 73, 422-429.

[78] Hanjalic, K., Popovac, M., Hadziabdic, M. A robust near-wall elliptic-relaxation eddy-viscosity turbulence model for CFD, Int. J. Heat Fluid Flow, 25, 1047–1051, 2004.

[79] Popovac, M., & Hanjalic, K. (2007). Compound wall treatment for RANS computation of complex turbulent flows and heat transfer. Flow, turbulence and combustion, 78, 177-202.

[80] Schiffner, Michael, Michael Jud, and Thomas Sattelmayer. "Reaction Kinetics Analysis of Dual Fuel Internal Combustion Engines Based on Ignition Delay Times Using n Heptane/Methane Fuel Blends." Proceedings of the 8th European Combustion Meeting, Dubrovnik, Croatia. 2017. https://doi.org/10.3390/en15114081

[81] Chen, Jundie, et al. "Effect of hydrogen blending on the high temperature auto-ignition of ammonia at elevated pressure." Fuel 287 (2021): 119563. DOI:10.1016/j.fuel.2020.119563

[82] Luo, Q.; Hu, J.-B.; Sun, B.; Liu, F.; Wang, X.; Li, C.; Bao, L. Effect of equivalence ratios on the power, combustion stability and NOxcontrolling strategy for the turbocharged hydrogen engine at low engine speeds. Int. J. Hydrogen Energy 2019, 44, 17095–17102.

[83] Peters, N., “Turbulent Combustion,” Meas. Sci. Technol. 12 (2001): 2022.